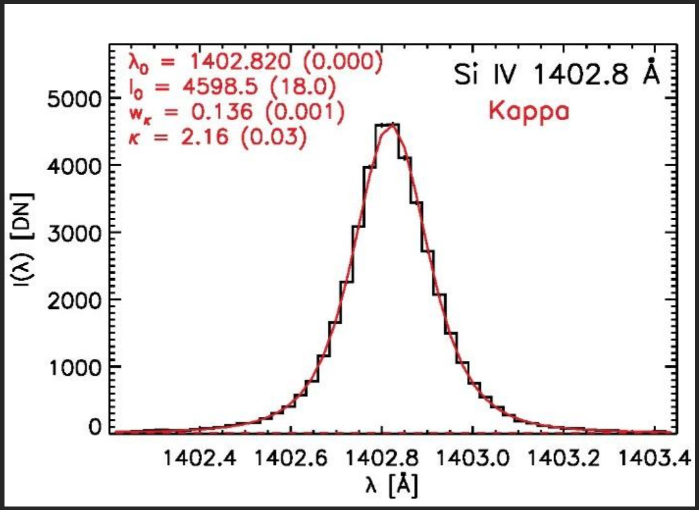

Optically Thin Solar Spectra out of Equilibrium

Jaroslav Dudík

Astronomical Institute of the Czech Academy of Sciences

Lecture 3

Selected Chapters in Astrophysics

Faculty of Mathematics and Physics, Charles University, 2018-10-25

Outline

I. **Basic Atomic Processes: Ionization, Recombination, Excitation and Statistical Equilibrium**

II. **Non-Equilibrium Ionization (NEI)**

Highly dynamic phenomena seen by IRIS and Hi-C
Simulations: Evolution of ionization stages
Occurrence in cooling loops and rapidly heated loops (nanoflares)
Effects and Observables

III. **Non-Maxwellian Distributions of Electrons and Ions**

Why, What, Where
High-energy tails in flares and elsewhere
Consequences for UV/EUV line formation; DEMs
Detection, or lack thereof
Combination with non-equilibrium ionization

Atomic Processes

Ionization

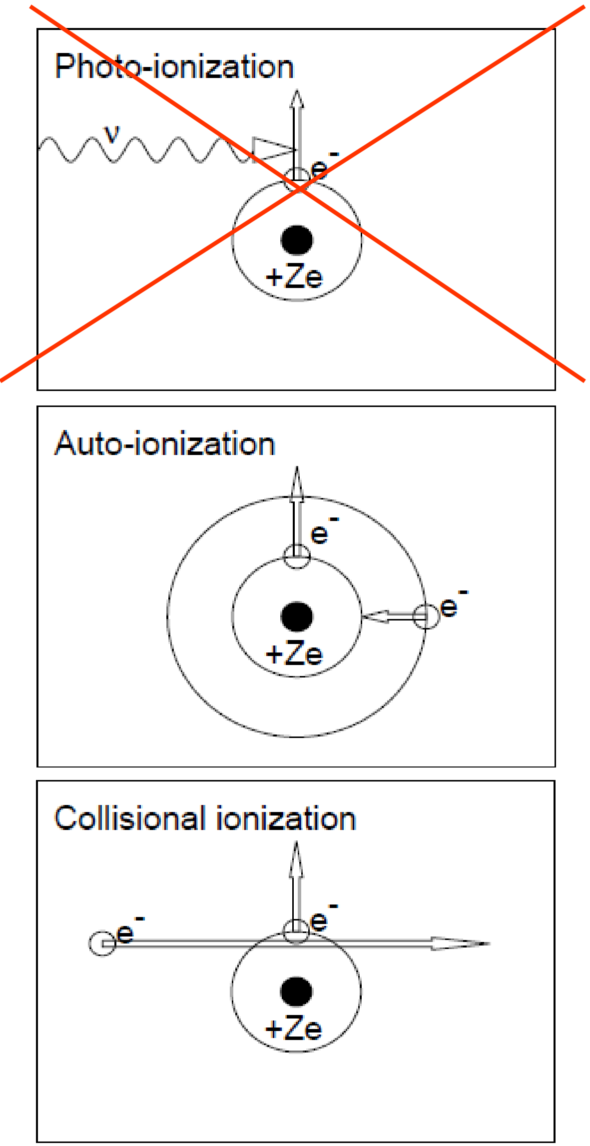

Recombination

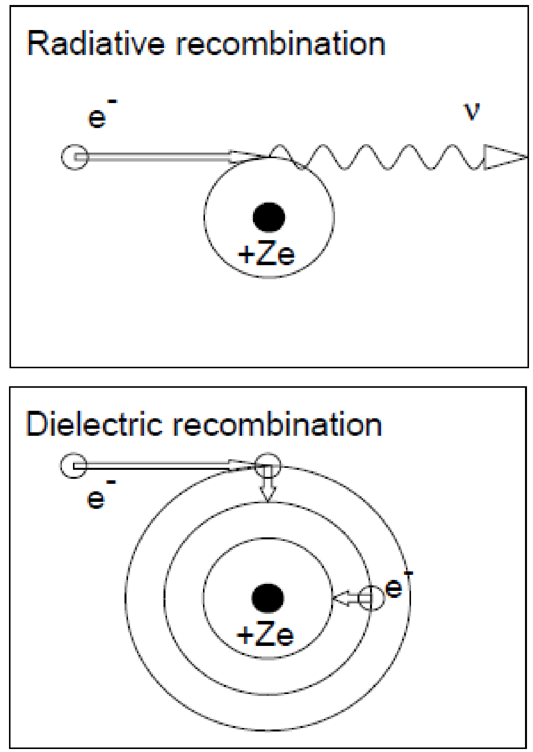

Excitation/Deexcitation

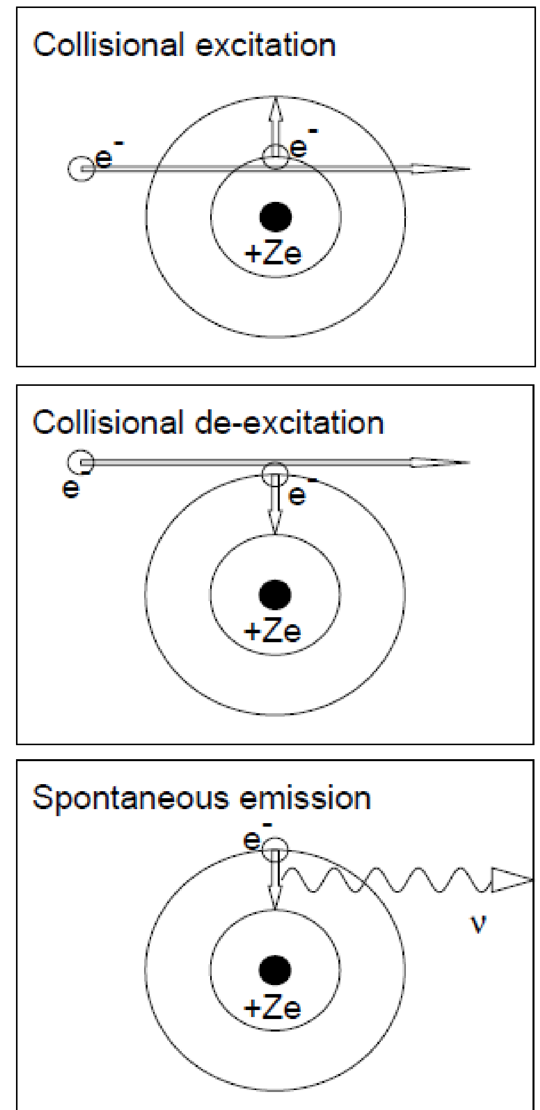

Aschwanden (2005), Physics of the Solar Corona

Line Intensities: Equilibrium

$$I_{ji} = \int A_X G_{X,ji}(T, n_e, \kappa) n_e n_H \mathrm{d}l\,,$$

excitation fraction *ionization fraction Y_k*

$$\varepsilon_{ji} = \frac{hc}{\lambda_{ji}} A_{ji} n(X_j^{+k}) = \frac{hc}{\lambda_{ji}} \frac{A_{ji}}{n_e} \frac{n(X_j^{+k})}{n(X^{+k})} \frac{n(X^{+k})}{n(X)} A_X n_e n_H$$
$$= A_X G_{X,ji}(T, n_e, \kappa) n_e n_H,$$

- **Excitation fraction: Small equilibration timescales (~ 1s)**
- **Level population is then calculated assuming statistical equilibrium:**
  Collisional excitations (upward transitions) are balanced by spontaneous emission and collisional de-excitations (downward transitions)

$$\sum_{j>m} n(X_j^{+k}) n_e C_{jm}^{\mathrm{d}} + \sum_{j<m} n(X_j^{+k}) n_e C_{jm}^{\mathrm{e}} + \sum_{j>m} n(X_j^{+k}) A_{jm}$$
$$= n(X_j^{+k}) \left(\sum_{j<m} n_e C_{mj}^{\mathrm{d}} + \sum_{j>m} n_e C_{mj}^{\mathrm{e}} + \sum_{j<m} A_{mj} \right),$$

- **Where the rates $C = \int v\sigma(v) f(v) \mathrm{d}v$**

Collisional Ionization Equilibrium

$$0 = n_{\mathrm{e}}(I_{i-1}Y_{i-1} + R_iY_{i+1} - I_iY_i - R_{i-1}Y_i \ + \cdots)$$

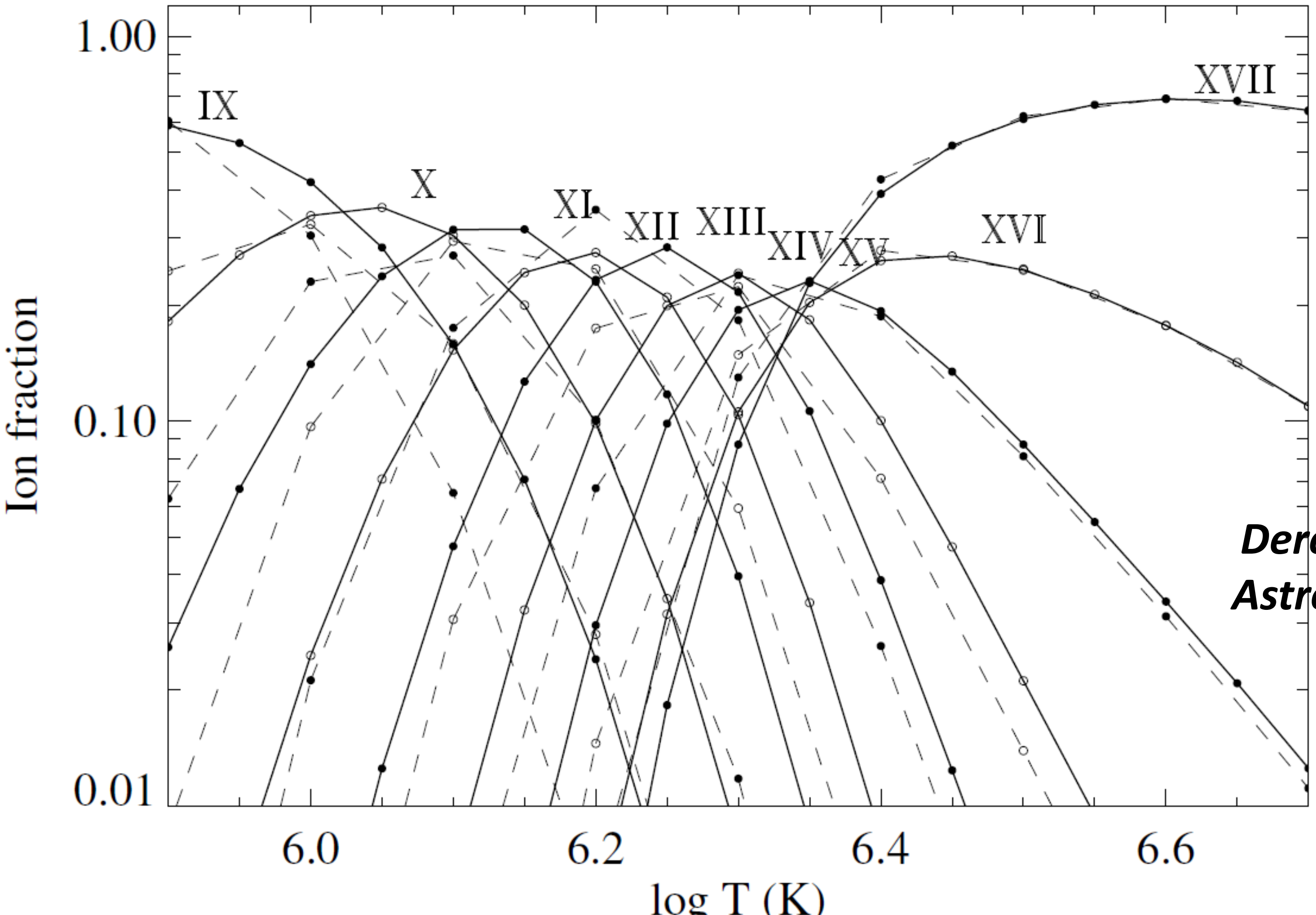

Dere et al. (2009), Astron. Astrophys. 498 915

The Case for Non-Equilibrium

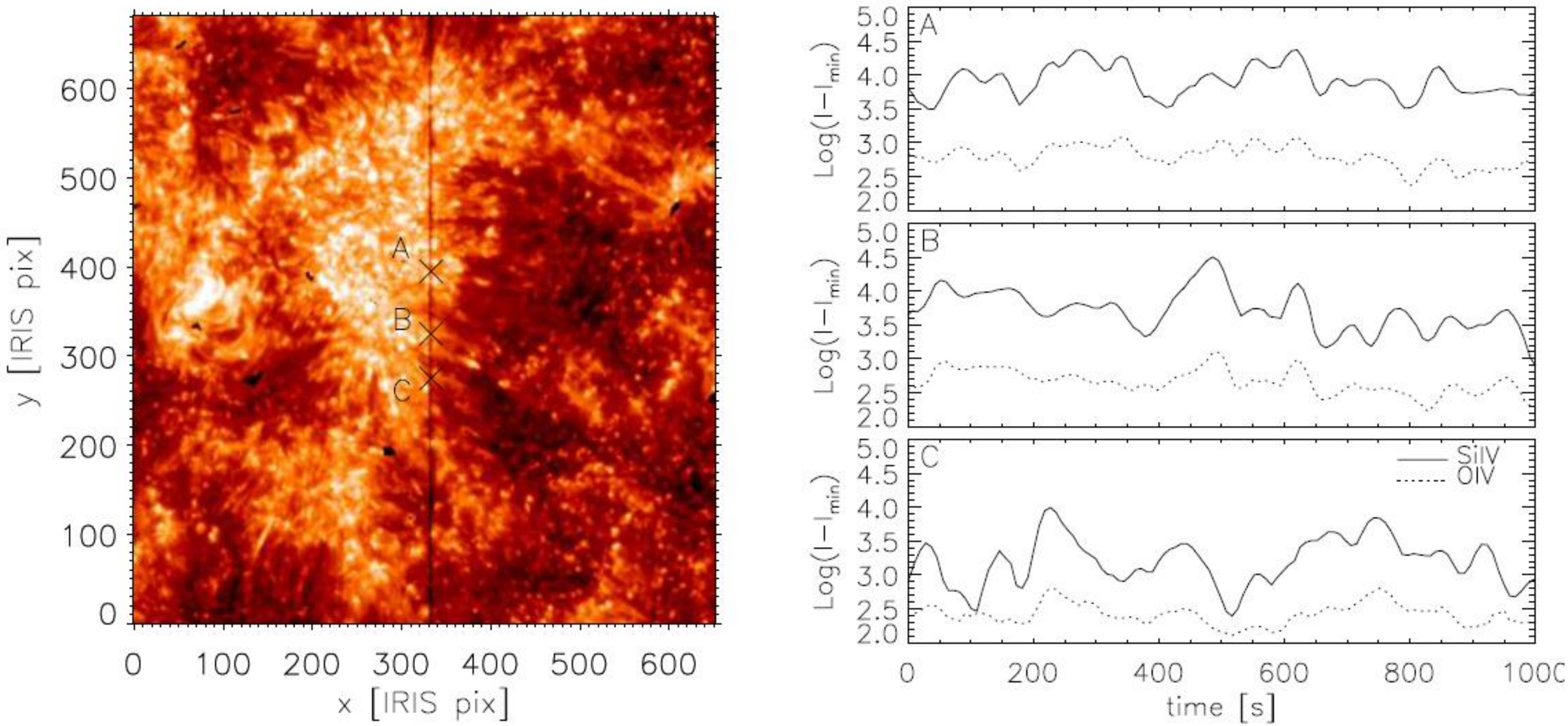

Bradshaw & Testa 2015, IRIS-4 talk

- Plage at the base of fan loops
- Strong intensity enhancements of TR lines on short timescales
- Si IV enhanced more than O IV

The Case for Non-Equilibrium

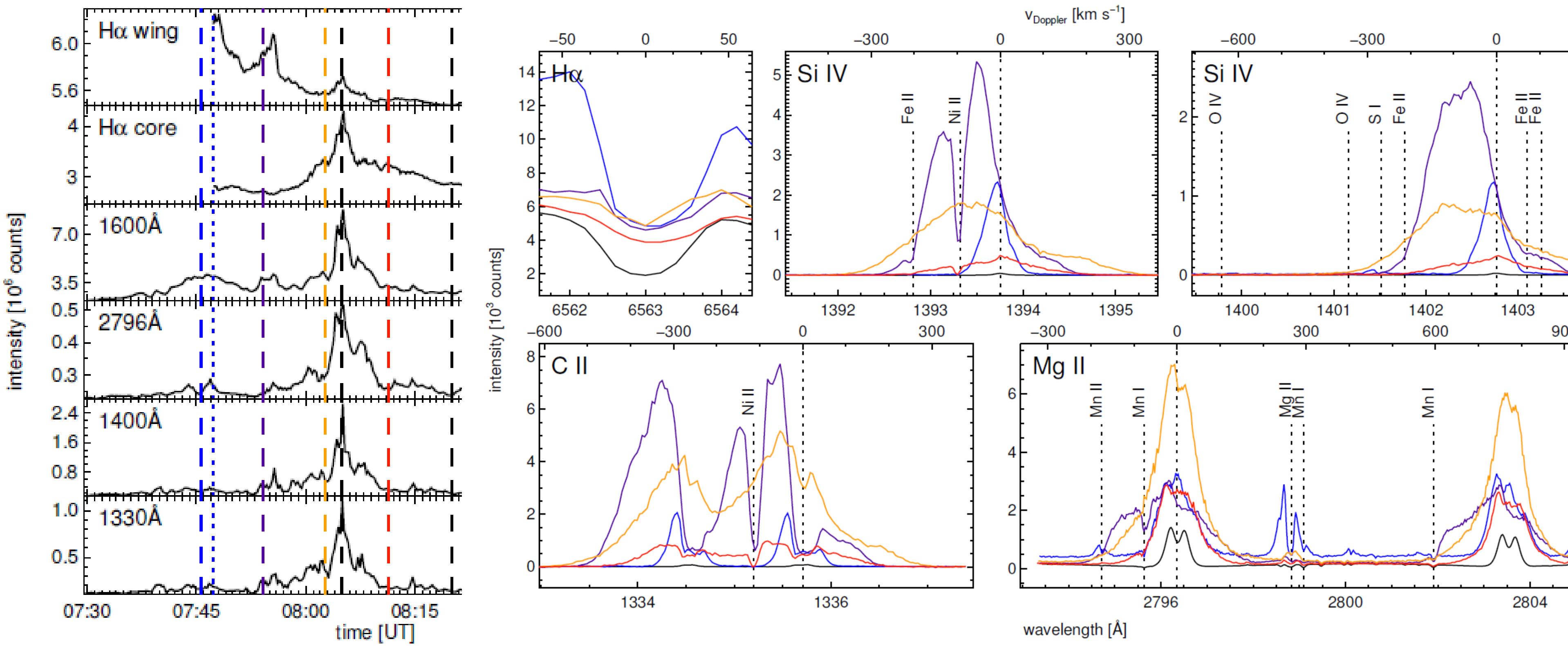

Vissers et al. 2015, ApJ, 812, 11

- **Flaring Arch Filaments (FAF): 1D bright filaments with AIA 171Å + 193Å**
- **Strong intensity enhancements of TR lines + blueshifts (flows!)**
- **Si IV profiles similar to C II profiles (+ blended by thin absorption lines)**

The Case for Non-Equilibrium

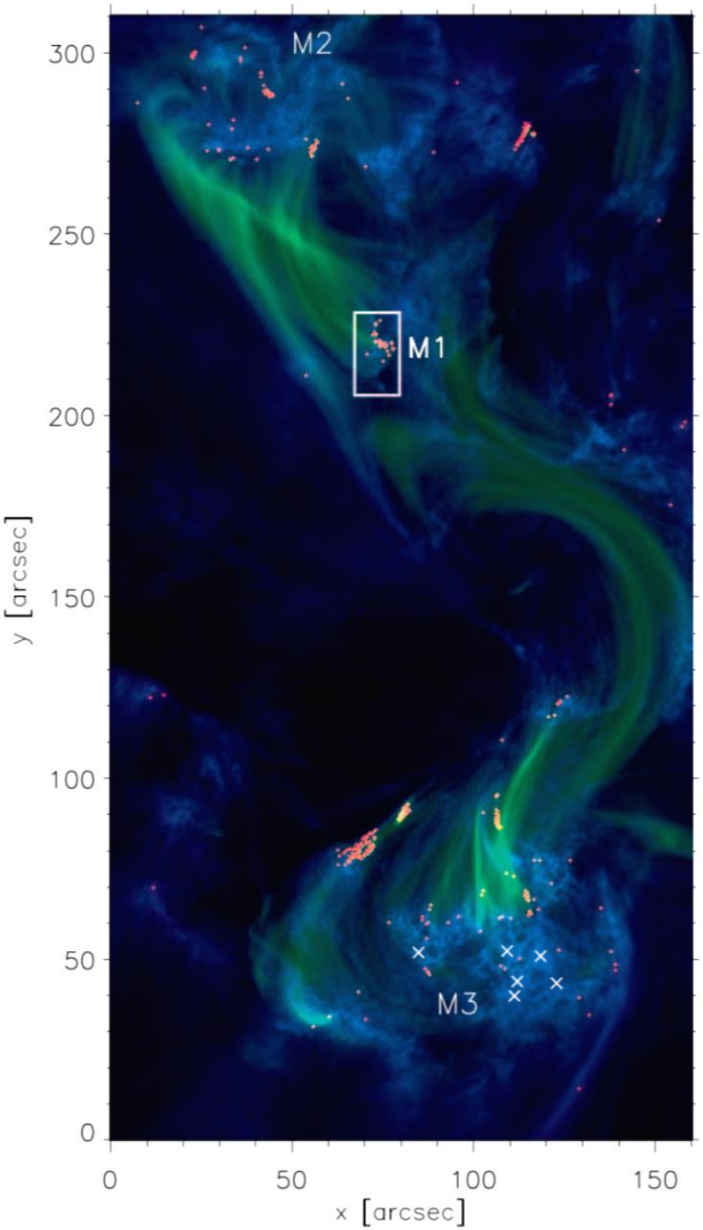

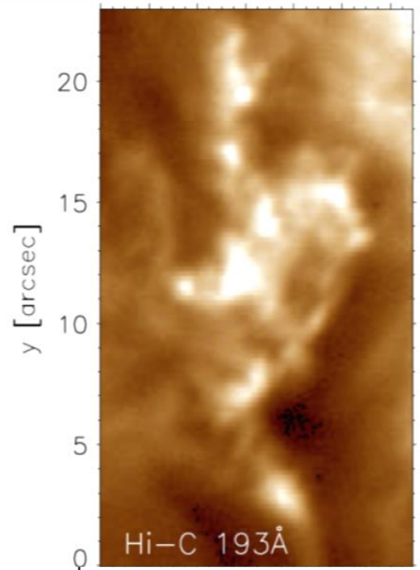

- Intensity enhancements at 193Å moss seen by Hi-C
- Footpoints of Fe XVIII loops
- Slipping **reconnection**
- **Variability down to 10s of seconds**

Testa et al. 2013, ApJ, 770, 1

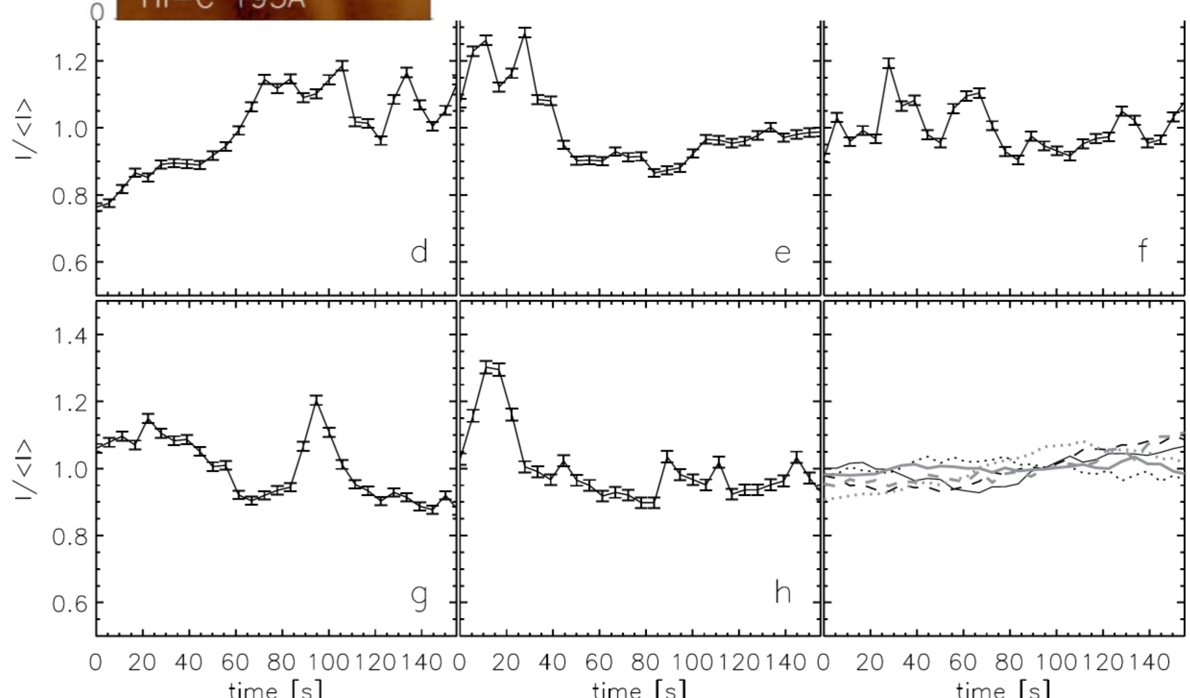

The Case for Non-Equilibrium

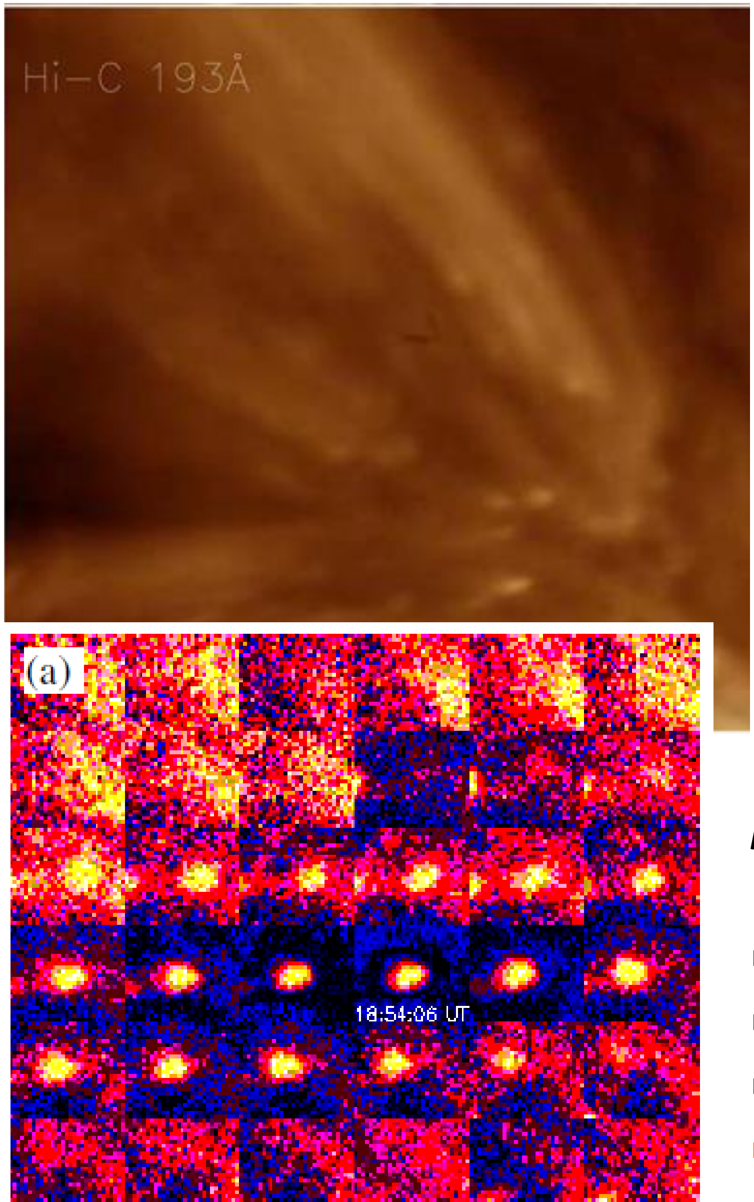

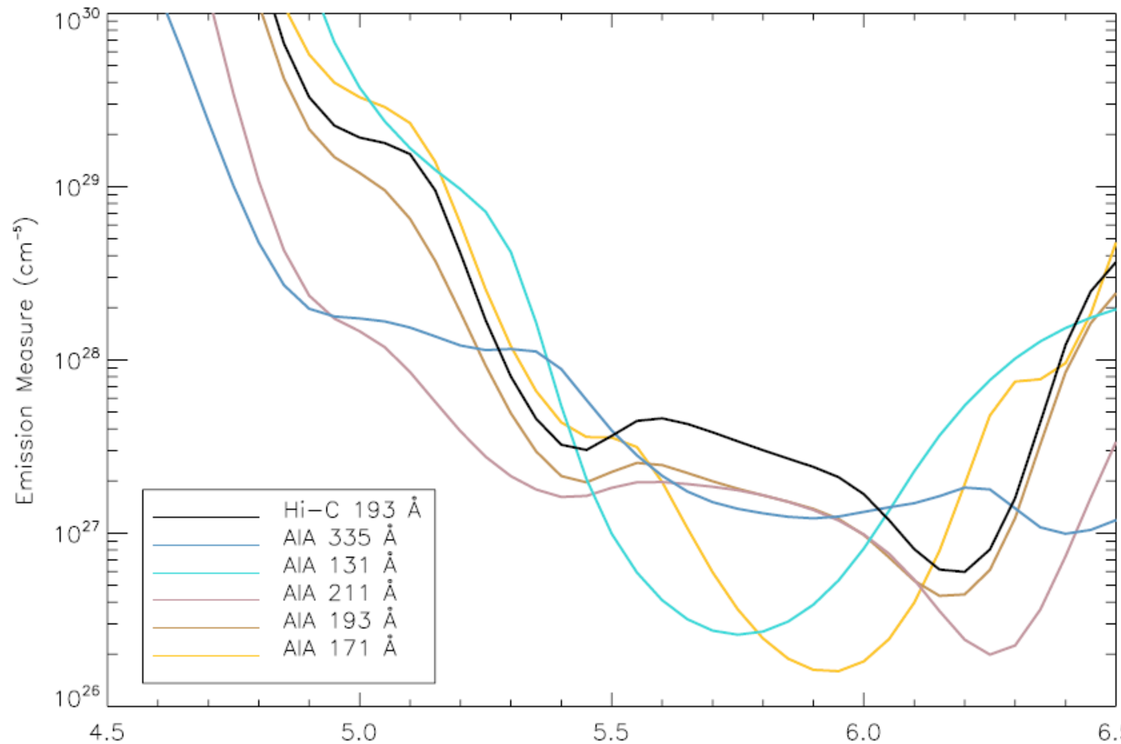

Régnier et al. 2014, ApJ, 784, 134

- **EUV bright dots seen by Hi-C**
- **At footpoints of 193Å open loops**
- **Likely at log(T/K) = 5.5**
- **Variability on 11-44 s**

Non-Equilibrium Ionization (NEI)

$$\frac{\partial Y_i}{\partial t} + \frac{\partial}{\partial s}(Y_i v) = n_e(I_{i-1}Y_{i-1} + R_i Y_{i+1} - I_i Y_i - R_{i-1}Y_i \ \ + \cdots)$$

e.g., Bradshaw & Mason (2003), A&A 401, 699

where

Y_i – population of ion +*i*

v – plasma velocity along *s* (1D loop)

I_i – total ionization rate of ion +*i*

R_i – total recombination rate of ion +*i*

If v = 0:

- **Coupled set of Z+1 first-order differential equations for Y_i**
- **Can be re-cast as Z uncoupled first-order diff eqs using eigenvector basis**
- **Solution is a set of Z separate exponential functions**
- **Ionization equilibration timescale is given by the smallest eigenvalue λ_j**

$$Y_i(t, T_e) - Y_{i,\mathrm{eq}}(T_e) = \sum_j W_{ji}(T_e) c_j \exp\left(-n_e \lambda_j t\right)$$

Smith & Hughes (2010), ApJ, 718, 583

see also Golub et al. (1989), SoPh 122, 145; Reale & Orlando (2008), ApJ 684, 715

NEI: Timescales

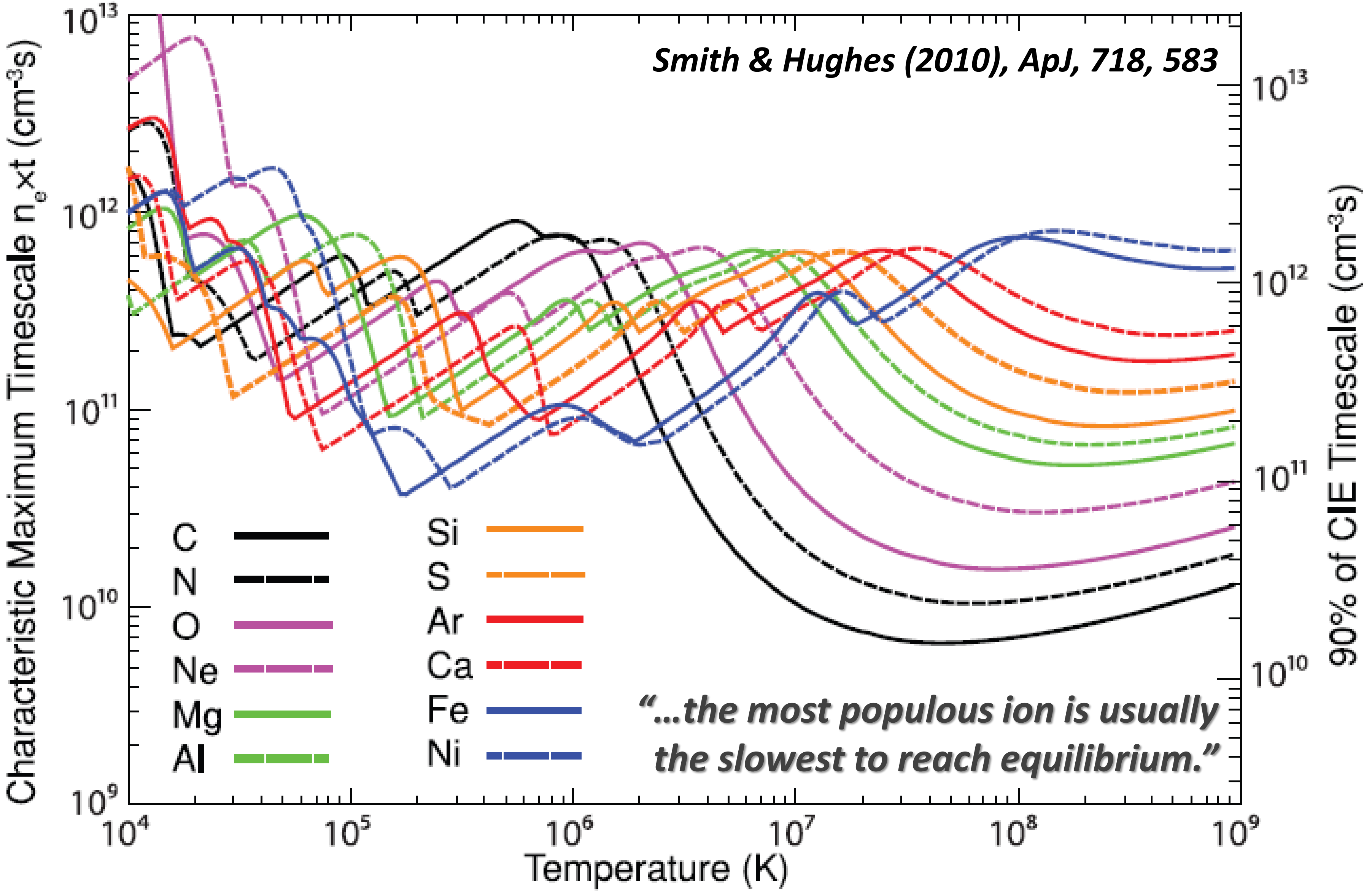

Effect on Line Contribution Function

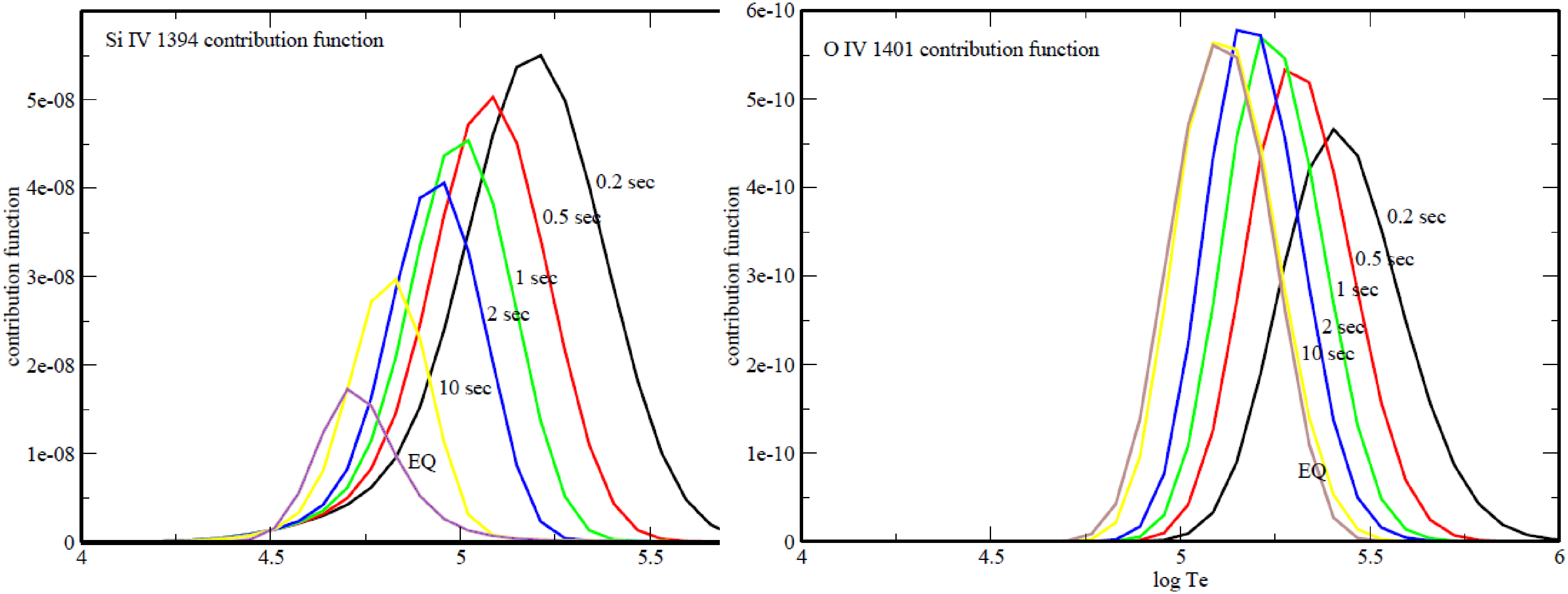

Doyle et al. (2013), A&A, 557, 9

- **At log(n_e) = 10, Si IV takes ≈100 s to reach equil.; O IV only ≈10 s**
- **For short bursts (less than 2 s), Si IV produces intensity enhancement of a factor of 3 compared to O IV**
- **This is due to the cross-section behavior with *E* (Si IV are allowed line, O IV intercombination lines)**

Non-Equilibrium Ionization (NEI)

$$\frac{\partial Y_i}{\partial t} + \frac{\partial}{\partial s}(Y_i v) = n_e(I_{i-1}Y_{i-1} + R_i Y_{i+1} - I_i Y_i - R_{i-1} Y_i \ + \cdots)$$

Bradshaw & Mason (2003), A&A 401, 699
A&A 407, 1127

If *v* ≠ 0:

- **Ionization fraction becomes coupled to (M)HD equations via *v***
- **Evolution of T_e becomes dependent on heating and radiative losses**
- **Radiation is dependent on ionization fractions**
- **Self-consistent loop modeling required (e.g., HYDRAD code)**

- **Rapid heating: ionizing plasma**
- **Rapid cooling: recombining plasma**
- **Plasma temperature derived from ion population *may be incorrect***

Raymond & Dupree (1978)
Noci et al. (1989)
Spadaro et al. (1990)

Hansteen (1993)
Spadaro et al. (1994)
Edgar & Esser (2000)

NEI: Influence on line intensities

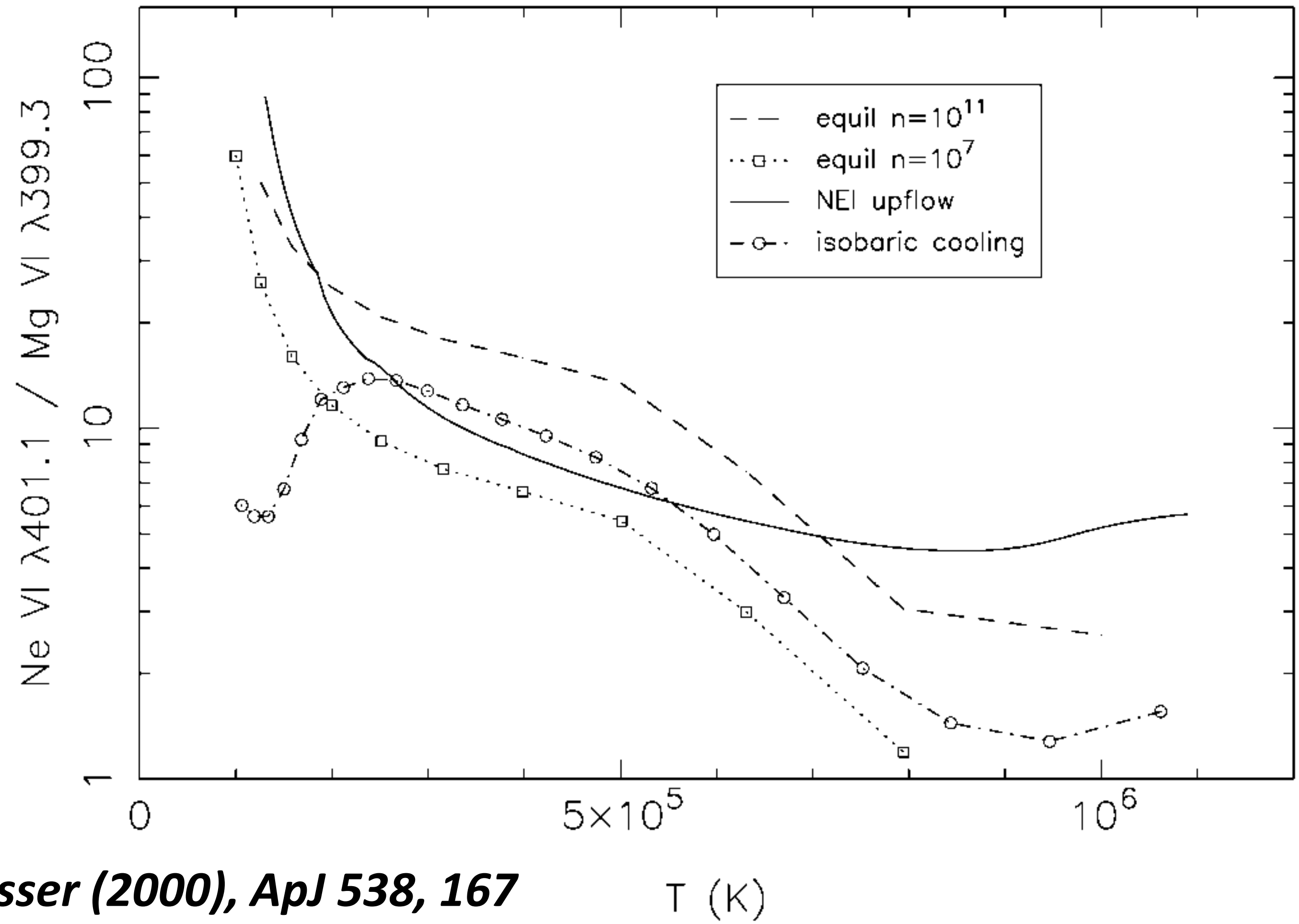

Edgar & Esser (2000), ApJ 538, 167

Calculation of Ne VI / Mg VI line intensity ratio

- **In equilibrium, Ne VI and Mg VI have similar contribution functions**
- **Sensitive to densities & assumed flows: NEI for solar wind upflow in TR**

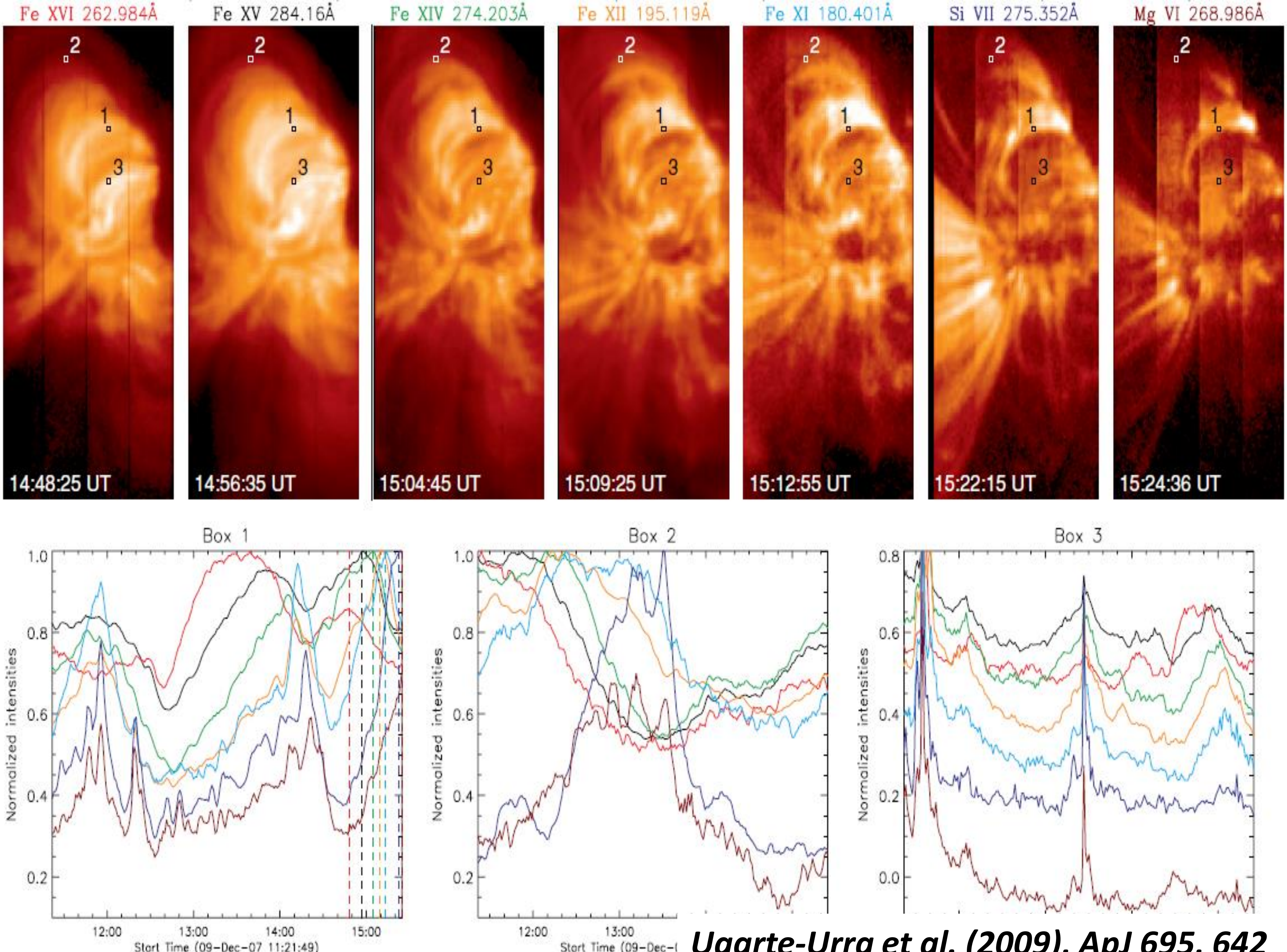

Ugarte-Urra et al. (2009), ApJ 695, 642

NEI: 1D Cooling Loop

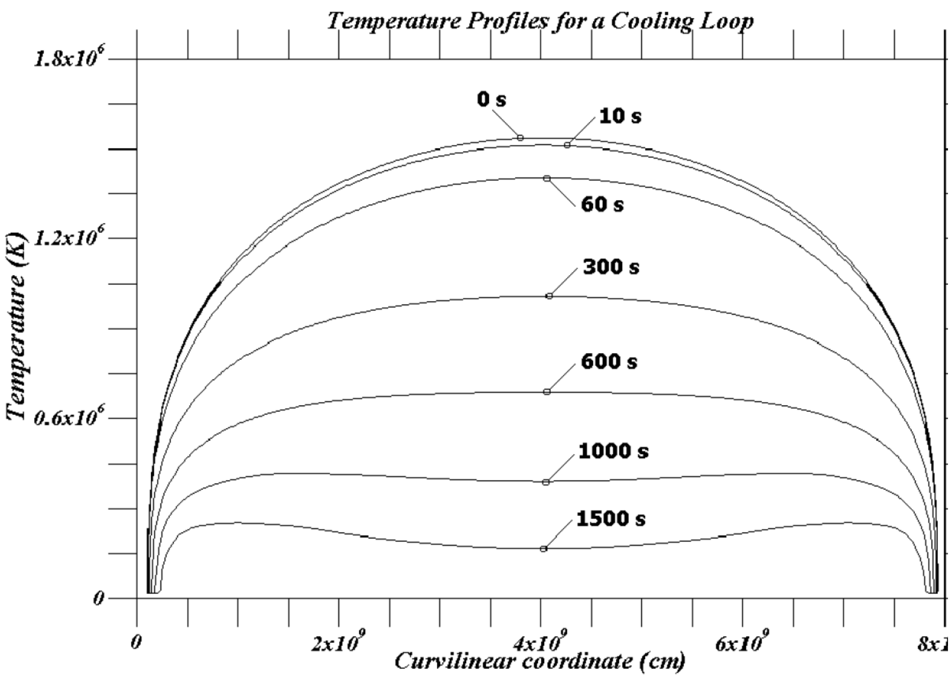

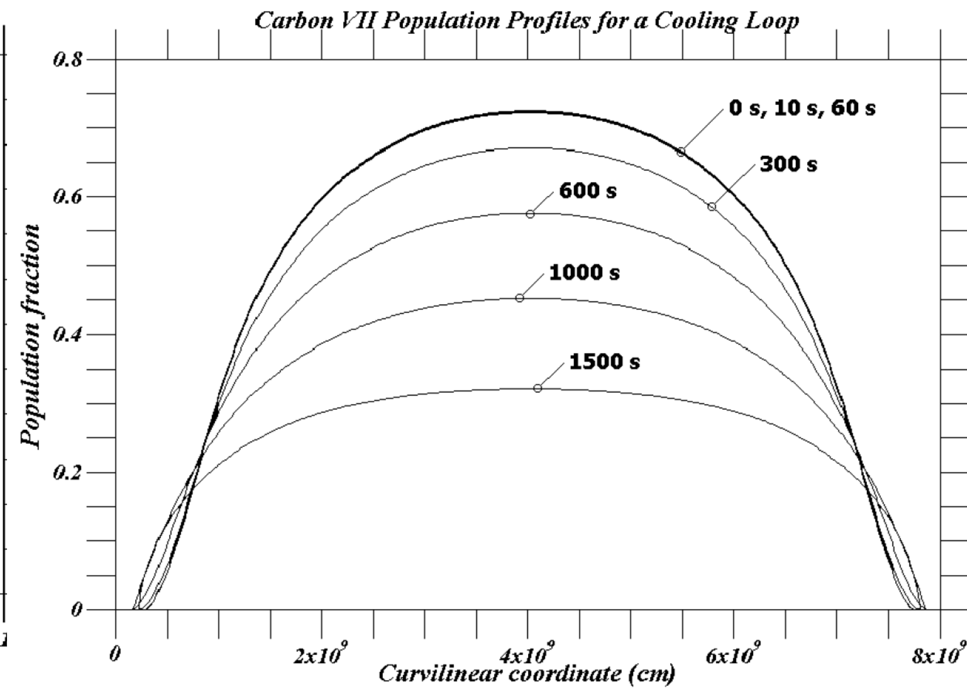

Bradshaw & Mason (2003), A&A 401, 699

Simulation of a cooling warm coronal loop with non-equilibrium ionization

- C VII formed at ≈1.5 MK in equilibrium
- C VII population in places where there should be none in equilibrium (low *T*)
- Recombination timescale for C VII at model densities: ≈ 2000 s
- Downflows from loop top carrying C VII to lower parts of the loop
- Emissivity differences of up to a factor of 3: loop cools more slowly than in eq

NEI: Coronal Heating at Loop Apex

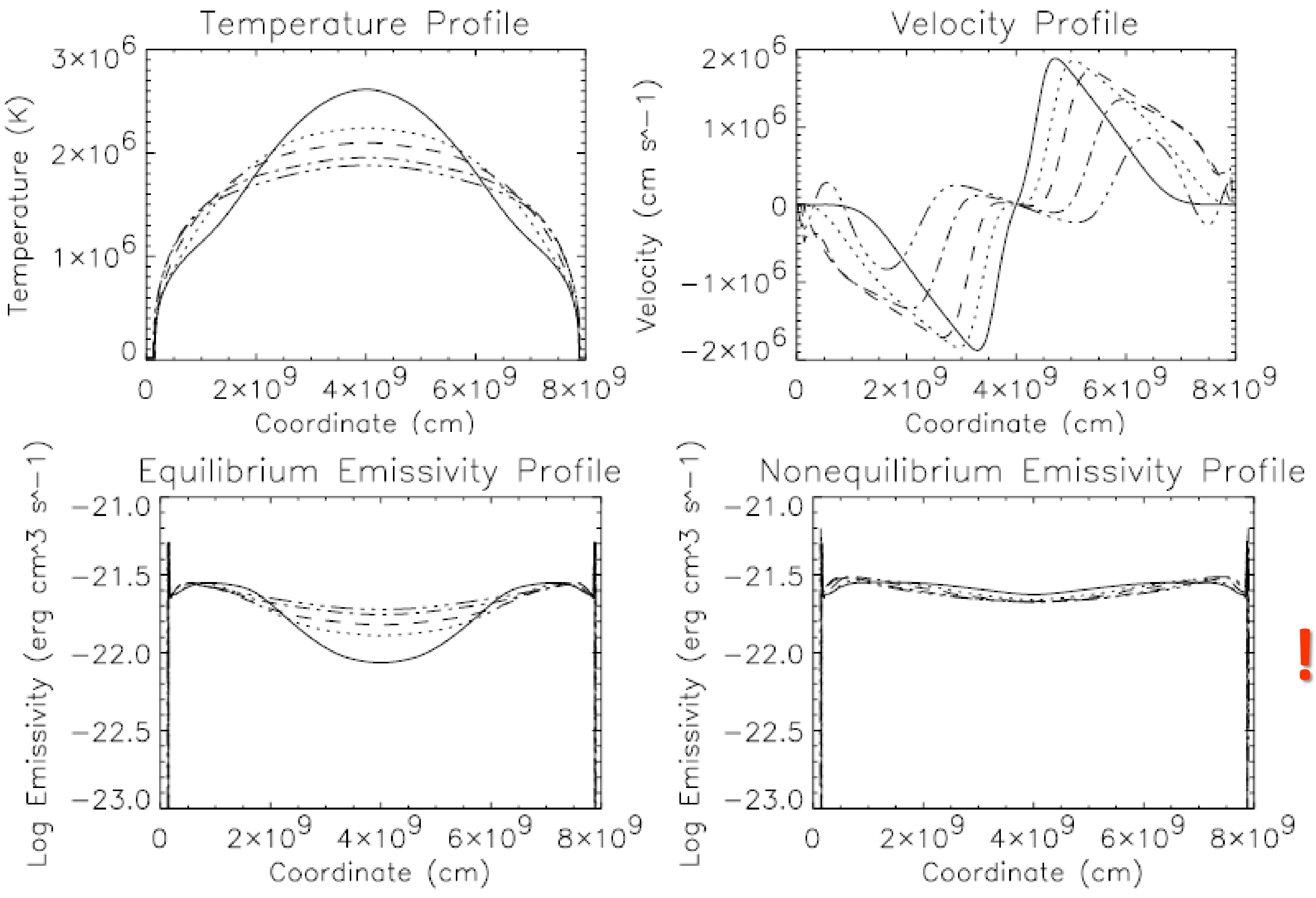

Bradshaw & Mason (2003), A&A 407, 1127

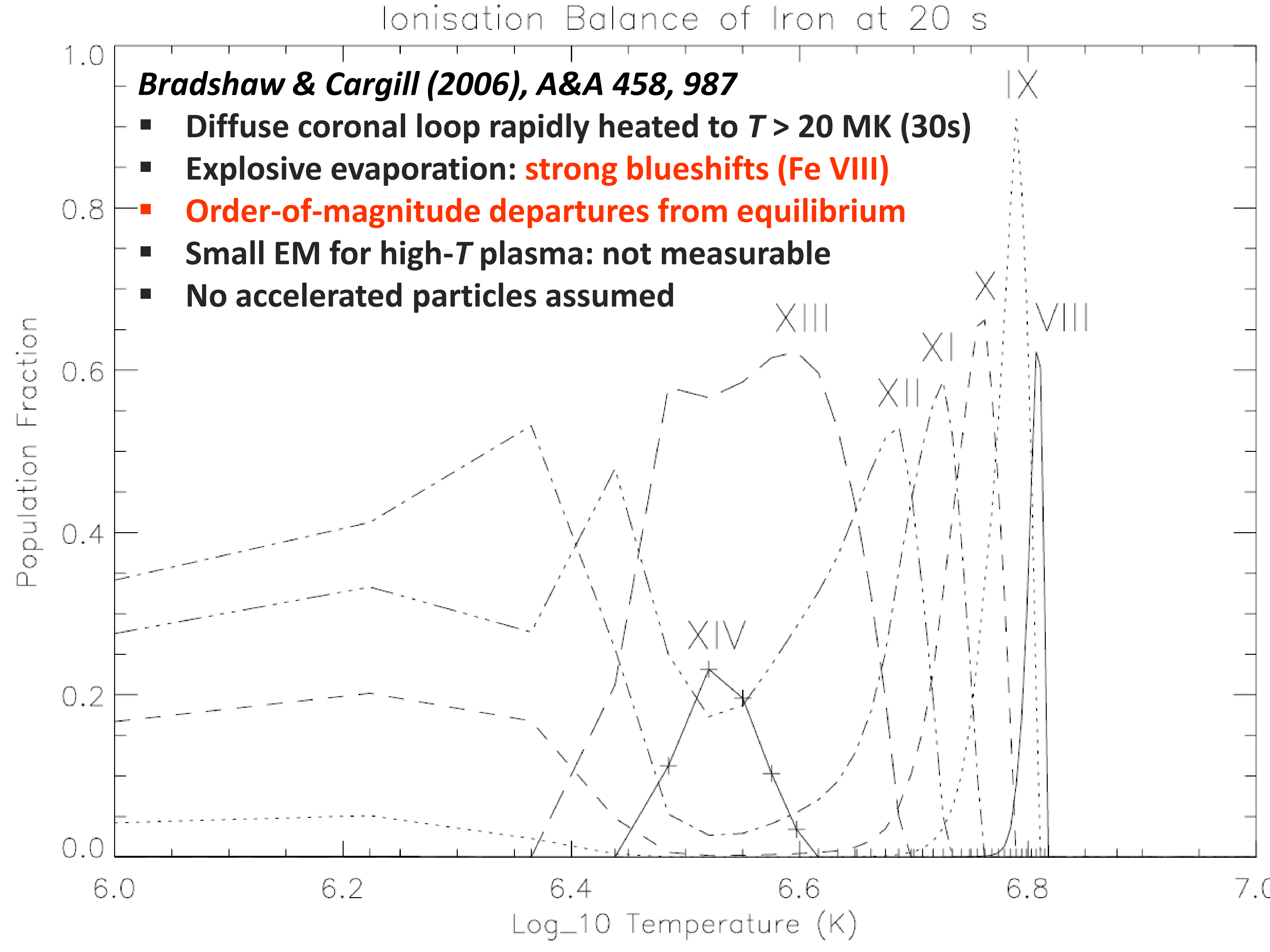
Ionisation Balance of Iron at 20 s
Bradshaw & Cargill (2006), A&A 458, 987
Diffuse coronal loop rapidly heated to T > 20 MK (30s)
Explosive evaporation: strong blueshifts (Fe VIII)
Order-of-magnitude departures from equilibrium
Small EM for high-T plasma: not measurable
No accelerated particles assumed
IX
X
VIII
XIII
XI
XII
XIV
Population Fraction
1.0
0.8
0.6
0.4
0.2
0.0
6.0
6.2
6.4
6.6
6.8
7.0
Log_10 Temperature (K)

NEI: Nanoflare Heating

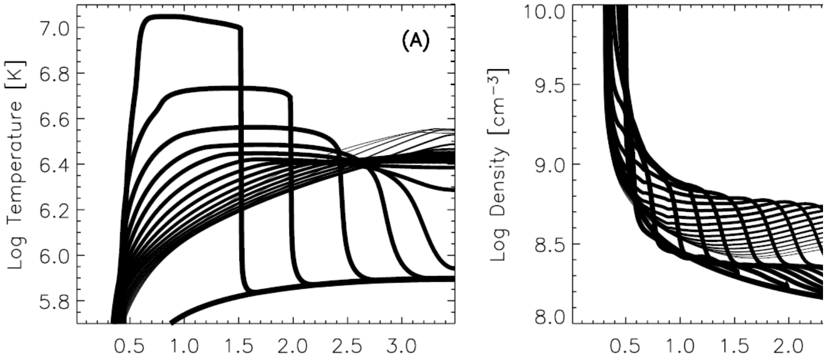

Reale & Orlando (2008), ApJ 684, 715

- **Single heating pulse**
- **Hot plasma not detectable if nanoflare durations < 1 min**

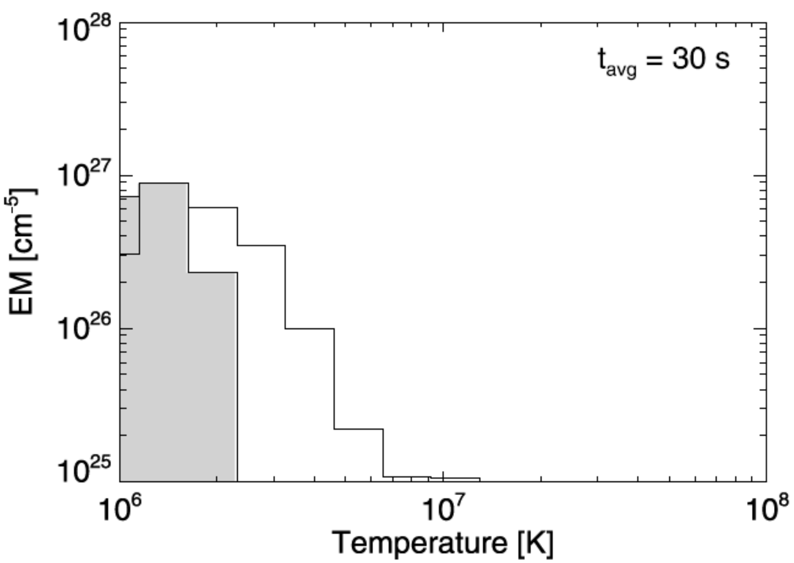

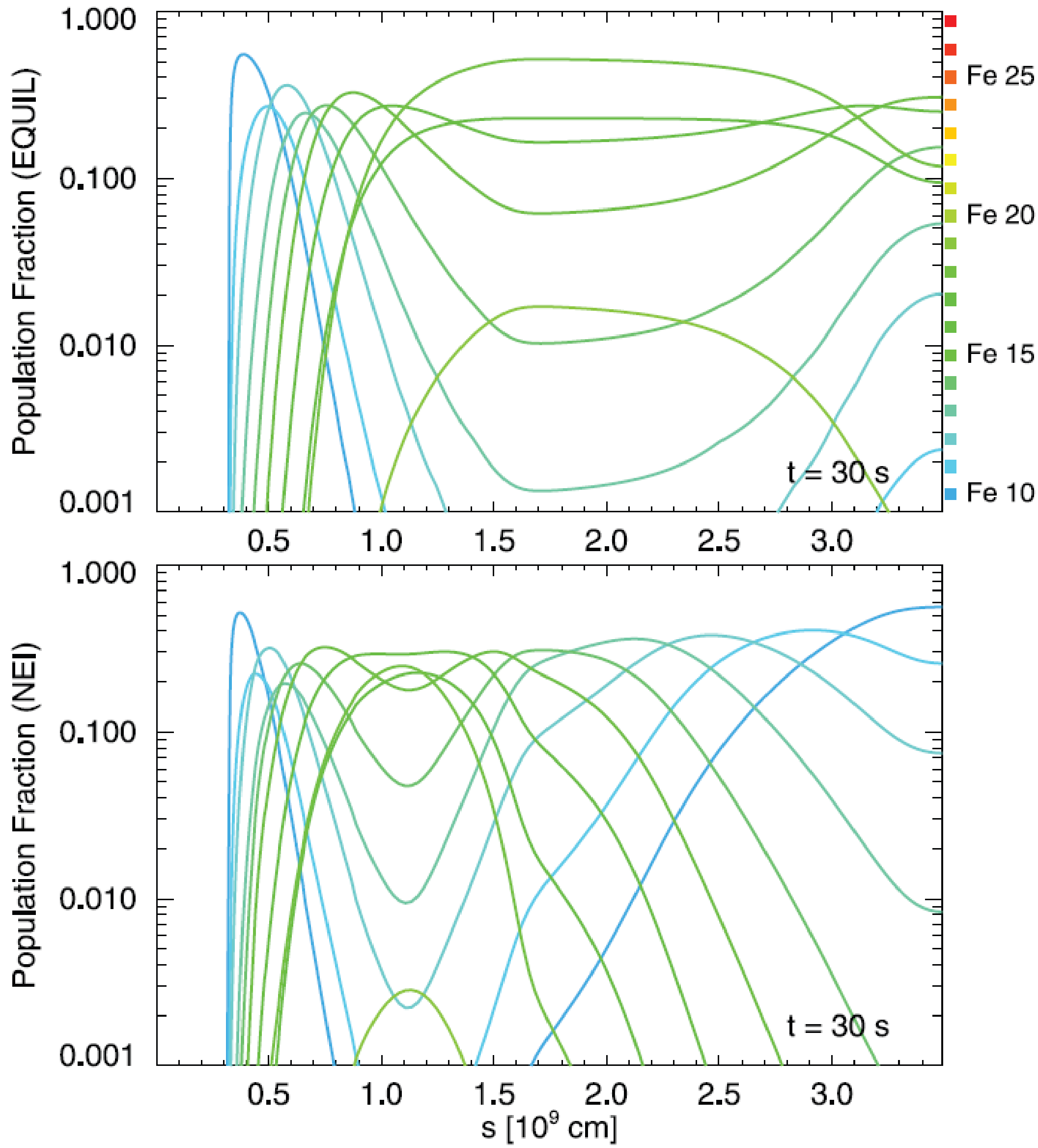

NEI: Nanoflare storm

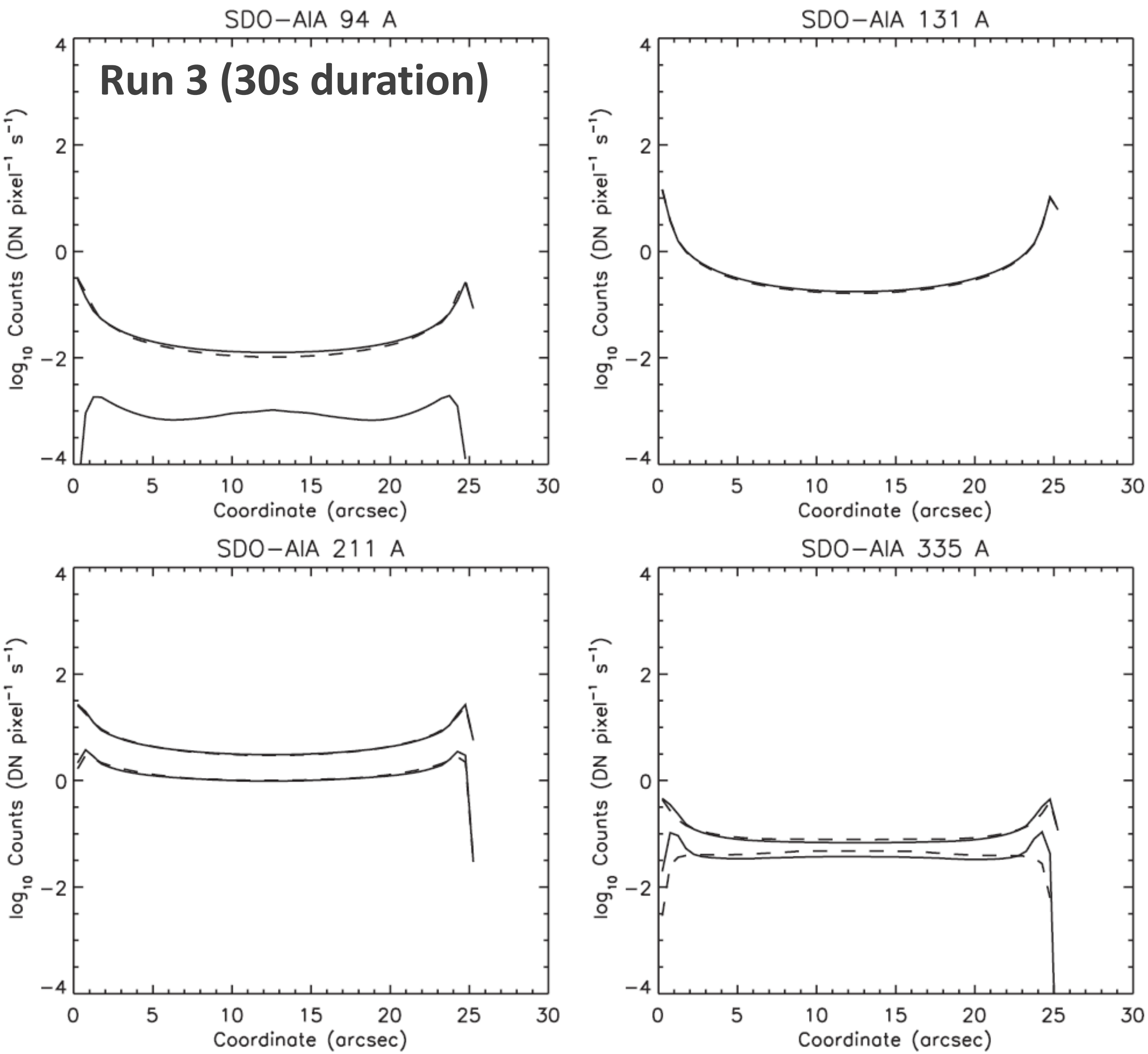

Bradshaw & Klimchuk (2011), ApJ 194

- Each strand heated separately (storm), complete cycle
- Hot plasma present, but AIA channels dominated by warm plasma near equil
- Difficult not to create loops at 1.5 – 6 MK
- Cooler lines formed long after nanoflare
- Longer heating create 1% hot 131Å emission
- Hot emission is still out of equilibrium

Side Note: Blind Spots

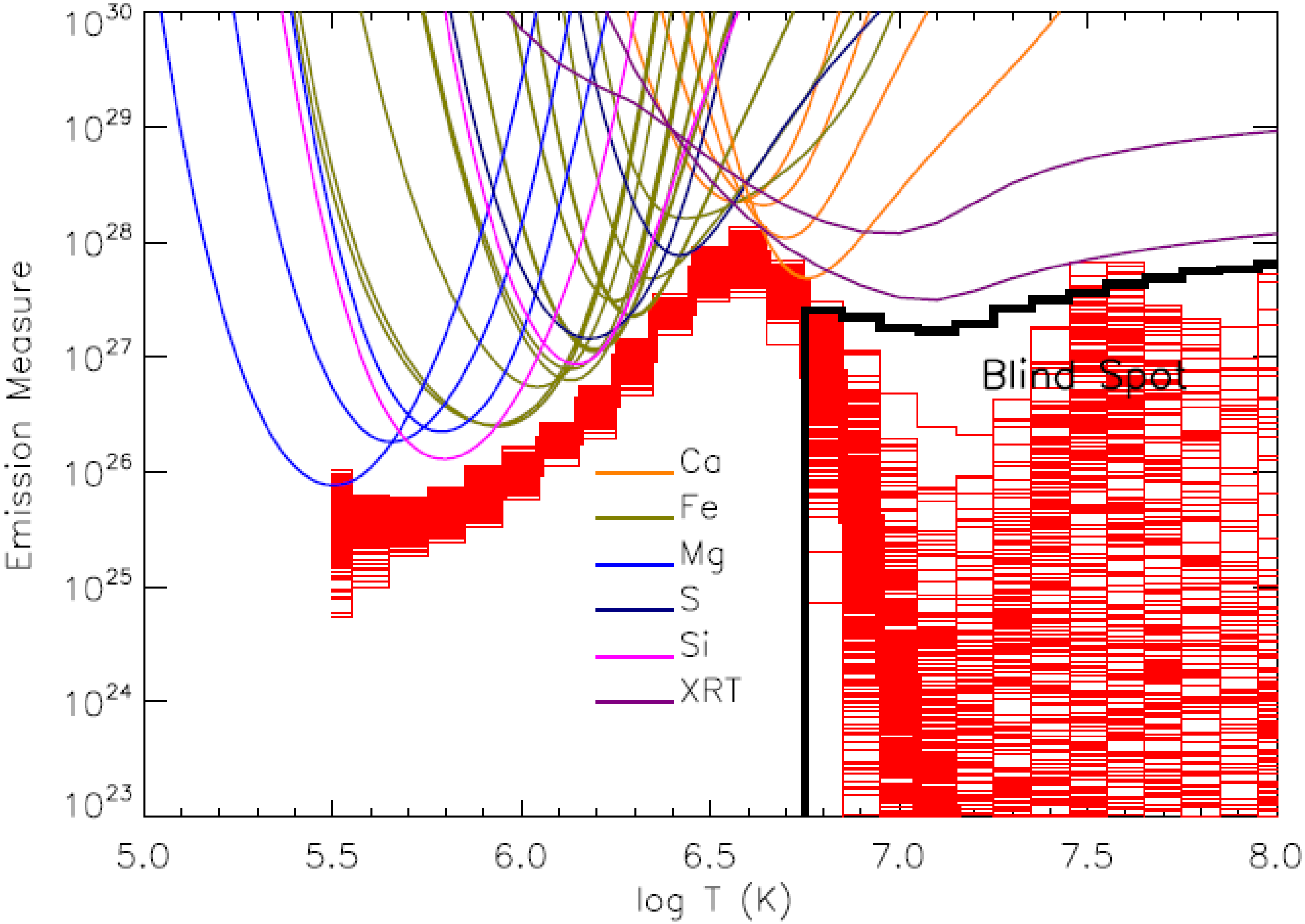

Winebarger et al. (2012), ApJ 746, 17

NEI in 3D: Bifrost

$$\frac{\partial Y_i}{\partial t} + \frac{\partial}{\partial s}(Y_i v) = n_\mathrm{e}(I_{i-1}Y_{i-1} + R_i Y_{i+1} - I_i Y_i - R_{i-1} Y_i \quad + \cdots)$$

↓

$$\frac{\partial n_k}{\partial t} + \vec{\nabla}.(n_k \vec{v}) = \sum_{j \neq k}^{N_l} n_j P_{jk} - n_k \sum_{j \neq k}^{N_l} P_{kj}$$

Olluri et al. (2013), AJ 145, 72

where

n_k – population density of ion level k

P_{jk} – transition rate coefficient $j \rightarrow k$

- **DIPER atomic package**
- **Fully 3D, solution uses operator splitting**
- **Levels are excitation or ionization levels, P_{jk} are radiative or collisional**
- **Assumes only a few levels for each atom: 12 for Si, 14 for O, 20 for Fe X–XV**
- **Optically thin atomosphere, otherwise global coupling & radiative transfer**

NEI in 3D: Bifrost

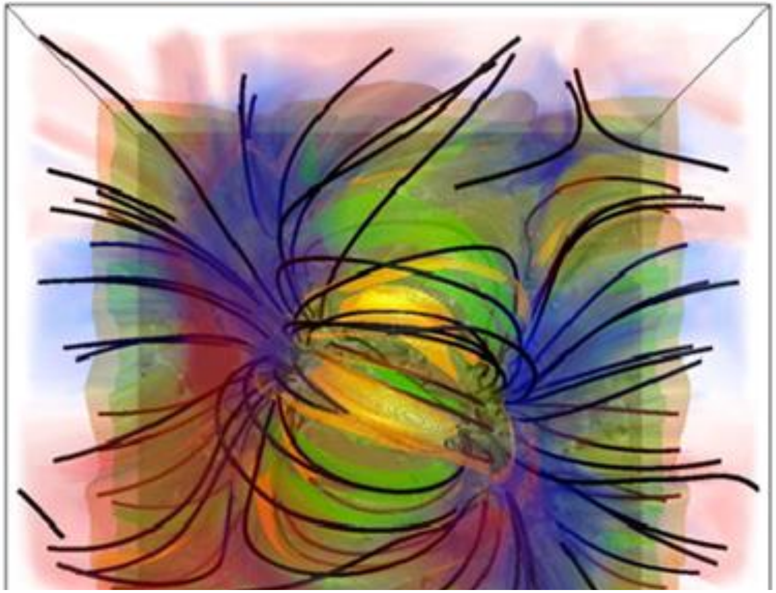

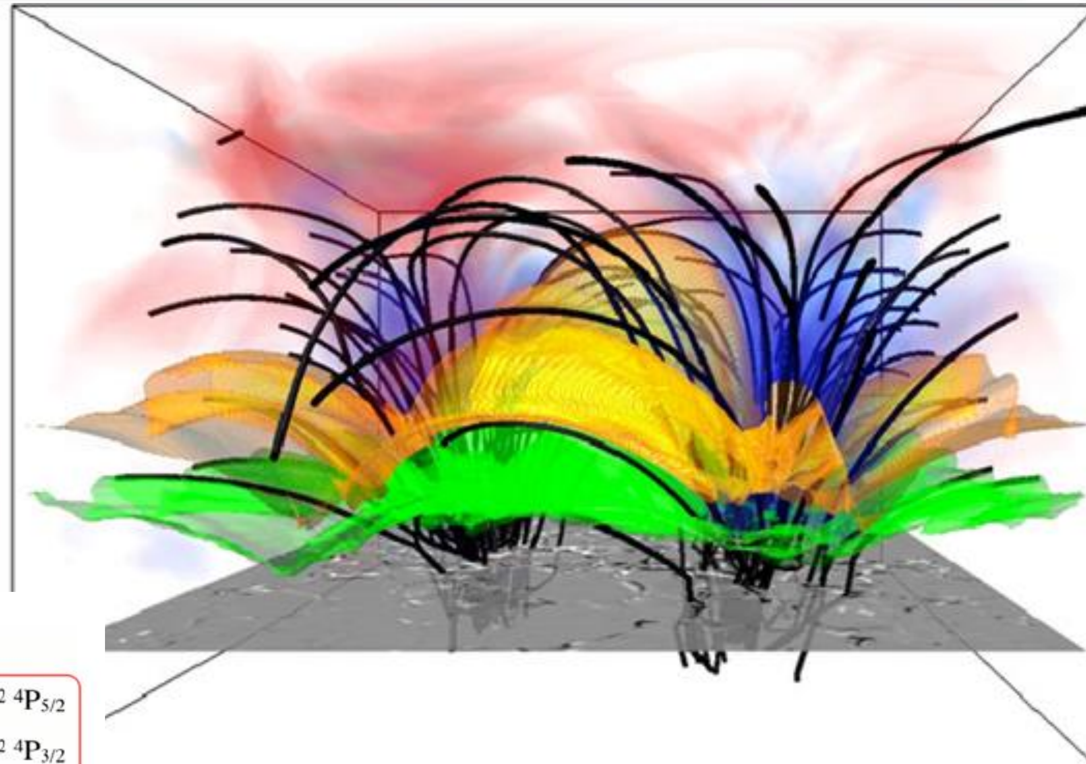

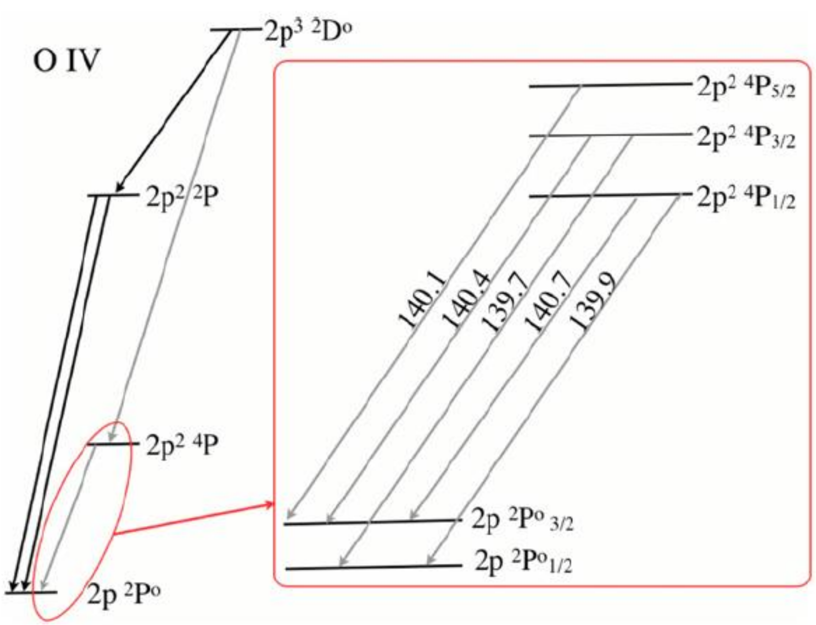

Gudiksen et al. (2011), A&A 531, A154
Olluri et al. (2013), ApJ 767, 43
Olluri et al. (2015), ApJ 802, 5

- Bifrost: 3D model of a quiet Sun
- 24 x 24 x 16 Mm^3, 48 G mean phot. field
- Coronal heating by many dissipation events
- Green & Yellow: 10^5 K & 10^6 K isosurfaces

NEI in 3D: Oxygen in Bifrost

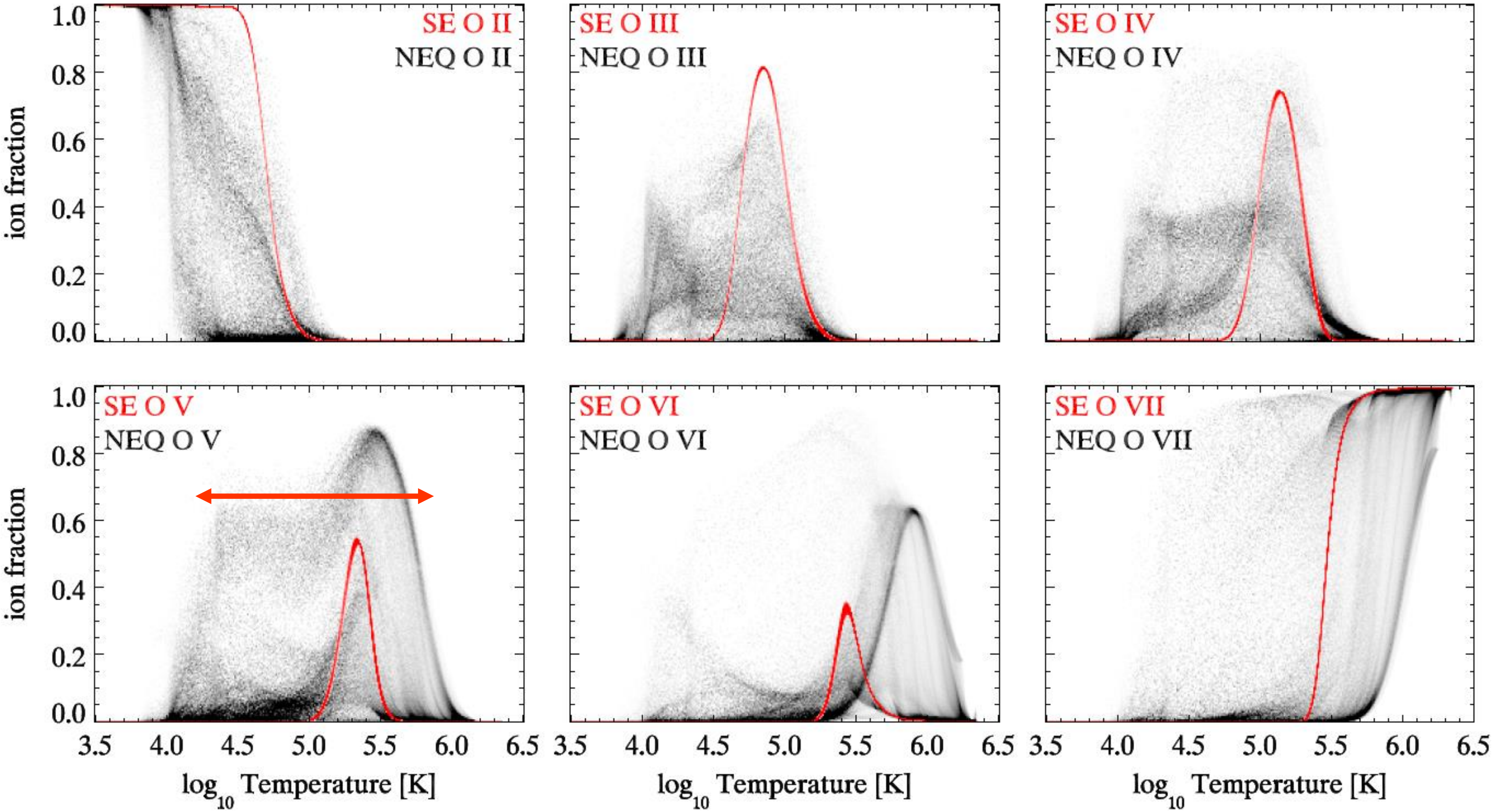

Olluri et al. (2013), ApJ 767, 43

- **Ions formed at wider range of temperatures than in equilibrium (CIE/SE)**
- **Advection, long recombination times (O III – IV), long ionization times (O V)**

Density Diagnostics (in Eq.)

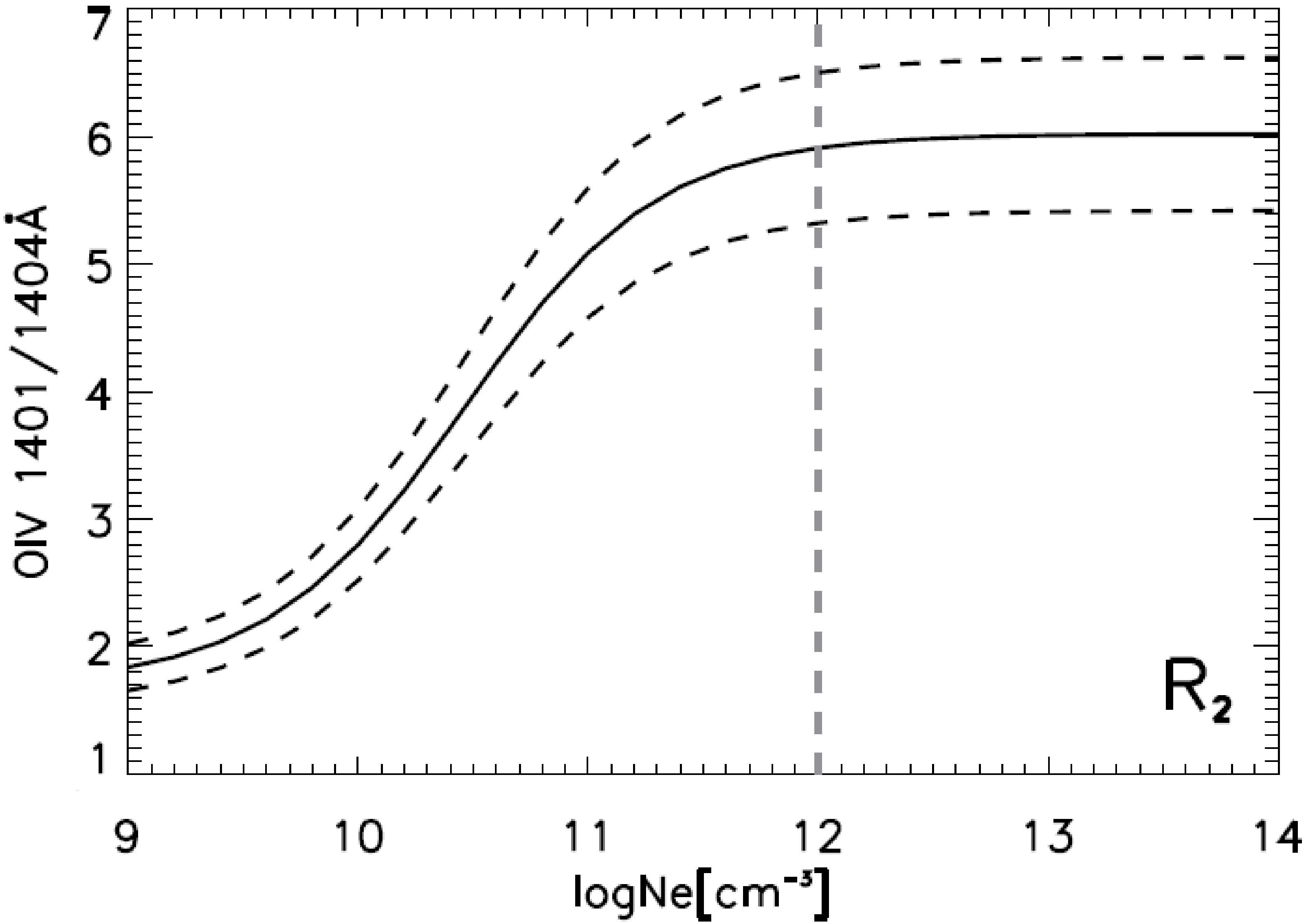

NEI in 3D: O IV diagnostics

Olluri et al. (2013), ApJ 767, 43

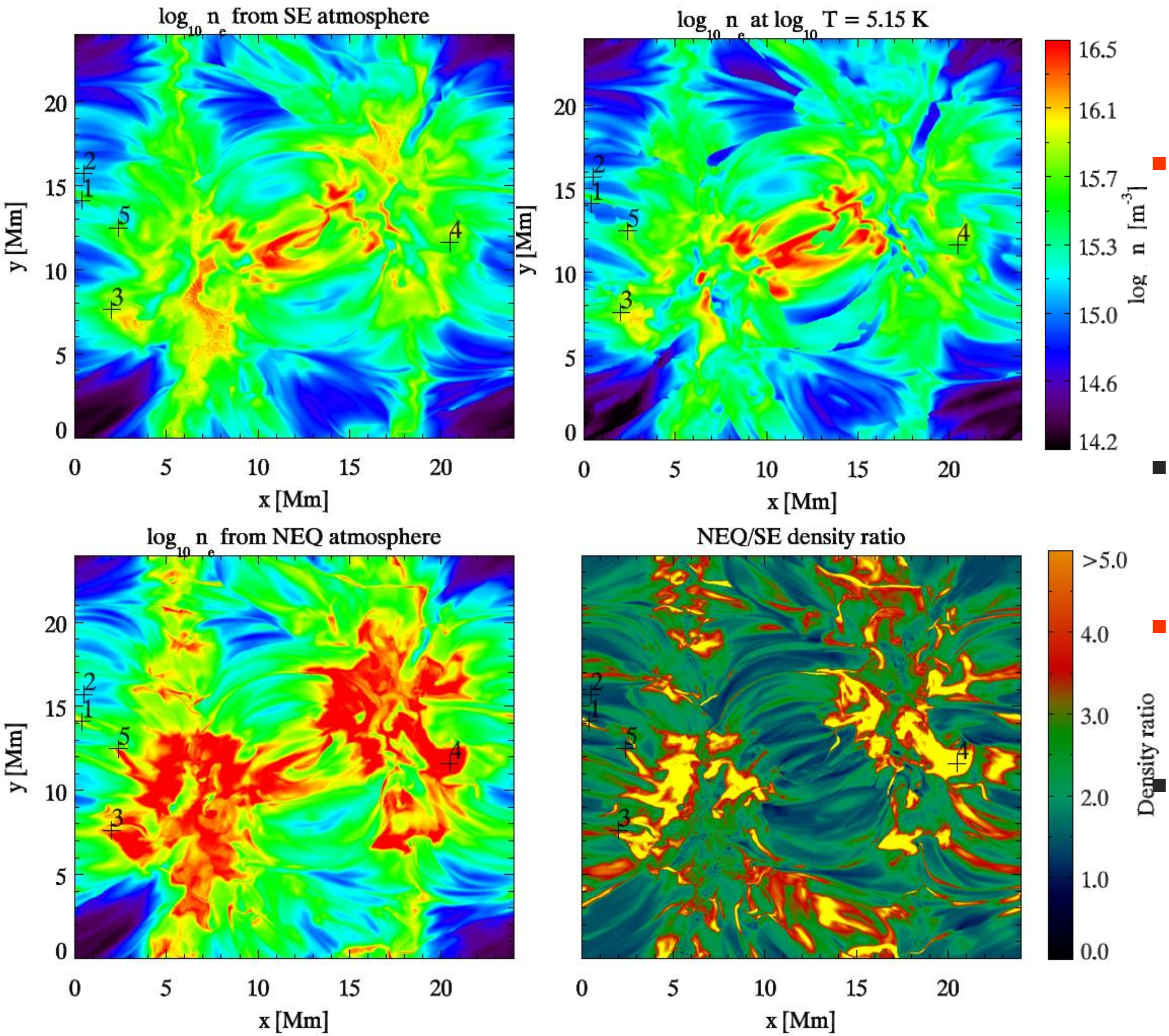

- *n_e* **diagnosed from NEI atmosphere** using line ratio technique is **very different from the *n_e* in the simulation**
- Because O IV is formed at lower *T* in NEI
- ***Line ratio is of limited use in NEI atmospheres***
- LOS effects: Deduced **n_e is a mean weighted by NEI emissivities** and is not related to *T*

Summary: NEI

NEI is important for dynamic phenomena

Long timescales for equilibration: Something, somewhere will be NEI

The advection term is important

Need for (M)HD models

Advection / flows contribute to ions existing in wider range of *T*

Emissivities are significantly affected

Short, bursty heating may not produce enough hot plasma especially if the heating recurs only after significant cooling

Plasma diagnostics using standard techniques could be affected and/or sometimes useless

We may measure densities in places where most of the emission originates independently of the respective equilibrium temperatures

The case for non-Maxwellians

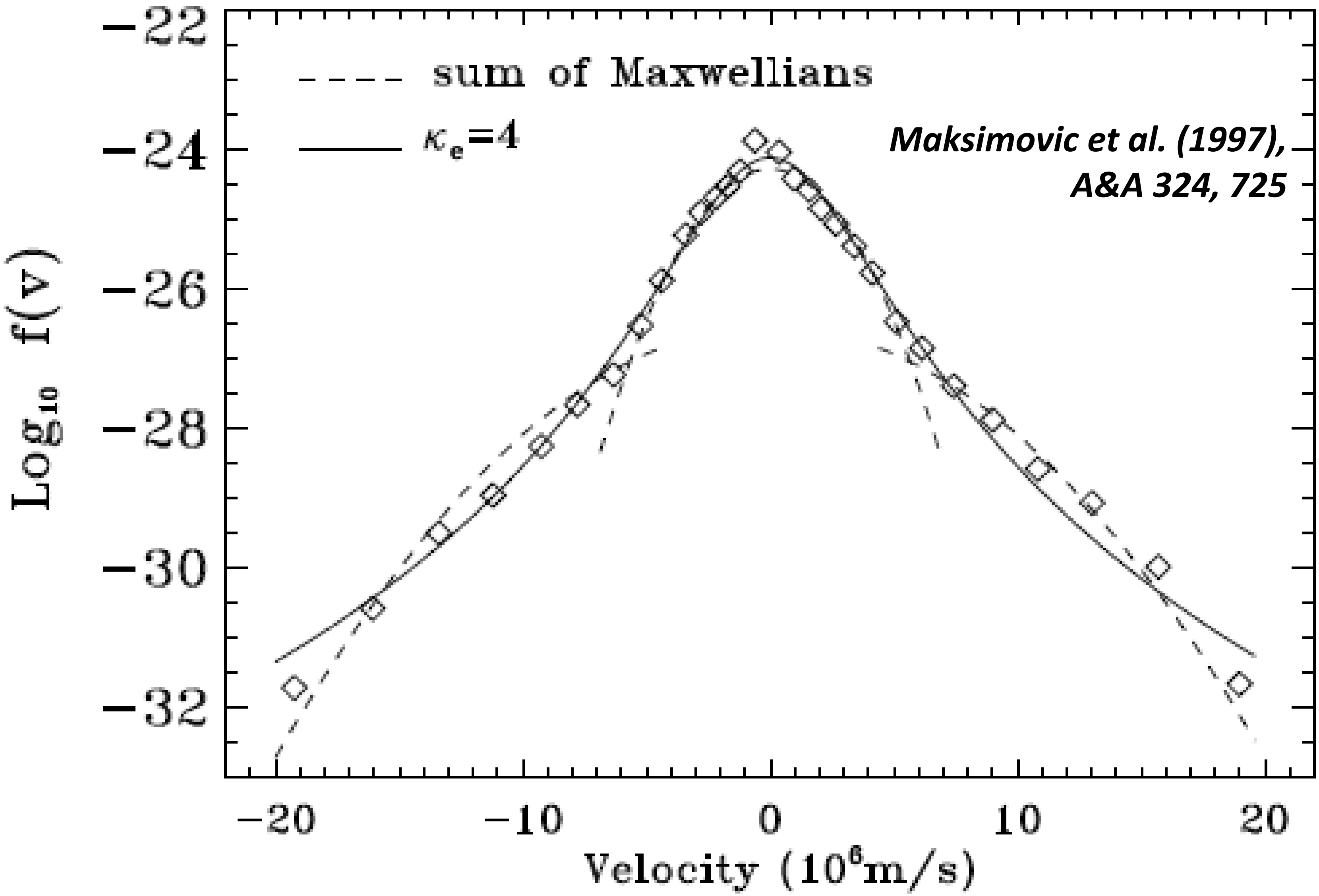

- Solar wind is non-Maxwellian

RHESSI + AIA: Constraints on *F*(*E*)

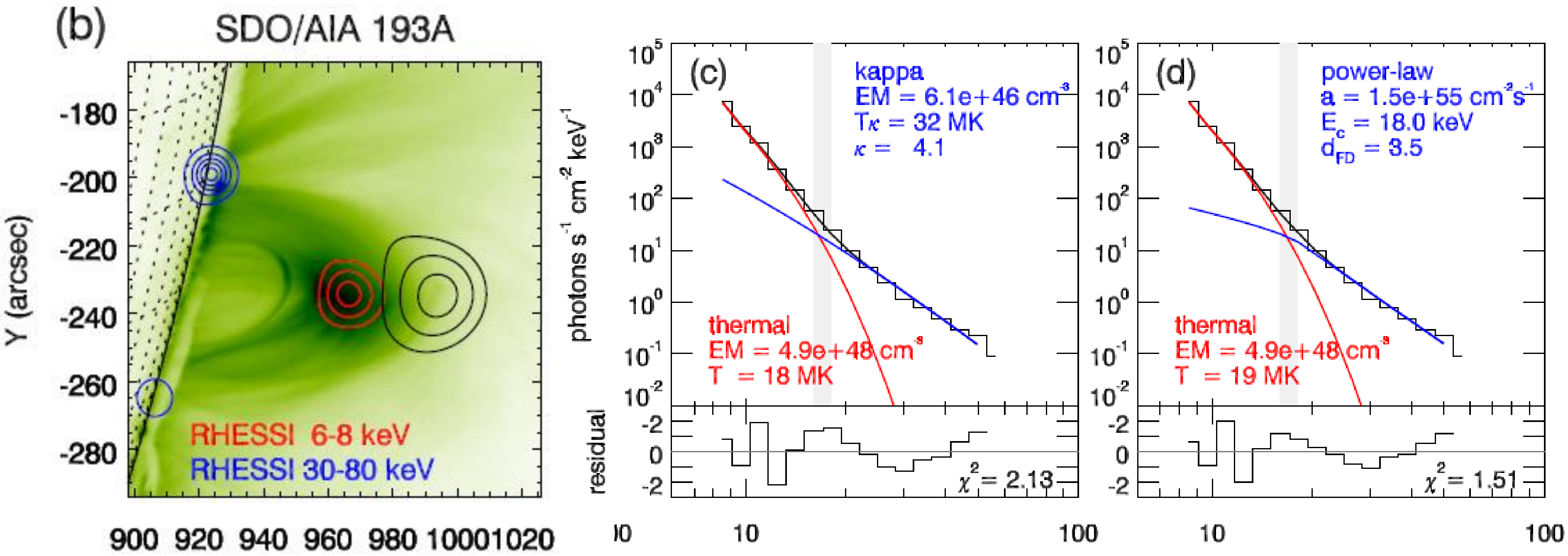

Oka et al. (2015), ApJ, 799, 195

- Analyzed several flares observed simultaneously by RHESSI and AIA
- High-energy tail observed by RHESSI fitted by a variety of models:
  - power-law tail
  - thermal + power-law
  - kappa-distribution

The case for non-Maxwellians

Oka et al. (2013) ApJ 764, 6

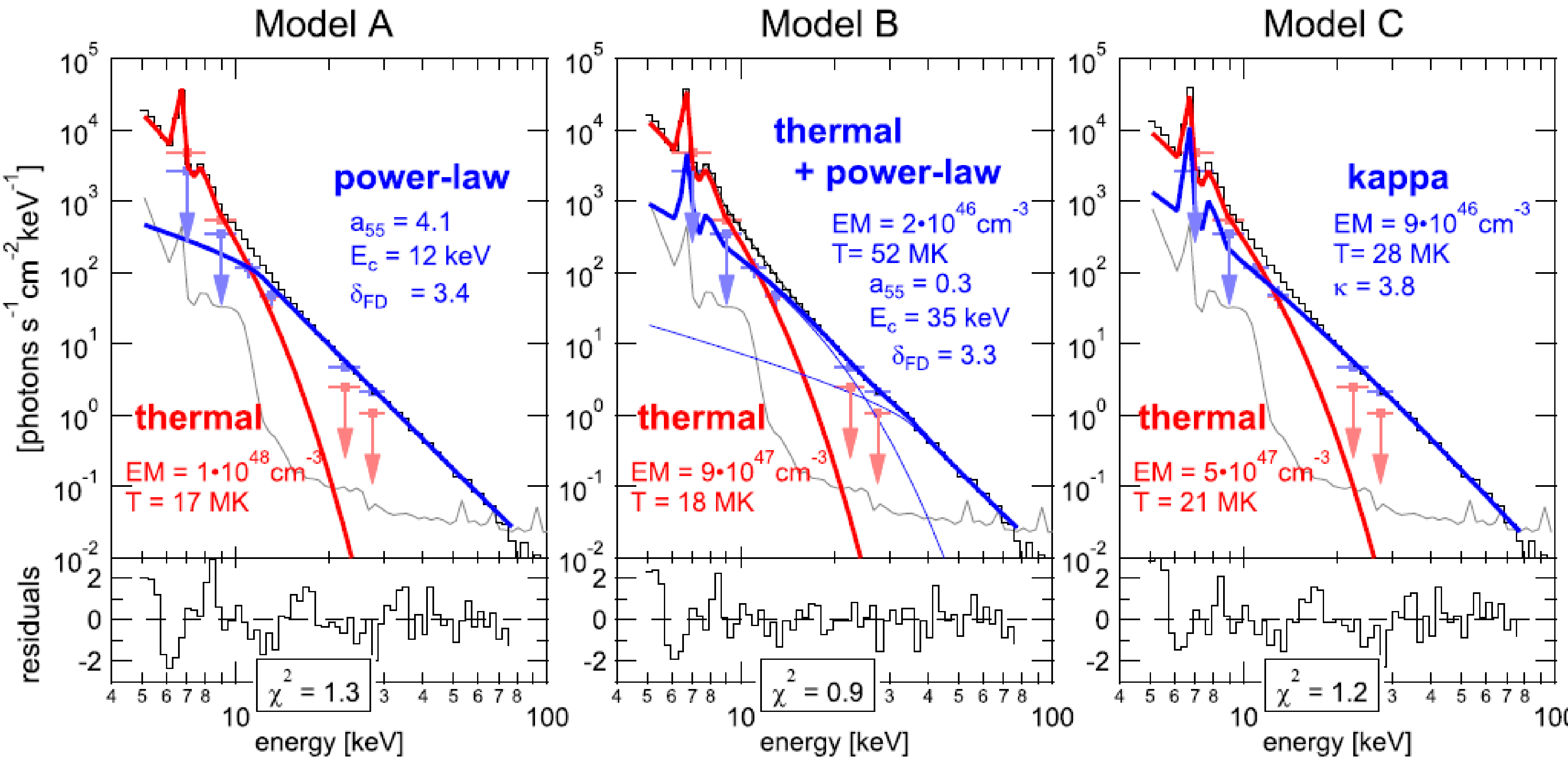

- Flares are non-Maxwellian (high-energy power-law tails)
- What about nanoflares? : Reconnection produces accelerated particles

  and so do waves (*Vocks et al. 2008, A&A 480, 527*)

RHESSI + AIA: Constraints on *F*(*E*)

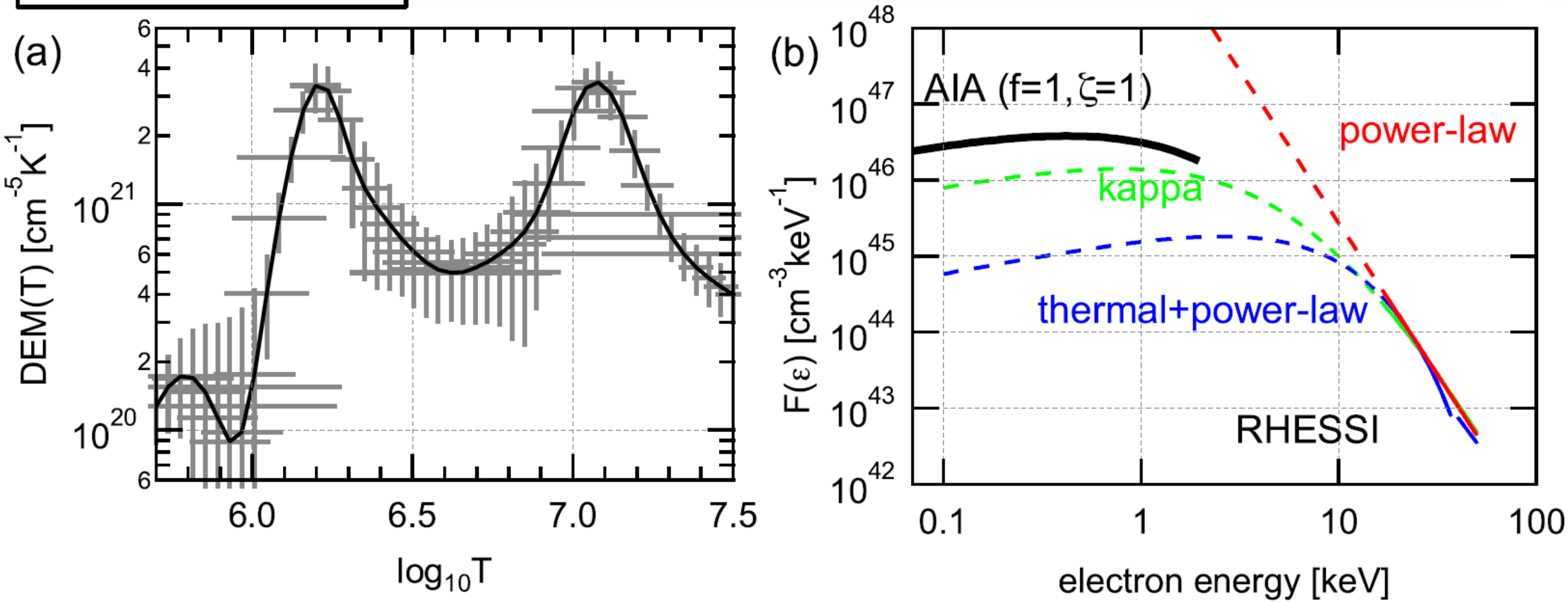

$$\langle n_{\mathrm{e}} V F(E)\rangle = \int_V n_{\mathrm{e}}(r) F(E,r)\,\mathrm{d}V = \int_T n_{\mathrm{e}}^2(r) f(E,r) \frac{\mathrm{d}V}{\mathrm{d}T}\,\mathrm{d}T$$

$$= \int_T \xi_f(T) f(E,r)\,\mathrm{d}T,$$

Oka et al. (2015), ApJ, 799, 195

- **DEM(*T*) obtained from AIA, then derived *F*(*E*) using the mean flux spectrum <nVF>**
- **Power-law fits to RHESSI incompatible with *F*(*E*) derived from AIA**
- **Kappa-distribution and thermal + power-law within the upper limits from AIA**

The case for non-Maxwellians

Gordovskyy et al. (2014), A&A 561, A72

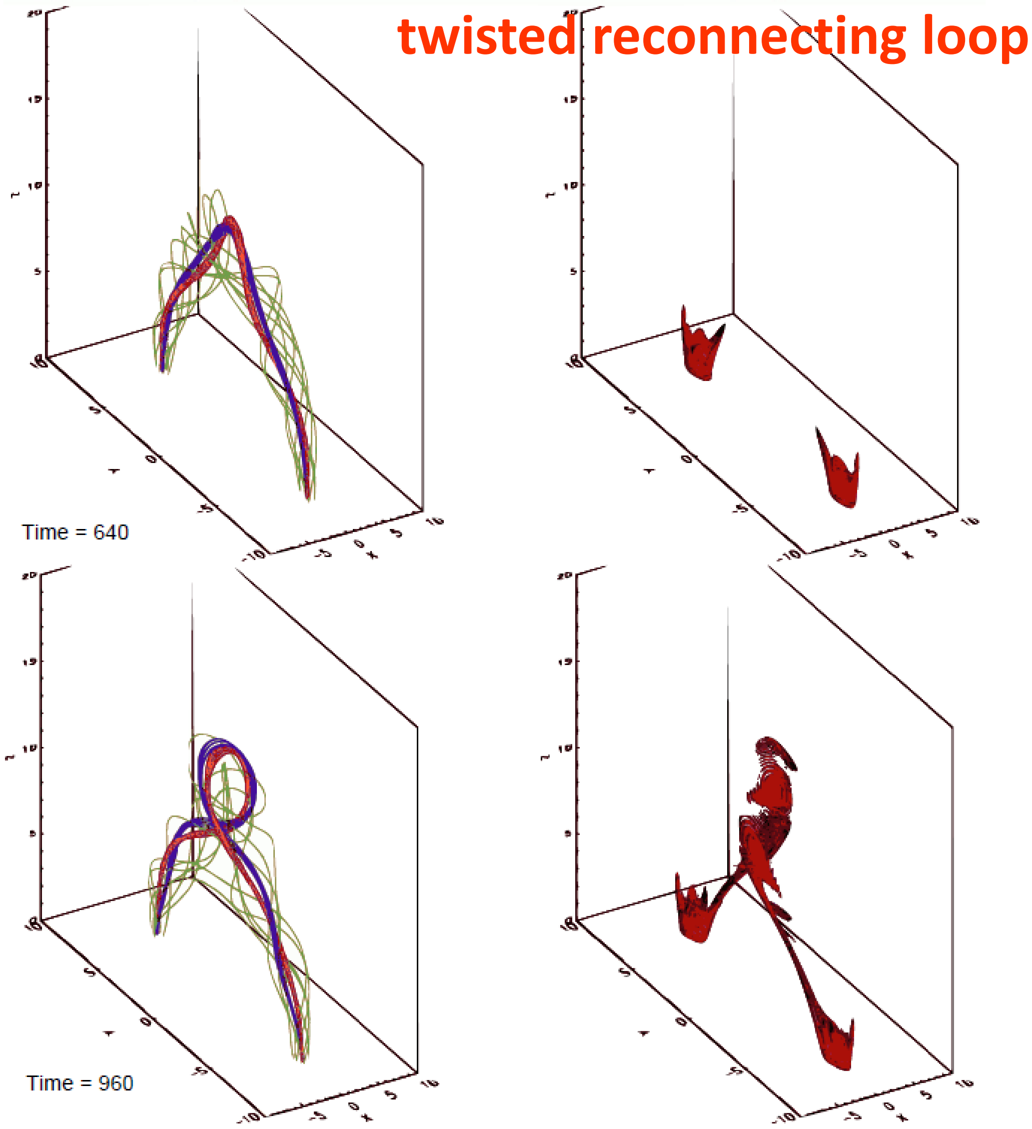

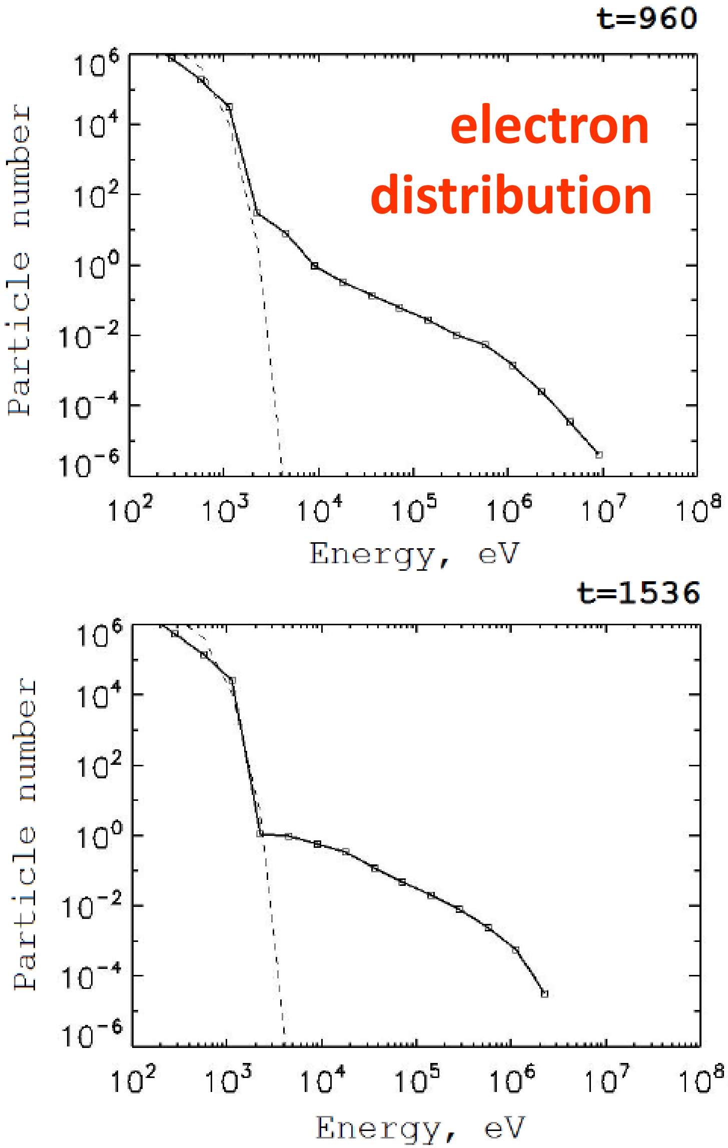

The case for non-Maxwellians

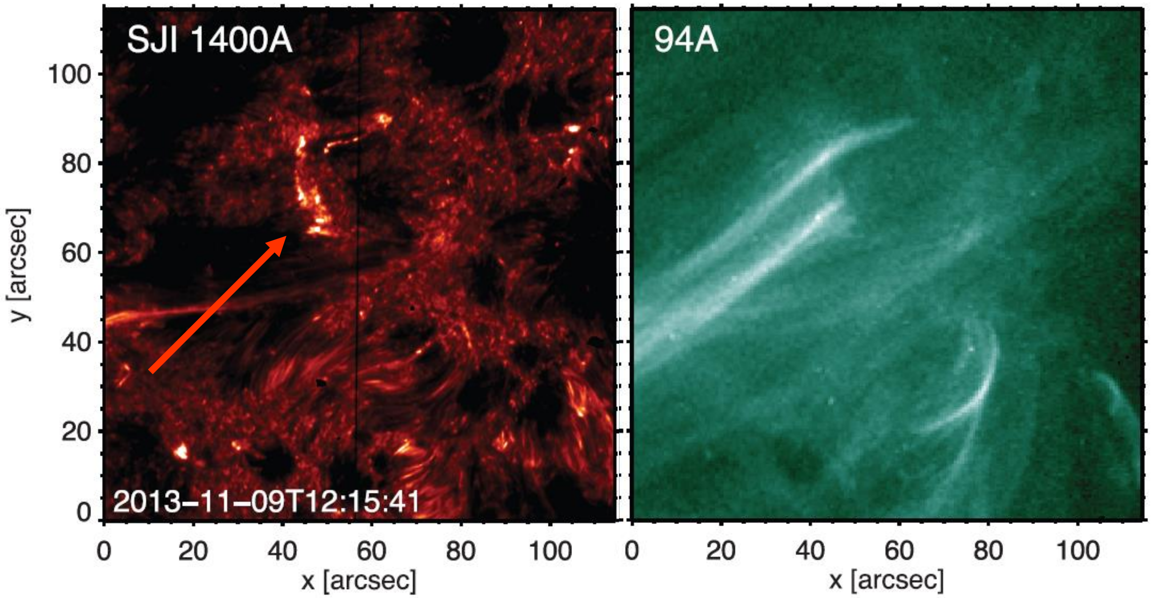

Testa et al. (2014), Sci 346, 6207

- **TR ribbon-like brightenings at footpoints of 94Å loops**
- **Blueshifts in Si IV can be reproduced by RADYN only if nanoflare-like heating by electron beams is assumed**
- **Heating without accelerated particles does not reproduce observations**

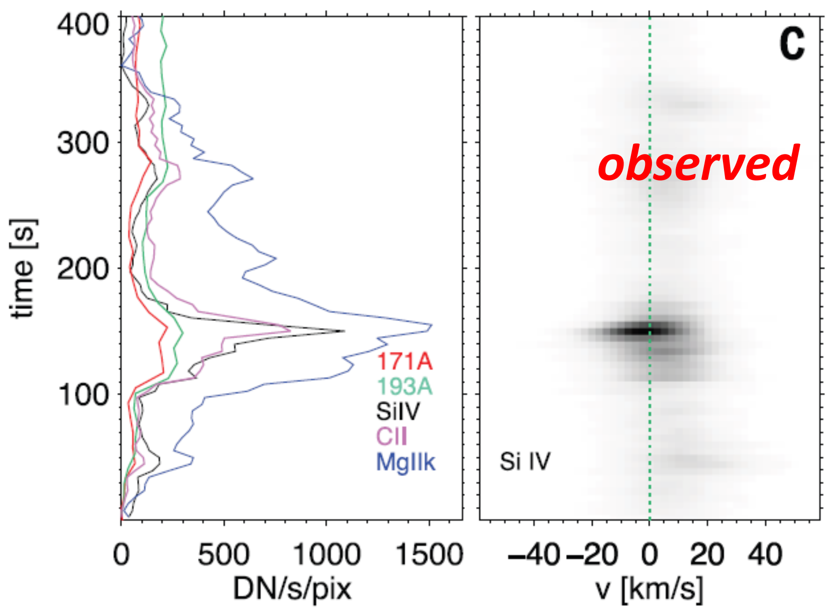

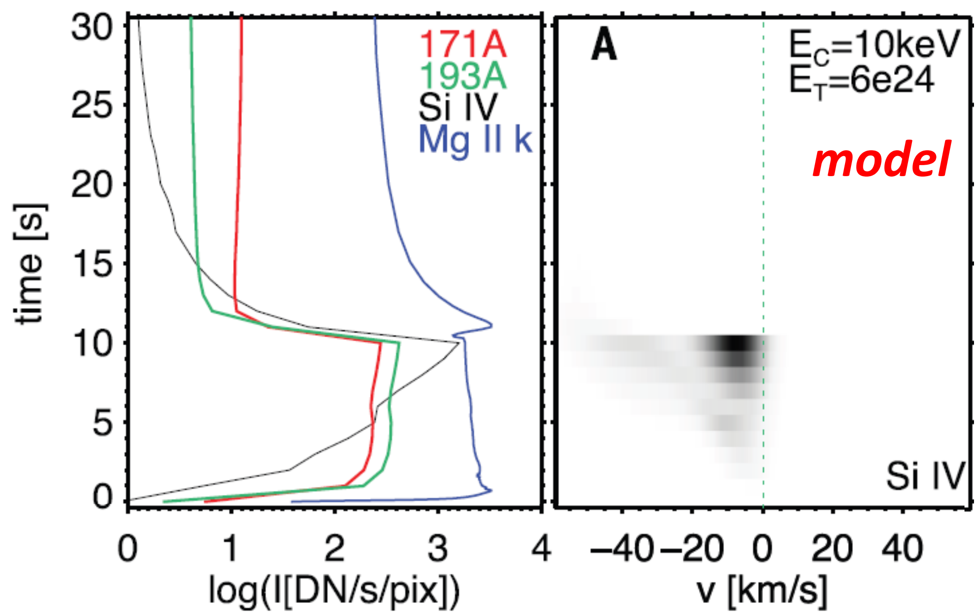

The κ-distributions

$$f_\kappa(E)dE = A_\kappa \frac{2}{\sqrt{\pi}\left(k_B T\right)^{3/2}} \frac{E^{1/2}}{\left(1+\frac{E}{\left(\kappa-3/2\right)k_B T}\right)^{\kappa+1}} dE$$

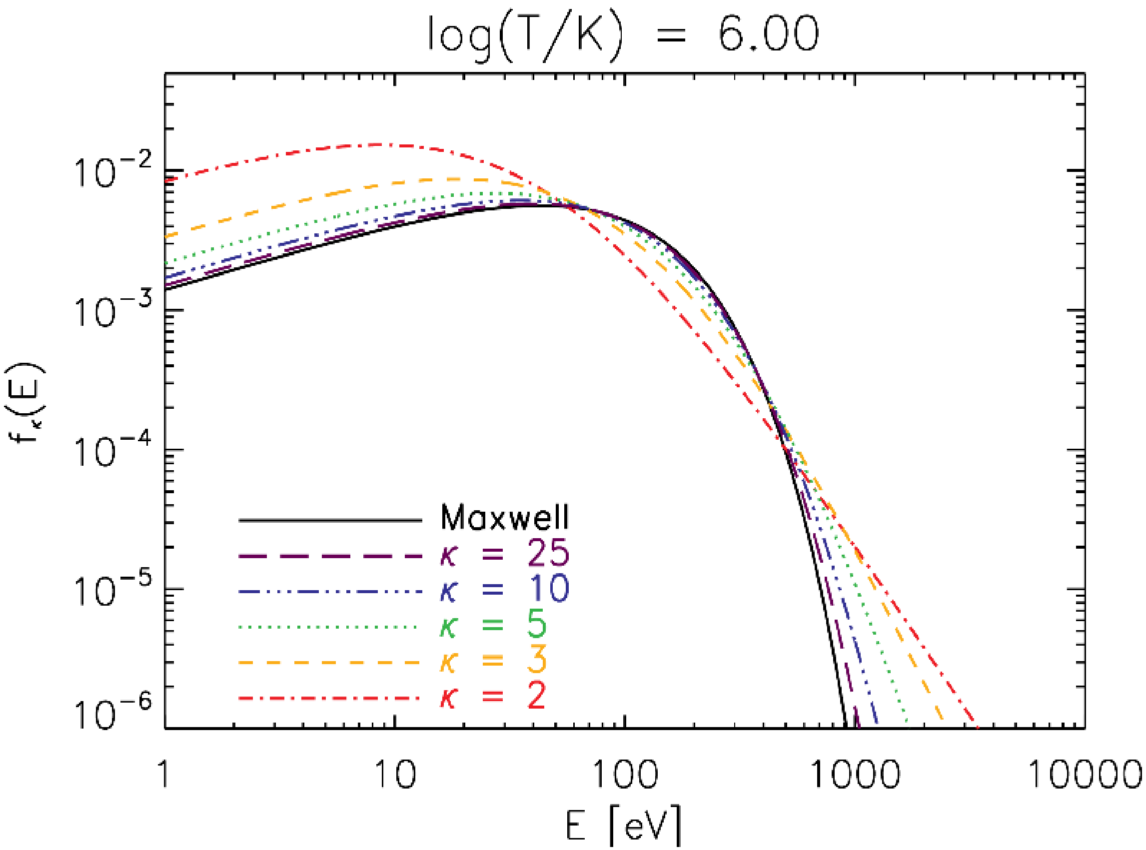

- **Maxwellian-like bulk**
- **Power-law tails (strongest possible)**
- **Differences from Maxwellian at all energies *E***

$$\left\langle E \right\rangle_\kappa = \frac{3}{2} k_B T_\kappa = \frac{3}{2} k_B T$$

Owocki & Scudder (1983)
Tsallis (1988, 2009)
Leubner (2004, 2005, 2008)
Livadiotis & McComas (2009, 2010)
Bian et al. (2014)

The κ-distributions

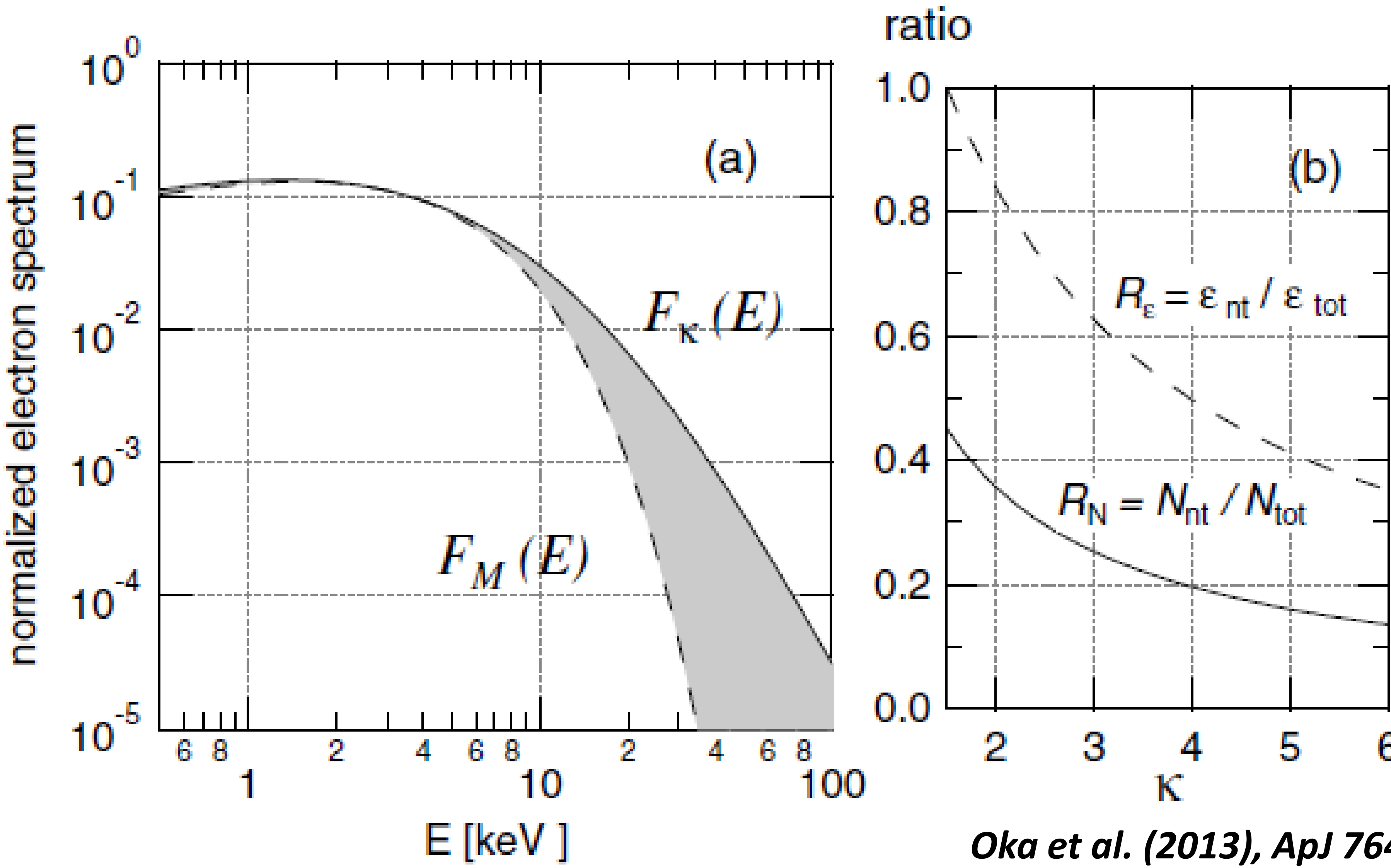

Oka et al. (2013), ApJ 764, 6

Non-Maxwellians: Line Intensities

$$I_{ji} = \int G_{ji}(T, n_e, \kappa) A_X n_e^2 \mathrm{d}l$$
$$= \int G_{ji}(T, n_e, \kappa) A_X \mathrm{DEM}(T) \mathrm{d}T\,,$$

excitation fraction

ionization fraction

$$G_{ji}(T, n_e, \kappa) = \frac{hc}{\lambda_{ji}} \frac{A_{ji}}{n_e} \frac{n_{X,i}^{+k}}{n_X^{+k}} \frac{n_X^{+k}}{n_X} \frac{n_H}{n_e}\,,$$

- **Ionization fractions:** from ***Dzifčáková & Dudík (2013), ApJS 206, 6***
- **Excitation fractions:** obtained from the original collision strengths Ω

Dudík et al. (2014), A&A 570, A124

or using indirect approximative method

Dzifčáková (2006), SoPh 234, 243

Dzifčáková & Kulinová (2011), A&A, 531, A122

Dzifčáková et al. (2015), ApJS 217, 14

κ-distr.: Ioniz./Recomb. Rates

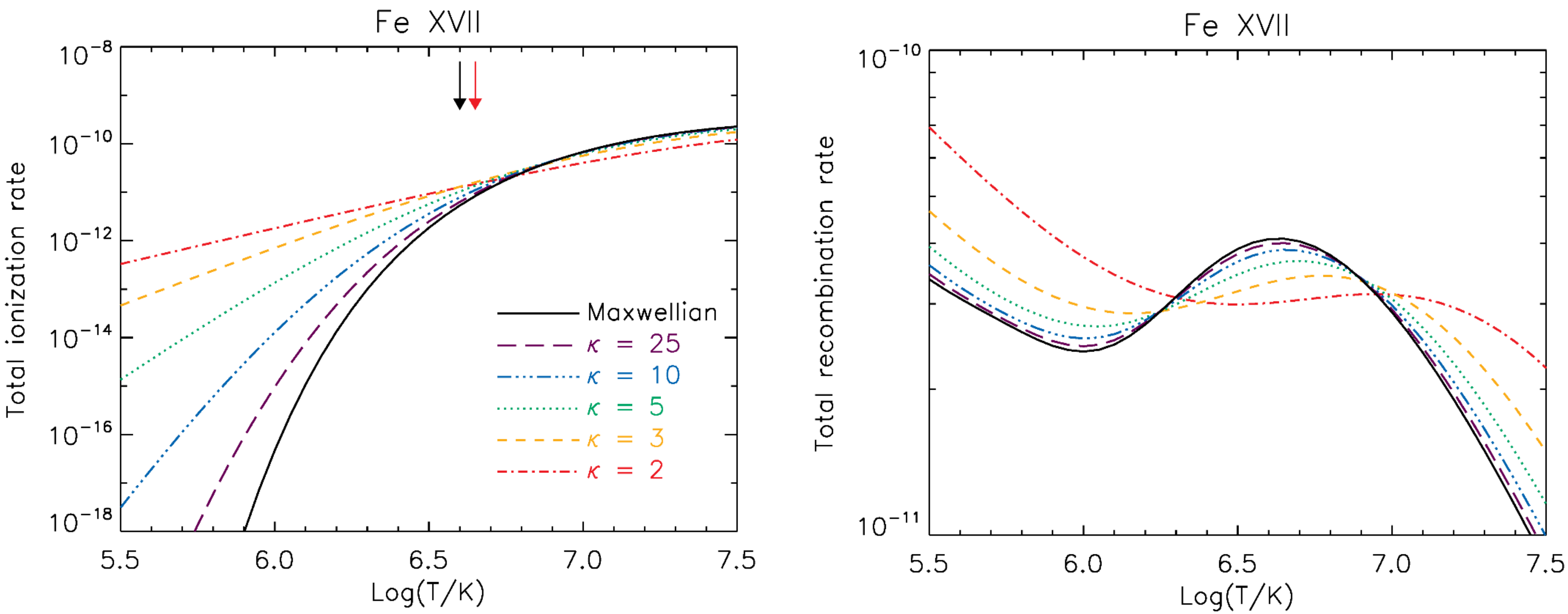

Dzifčáková & Dudík (2013), ApJS 206, 6

- **Ionization rate dominated by high-energy electrons (power-law tail)**
- **Recombination rate dominated by low-energy electrons**
- **The location of the peak of the relative ion abundance *in equilibrium* is determined by these rates**

κ-distr.: Ionization Equilibrium

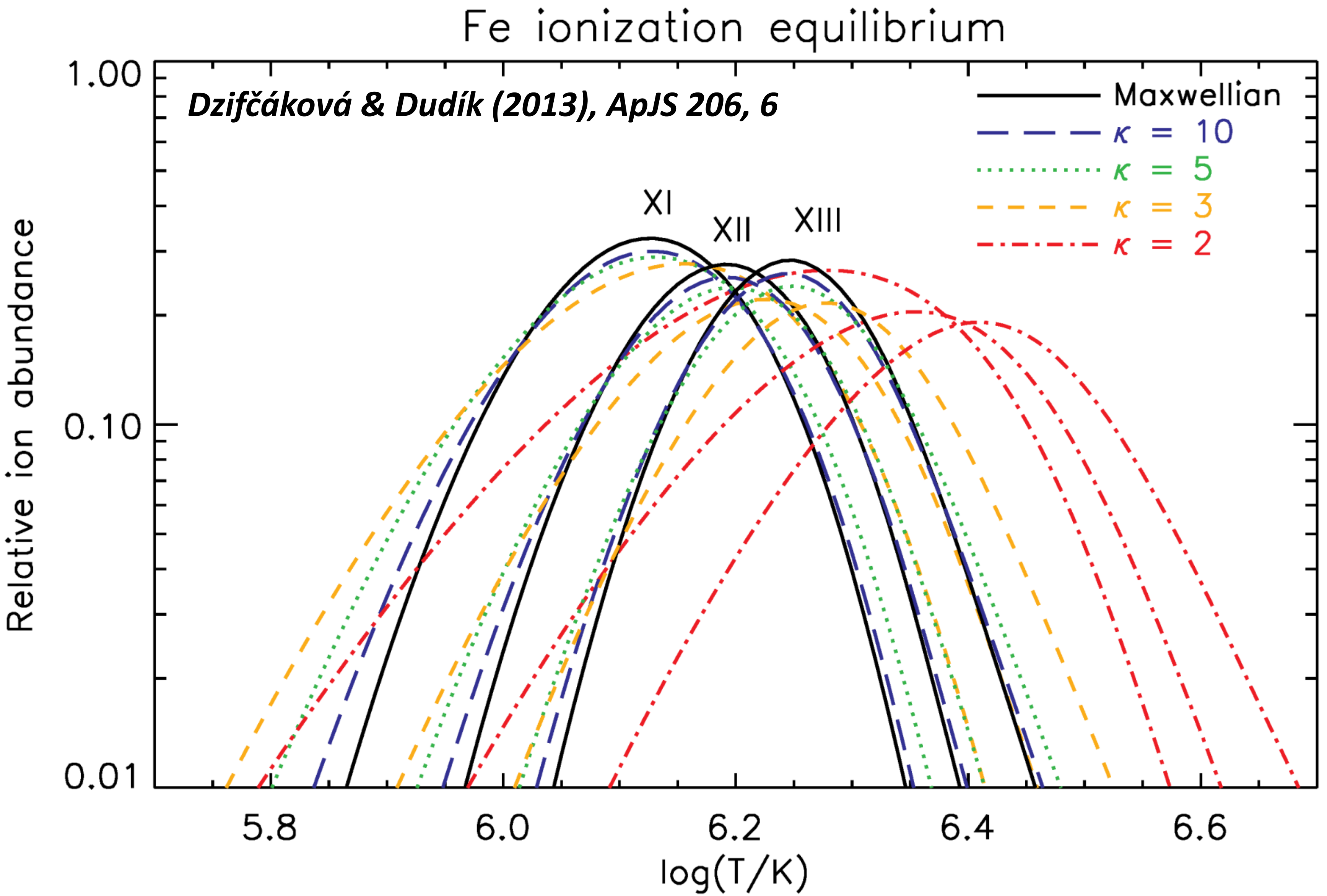

κ-distr.: Ionization Equilibrium

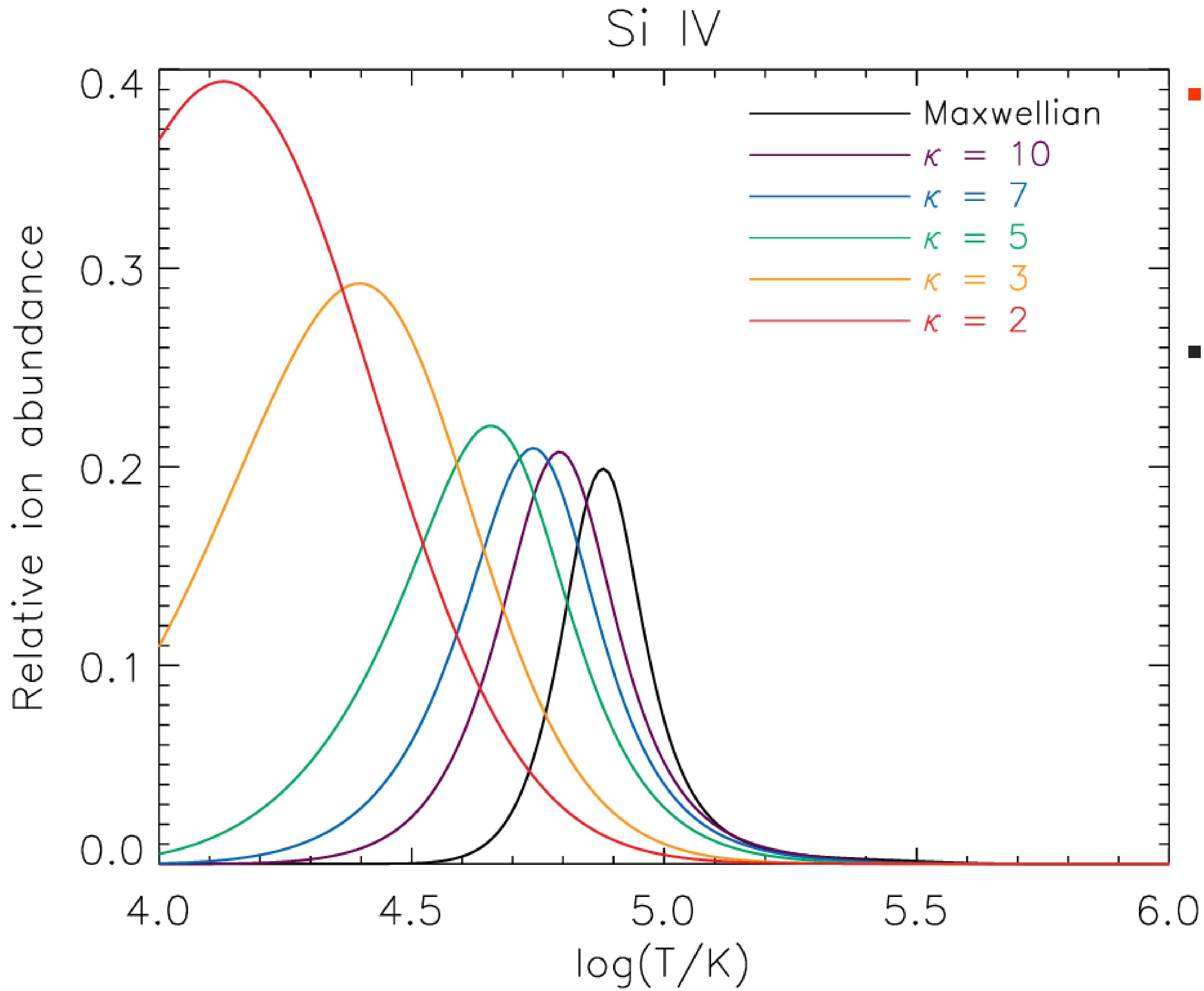

- **TR ions typically shifted to lower *T***
- **Some can have enhanced abundances compared to Maxwellian case**

Excitation Rates: Direct Method

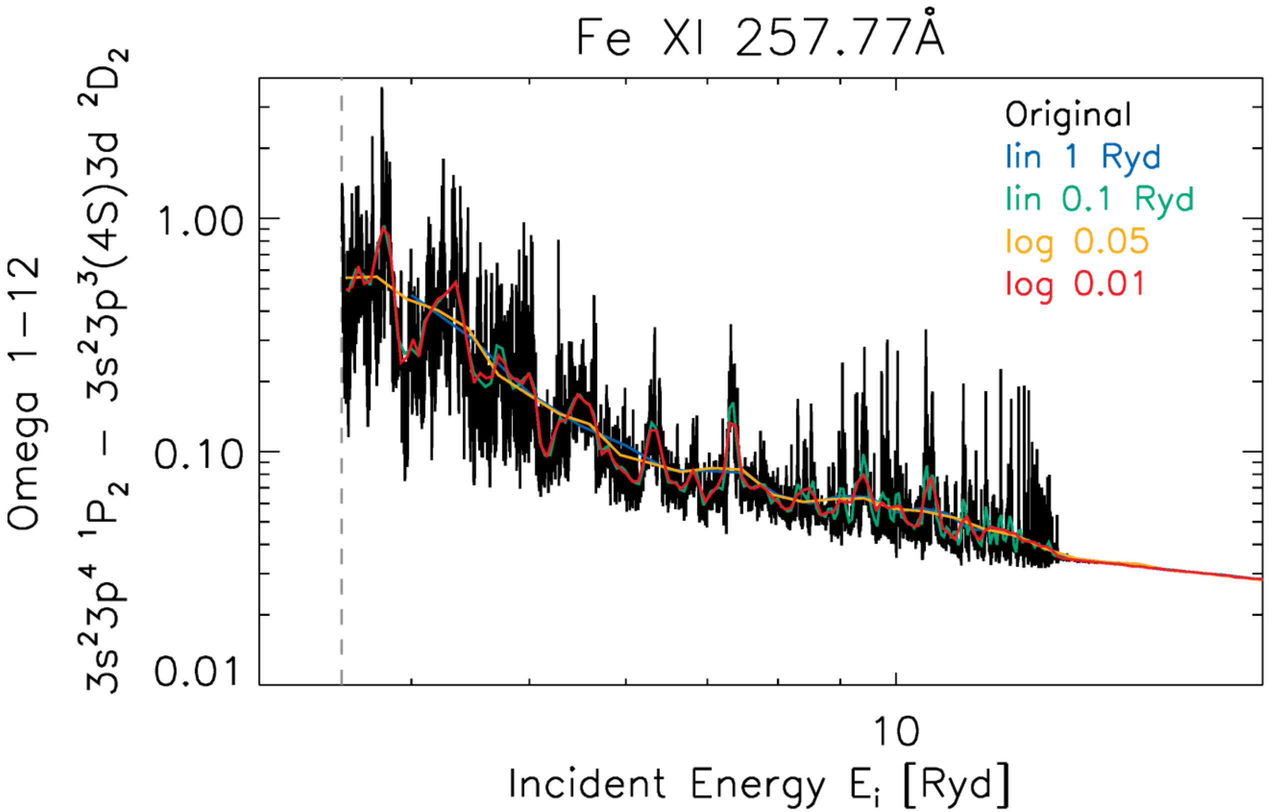

- **Excitation rate integrated directly from the cross-section**
- ***Problem*: huge cross-section files for a single ion (about 30 GB)**
- **Has been done for selected ions**

- **Si IV, O IV**
  Dudík et al. (2014), ApJL 780, 12

- **Fe IX – XIII**
  Dudík et al. (2014), A&A, 570, A124

$$\Upsilon_{ij}(T,\kappa) = \frac{\sqrt{\pi}}{2}\exp\left(\frac{\Delta E_{ji}}{k_B T}\right)\int_0^{+\infty}\Omega_{ij}(E_i)\left(\frac{E_i}{k_B T}\right)^{-\frac{1}{2}} f_\kappa(E_i)\mathrm{d}E_j$$

$$C^{e}_{ij}(T,\kappa) = \left(\frac{2\pi}{m_e k_B T}\right)^{1/2}\frac{2a_0^2}{\omega_i}I_H\exp\left(-\frac{\Delta E_{ji}}{k_B T}\right)\Upsilon_{ij}(T,\kappa)$$

Bryans (2006), PhDT

Excitation Rates: Indirect Method

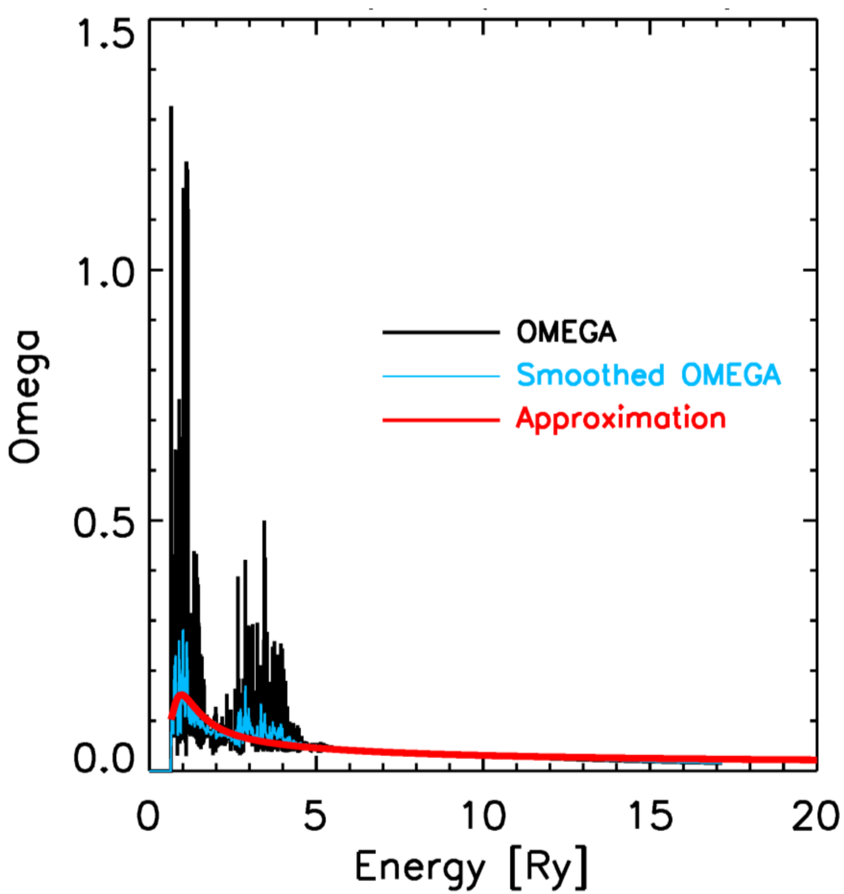

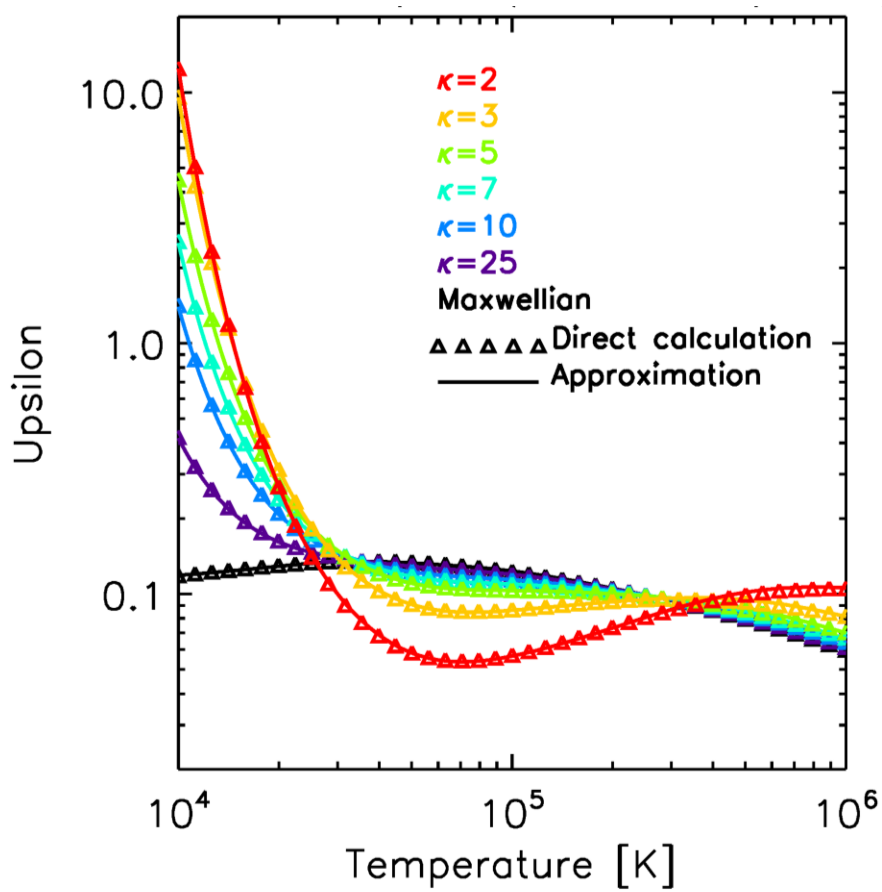

- Approximate the ϒ using an assumption on functional form of Ω
- Calculate the ϒ for κ-distributions using this approximation
- An overall precision of 5-10% is found (*Dzifčáková et al. 2015, ApJS 217, 14*)
- KAPPA database for several values of κ – http://kappa.asu.cas.cz

κ-distr.: Maxwellian Decomposition

$$f_\kappa(E,T) = \sum_i c_i f_{\mathrm{Maxw}}(E, a_i T)$$

Hahn & Savin (2015), ApJ, 809, 178

- Initial guess of a_i
- Coefficients c_i determined by matching the κ-distribution at a given set of energies E_j
- Iterations
- Relative error less than 5%
- Similar as in the indirect method

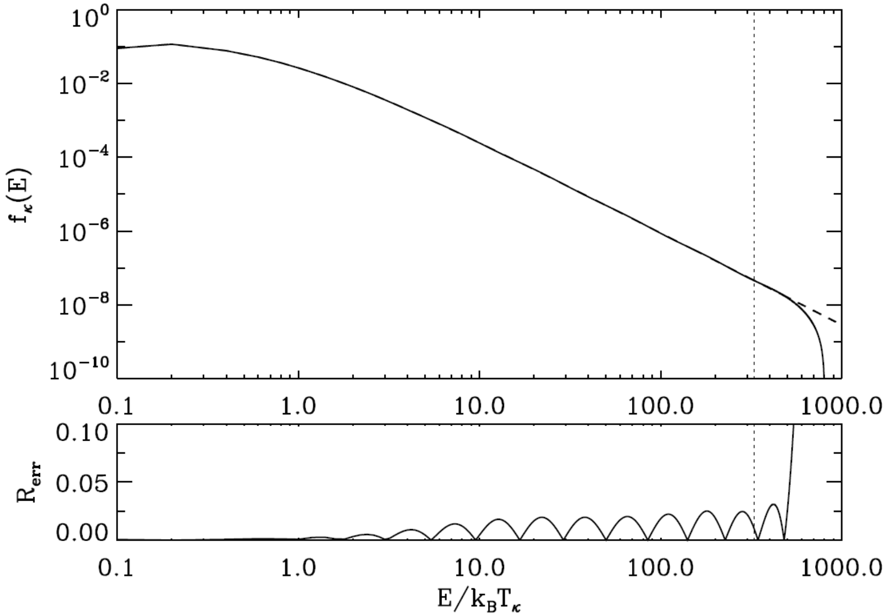

- A rate coefficient P_{jk} is given by (linearity)

$$P_{jk,\kappa}(T) = \sum_i c_i P_{jk,\,\mathrm{Maxw}}(a_i T)$$

κ-distr.: Line Spectra

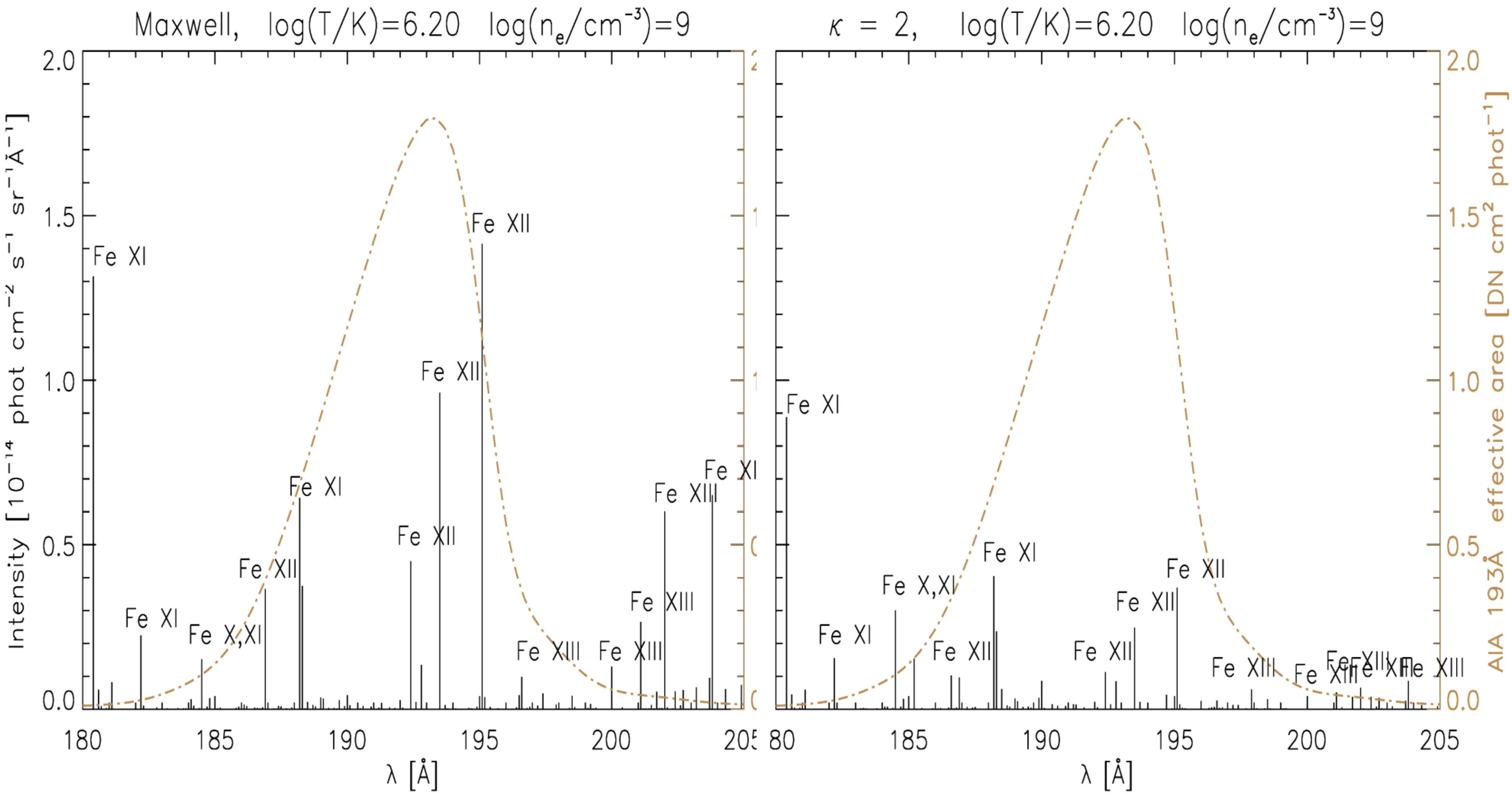

Dzifčáková et al. (2015), ApJS, 217, 14

- **Line intensities are significantly affected**
- **Complicated by *dependence on temperature and electron density***

κ-distr.: AIA Responses

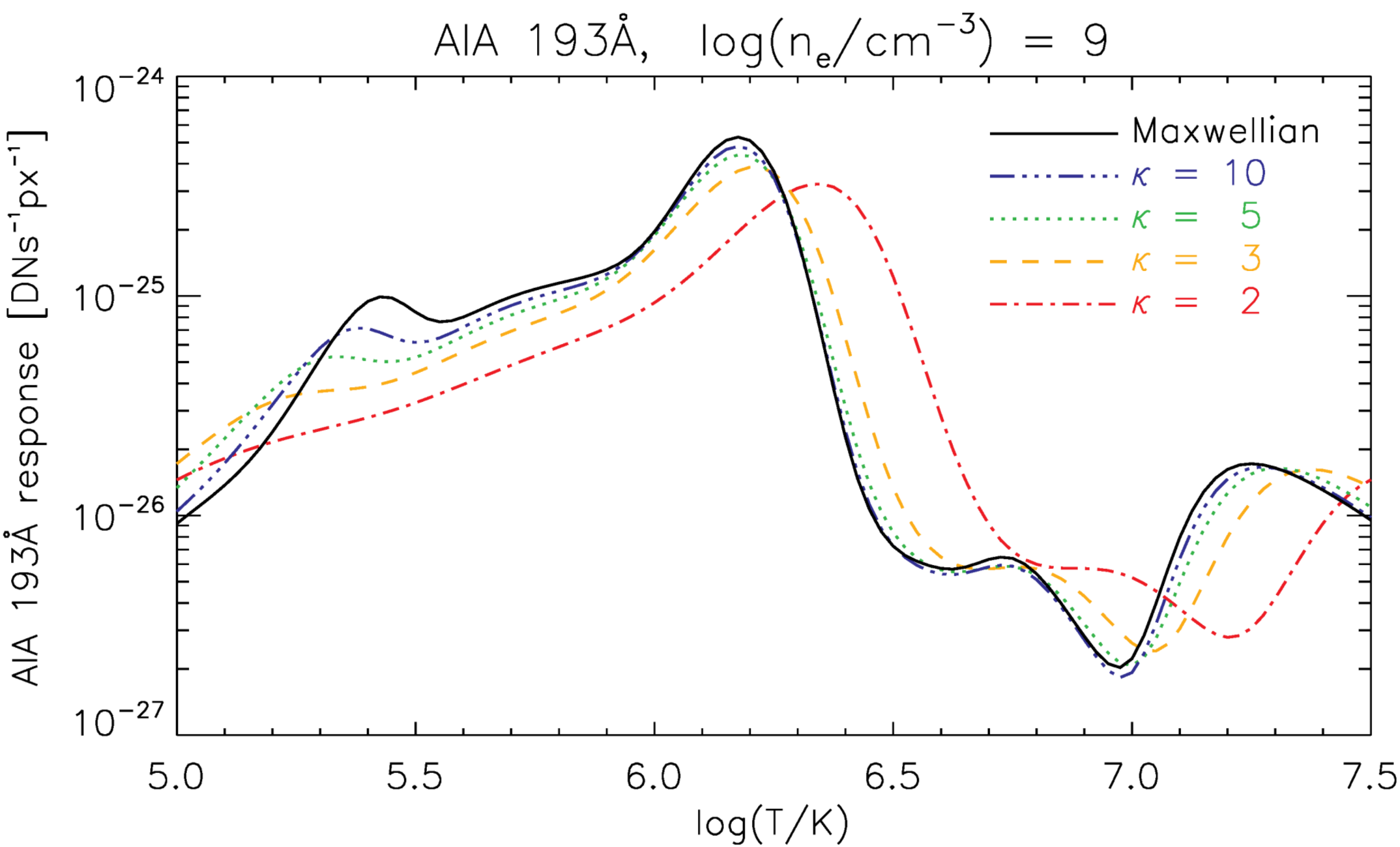

κ-distr.: AR core DEM slopes

Mackovjak et al. (2014), A&A, 564, A130

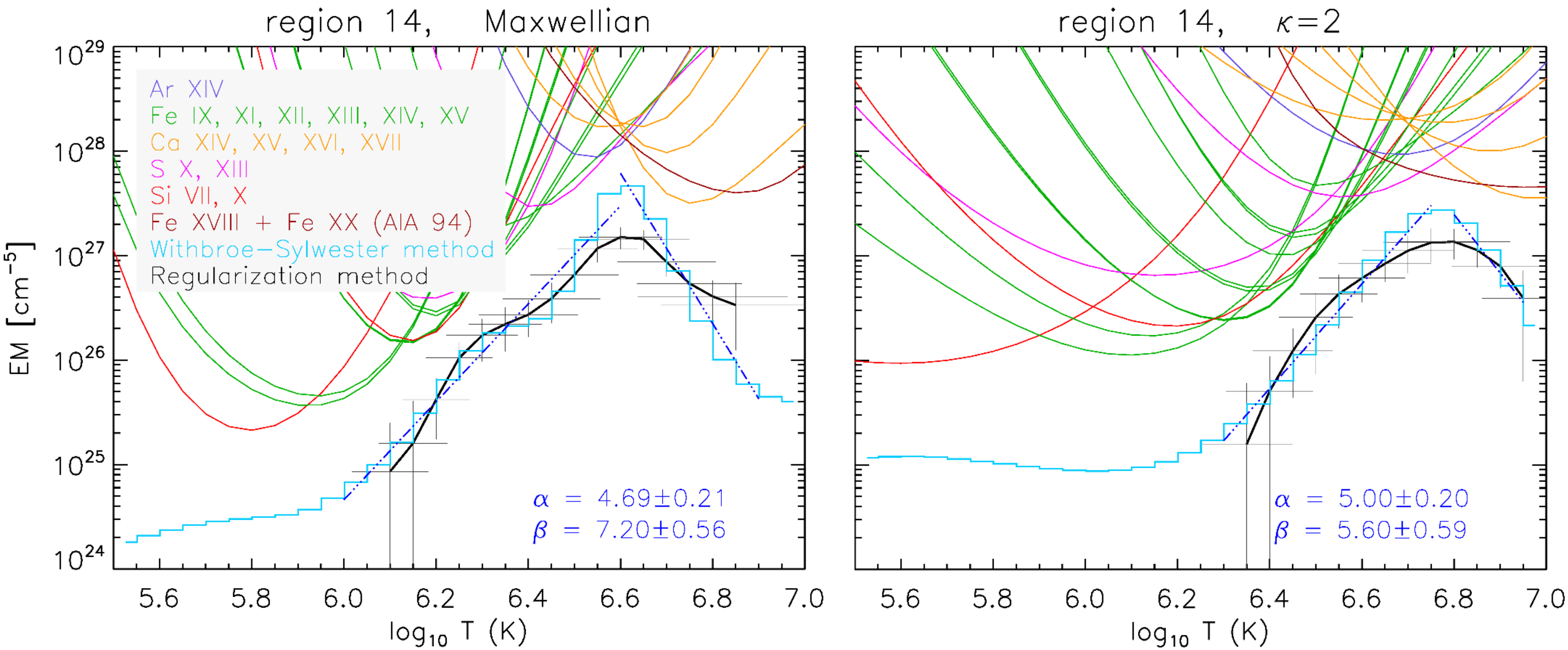

- AR core intensities from ***Warren et al. (2012), ApJ 759, 141***
- The low-*T* slope of the EM(*T*) does not change appreciably with κ
- This behavior does not depend on the AR core
- The high-*T* slope decreases

κ-distr.: Quiet Sun DEMs

Mackovjak et al. (2014), A&A, 564, A130

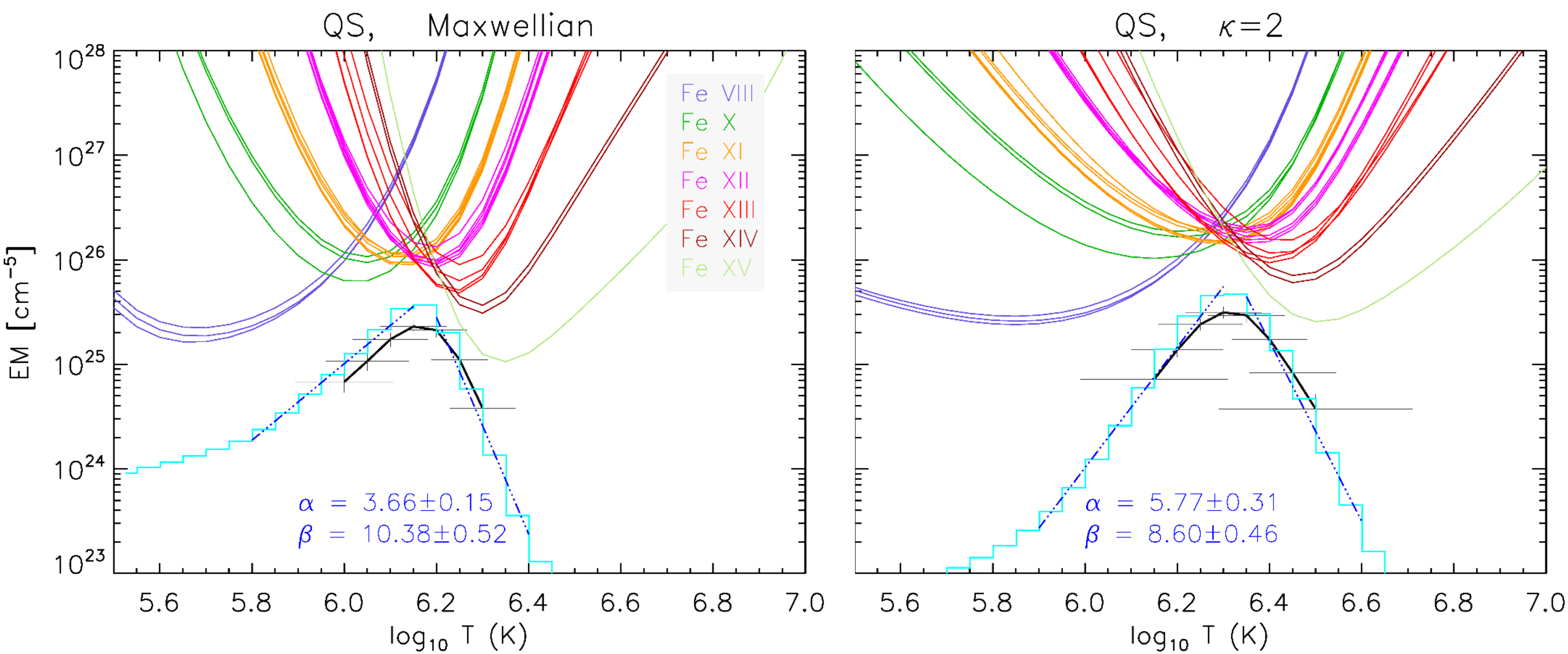

- QS intensities from ***Landi & Young (2010), ApJ 714, 636***
- Both low-*T* and high-*T* slopes of the EM(*T*) change with κ
- The κ = 2 case shows almost an isothermal crossing point
- Non-Maxwellian QS?

SDO/AIA: Transient Loop

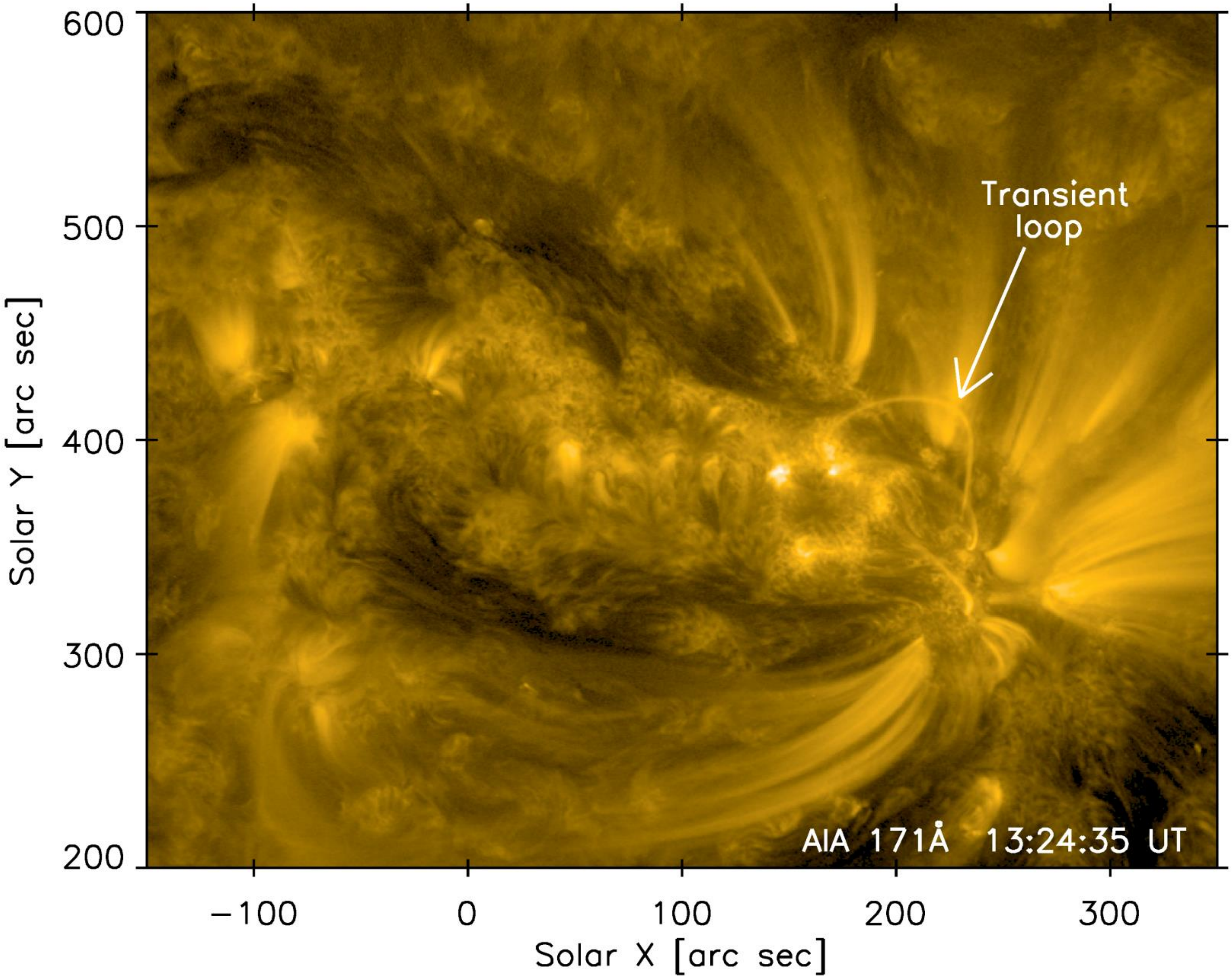

κ-distr.: Transient Loop Diagnostics

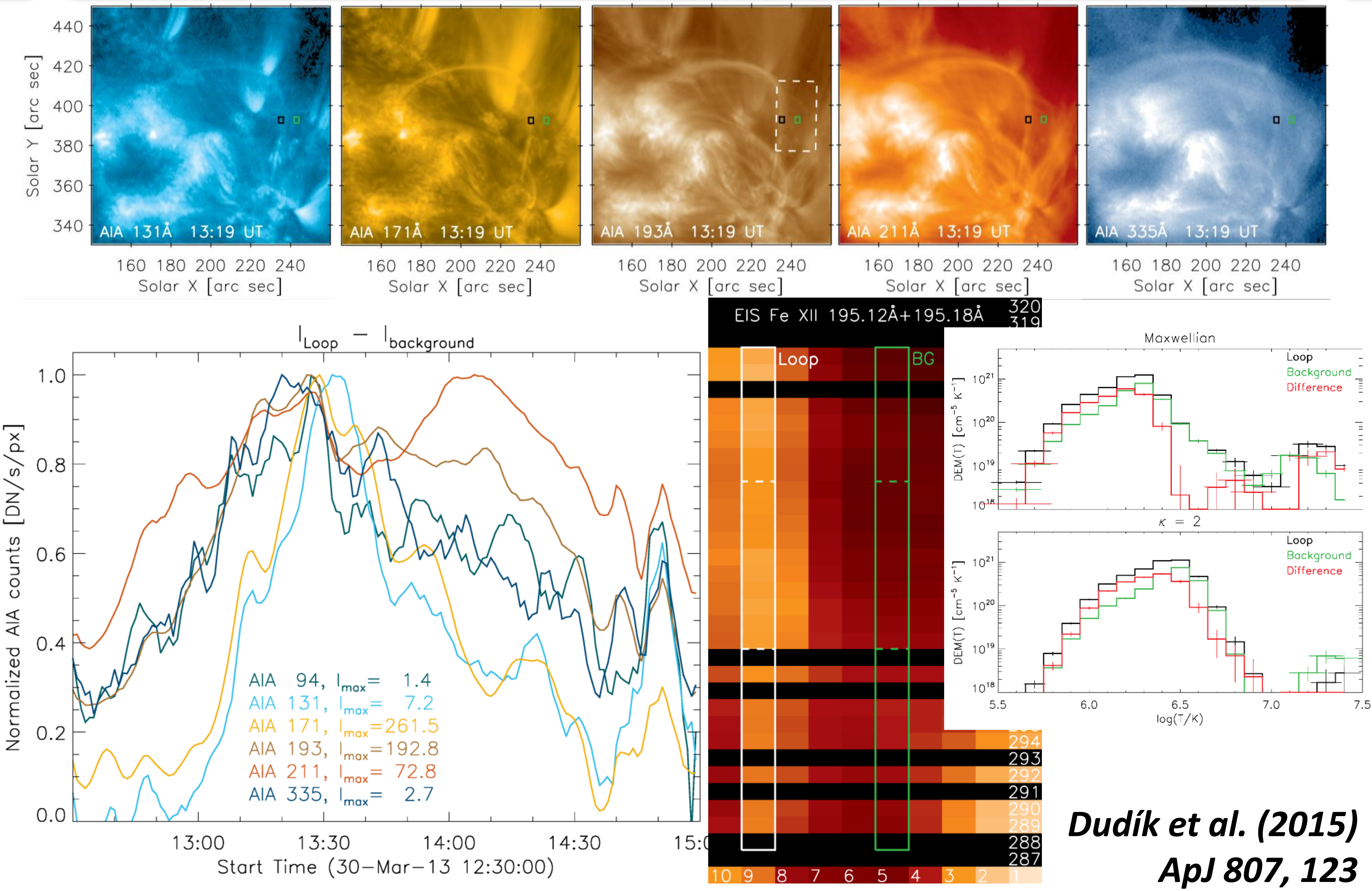

Dudík et al. (2015)
ApJ 807, 123

Density Diagnostics

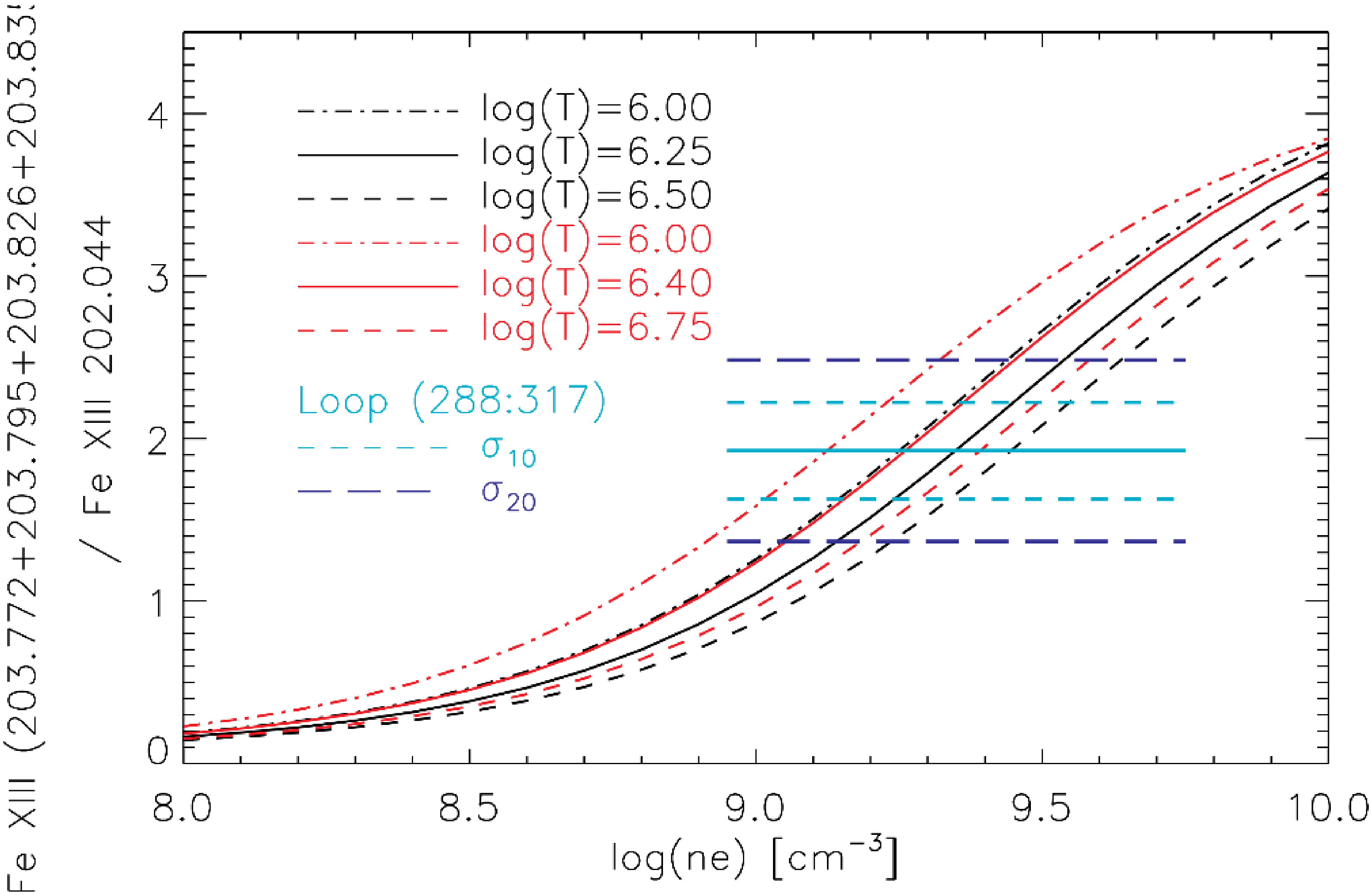

c.f. Dudík et al. (2014) A&A 570, A124

Diagnostics of κ

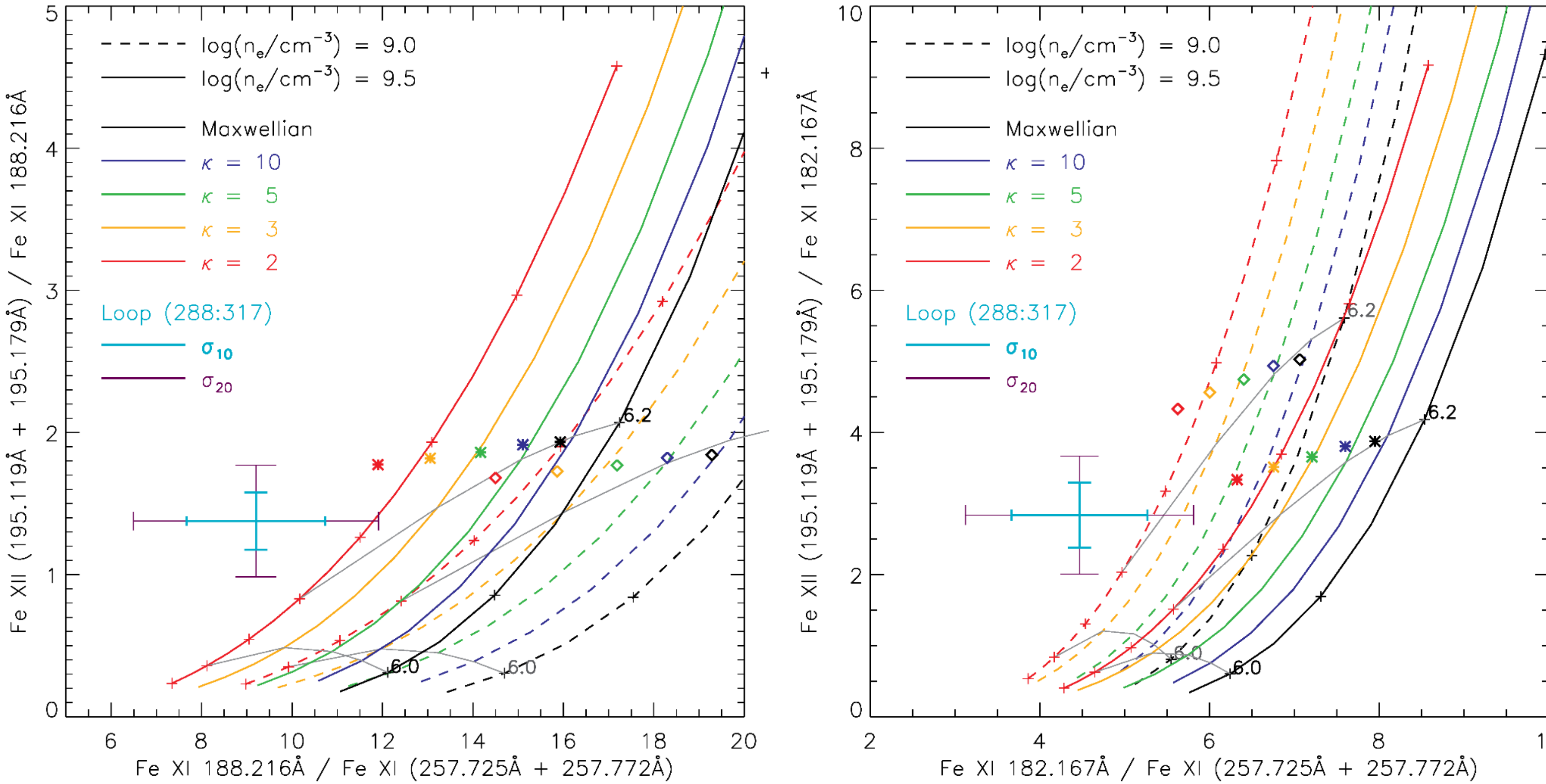

Dudík et al. (2015) ApJ 807, 123

- **Loop has *κ* ≤ 2 (is highly non-Maxwellian)**
- **This does not change if DEM is considered**

Side Note: EIS Calibration

Ion	λ [Å]	selfblending transitions [Å]	Loop (288:317)			Loop (300:309)		
			I	$\sigma_{10\%}(I)$	$\sigma_{20\%}(I)$	I	$\sigma_{10\%}(I)$	$\sigma_{20\%}(I)$
Fe XI	182.167	–	795	99	169	934	117	199
Fe XI	188.216	–	1638	172	332	1947	204	394
Fe XI	257.554	257.538, 257.547, 257.558	398	45	82	414	47	86
Fe XI	257.772	257.725	178	23	38	234	30	50
Fe XII	186.887	186.854, (186.931)	1406	145	283	1498	154	302
Fe XII	195.119	195.179, (195.078), (195.221)	2256	228	453	2506	254	503
Fe XIII	196.525	–	261	27	53	223	23	45
Fe XIII	202.044	–	1346	153	279	1779	202	368
Fe XIII	203.826	203.772, 203.795, 203.835	2591	270	524	2532	264	512

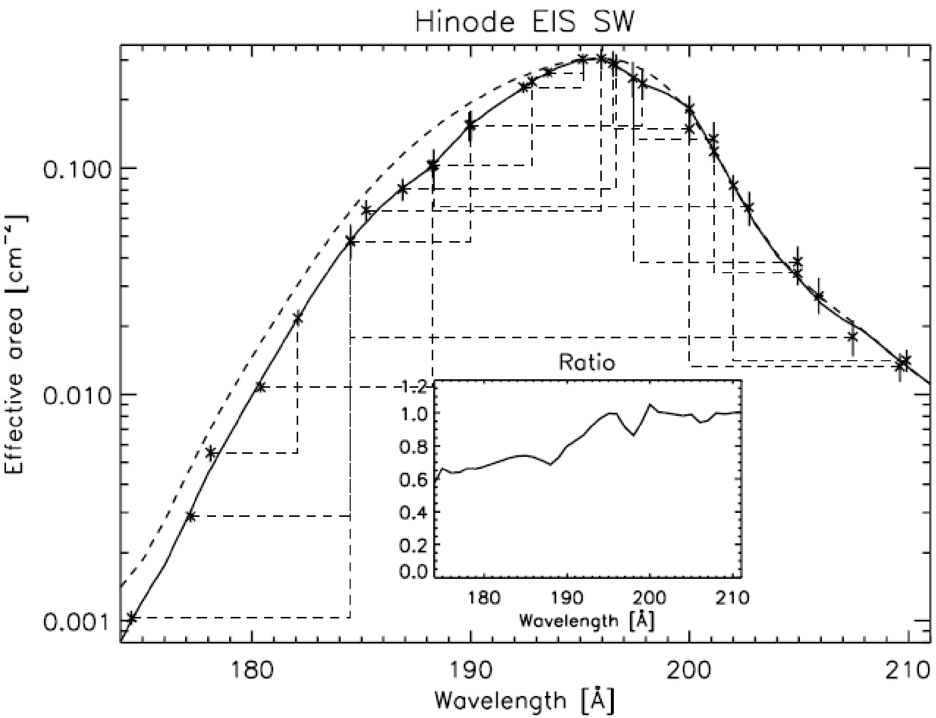

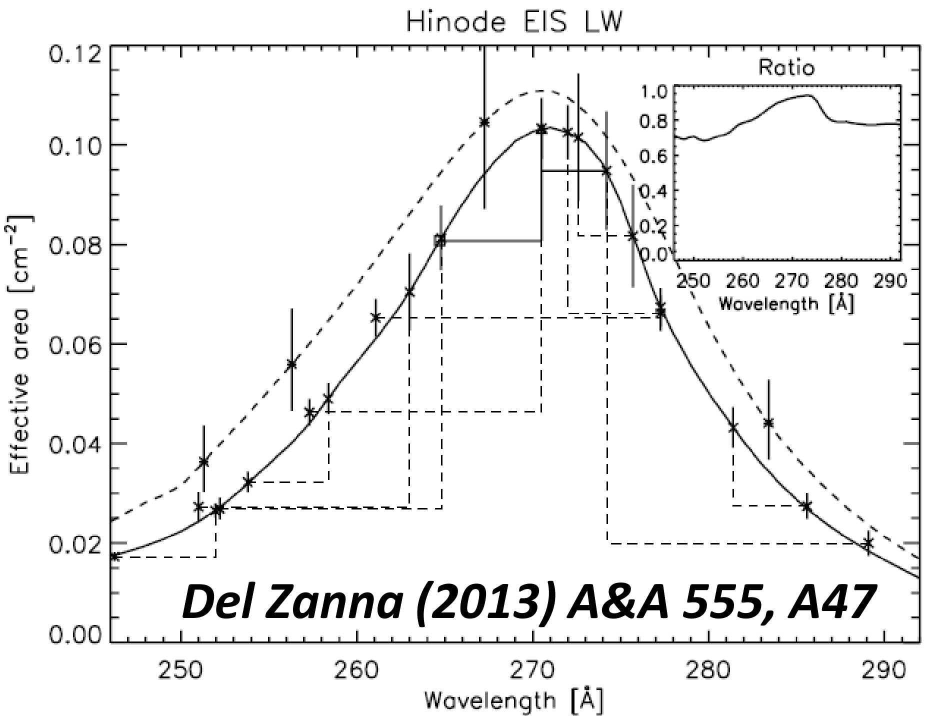

Del Zanna (2013) A&A 555, A47

Diagnostics in an X-Class Flare

X5.6, 2012 Mar 07, 00:02 – 00:24 – 00:40 UT, Active Region NOAA 11428

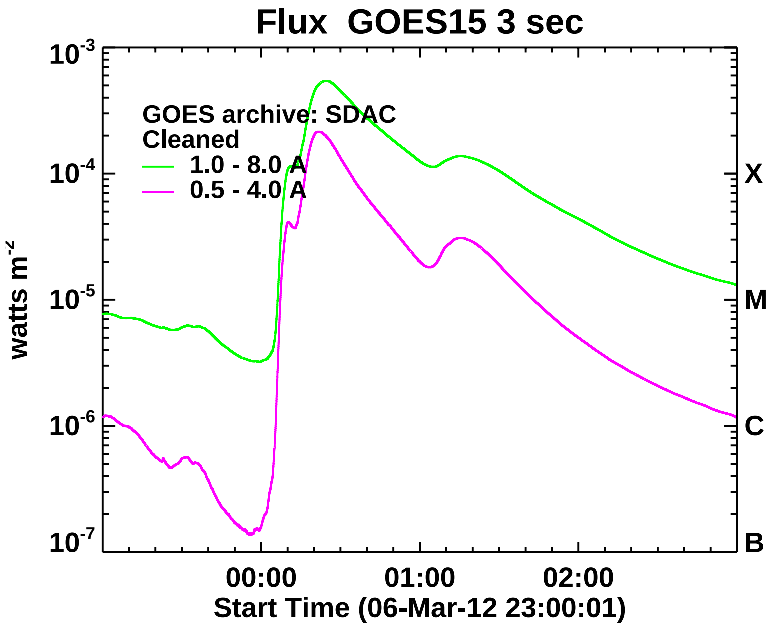

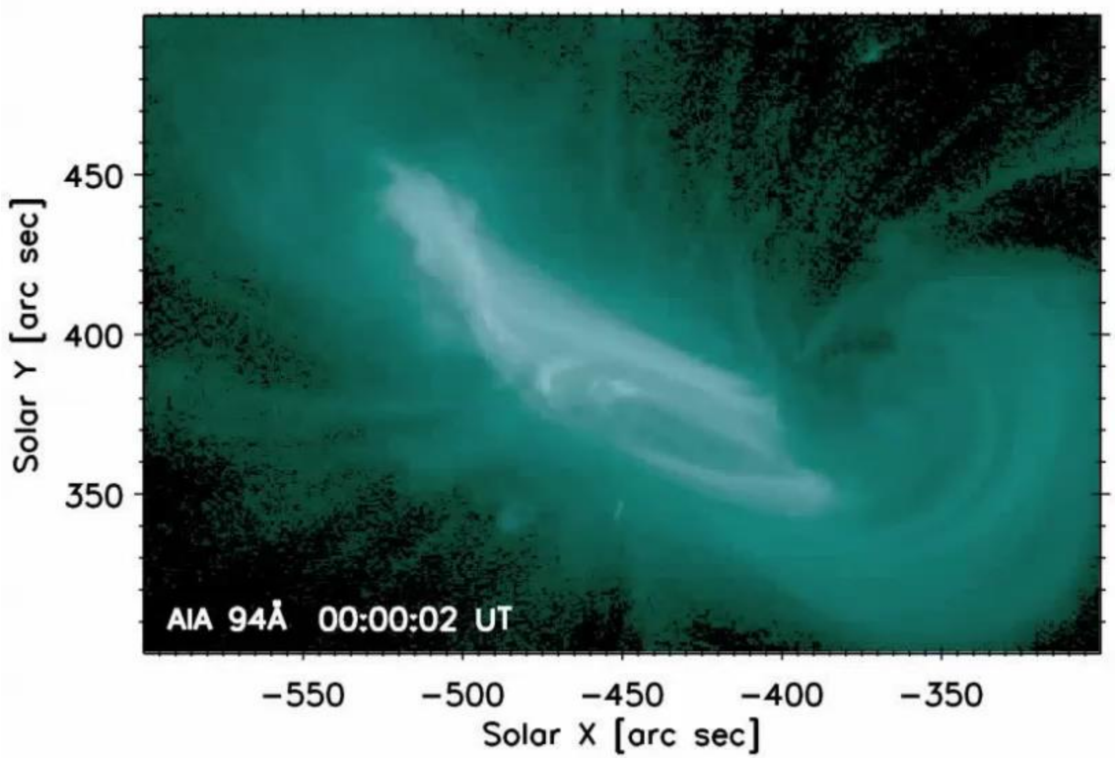

In the next slides, we analyze 1-min averaged data
00:10 – 00:40 UT (flare peak)
00:56 – 00:60 UT (gradual phase)

Diagnostics of the Distribution

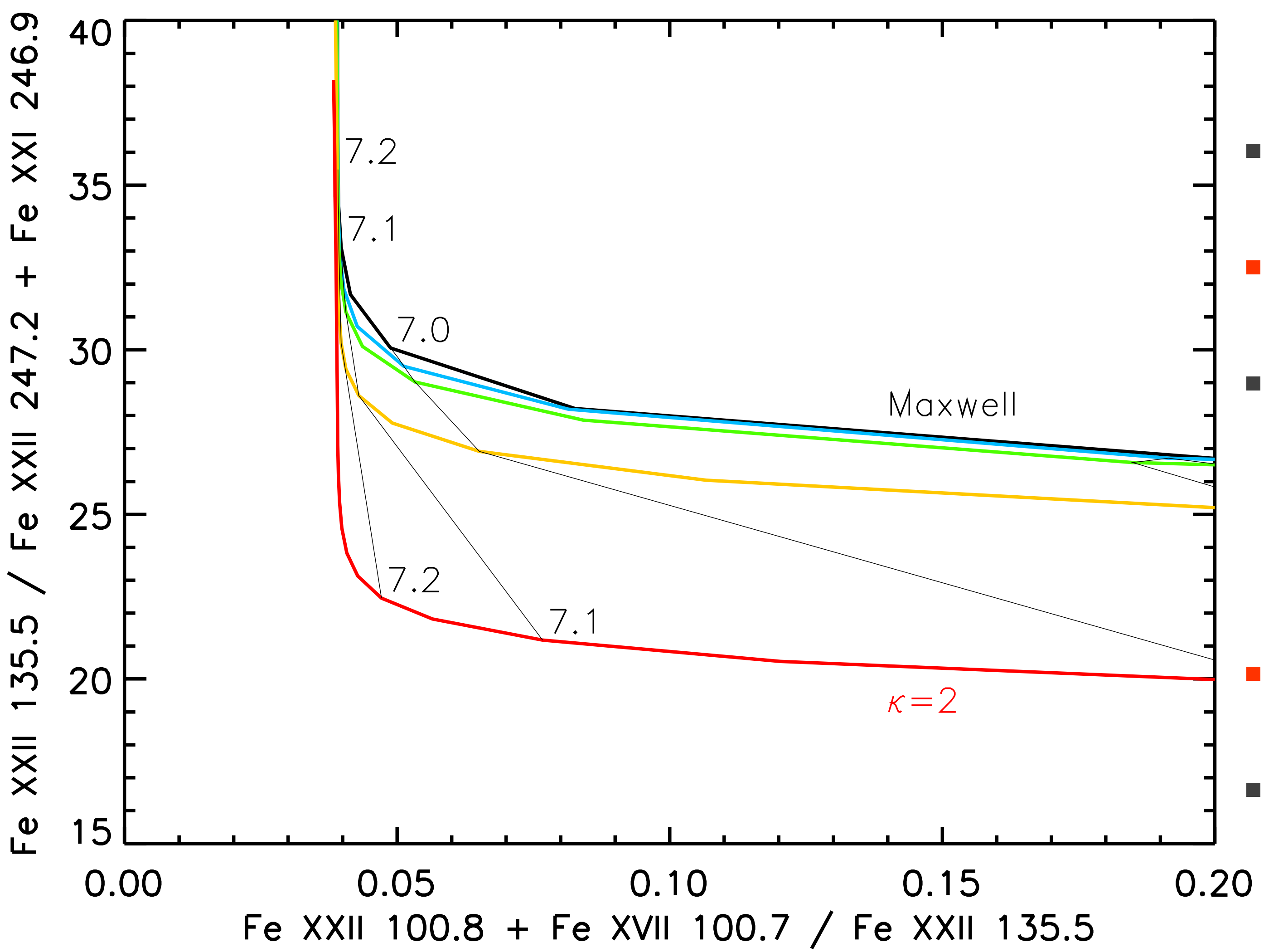

- **κ and *T* are always coupled**

- **Ratio-ratio diagram method:**
- **Use a ratio sensitive to κ**
- **Typically, this involves lines with widely different λ (excitation energies)**

- **Combine with a ratio sensitive to *T***
- **Typically, use a ratio of lines from the neighbouring ionization stages**

Diagnostics of the Distribution

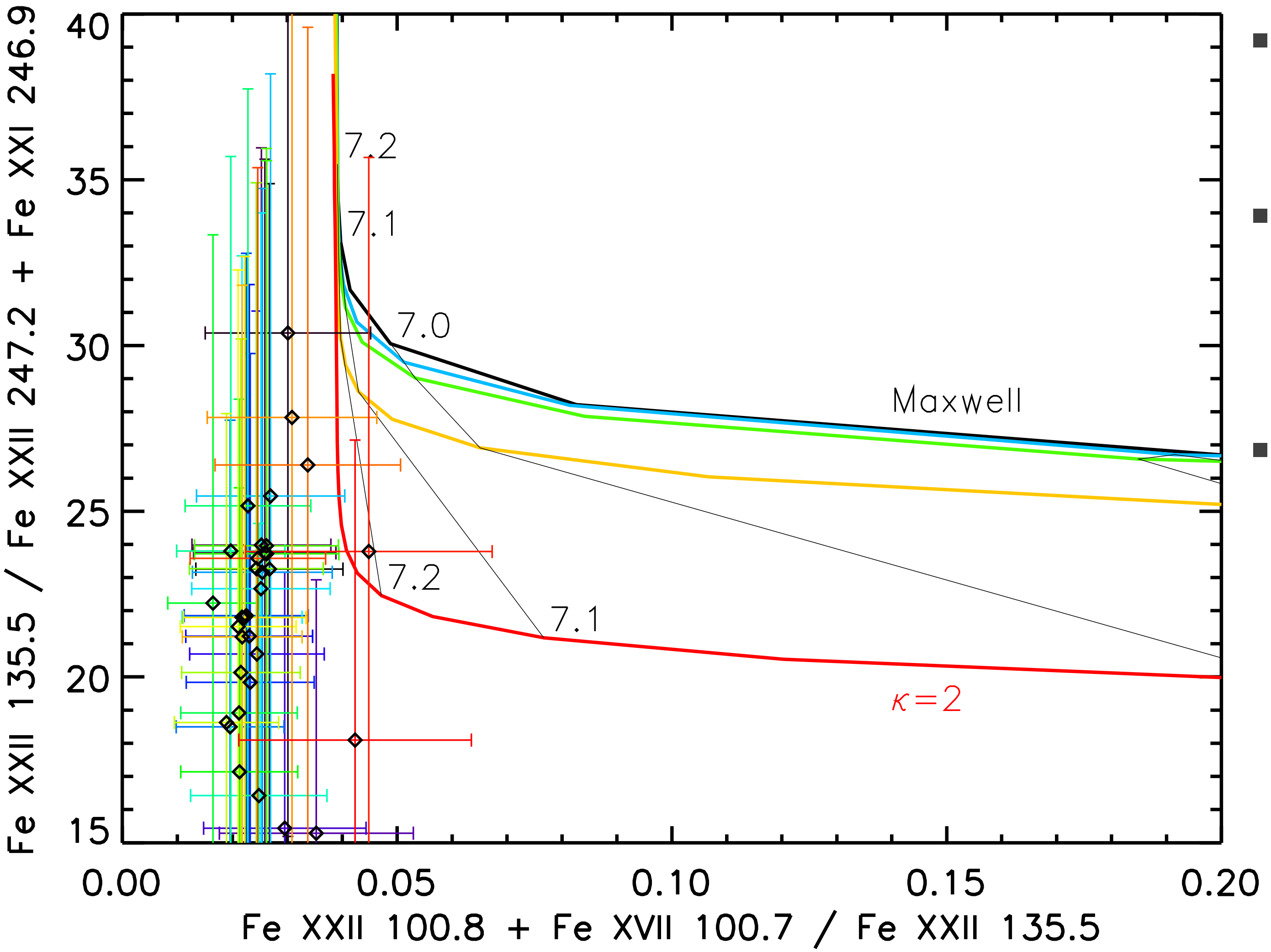

- **Ratio-ratio diagram method**
- **Data from SDO/EVE: Full-Sun X-ray and UV spectrometer**
- **Time in flare denoted by color: Blue – green – yellow – orange**

Dzifčáková et al. (2018), ApJ

The κ-distributions and TR lines

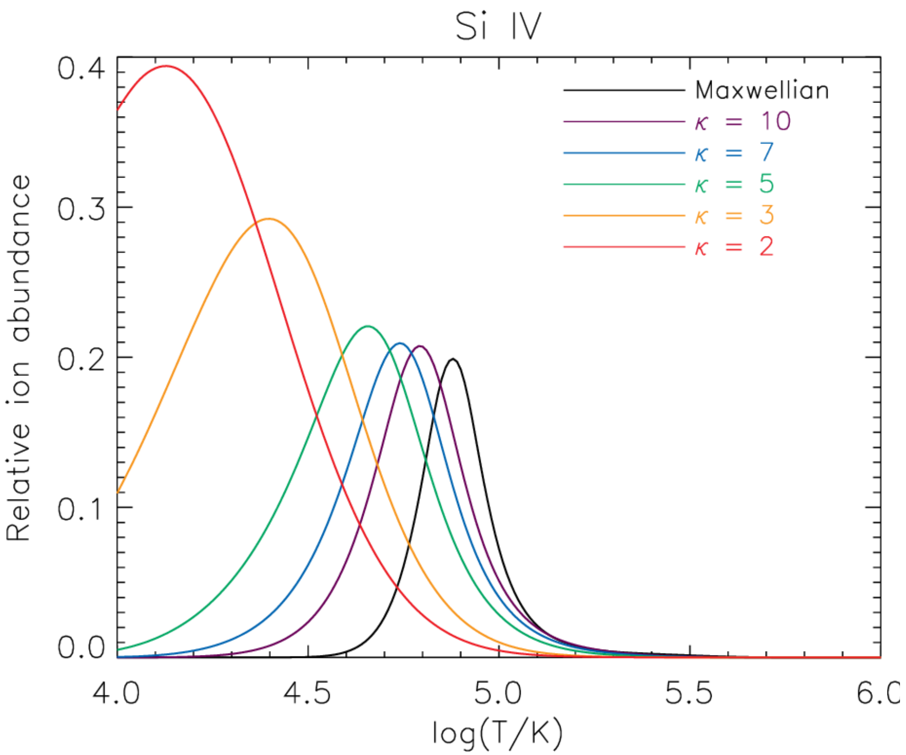

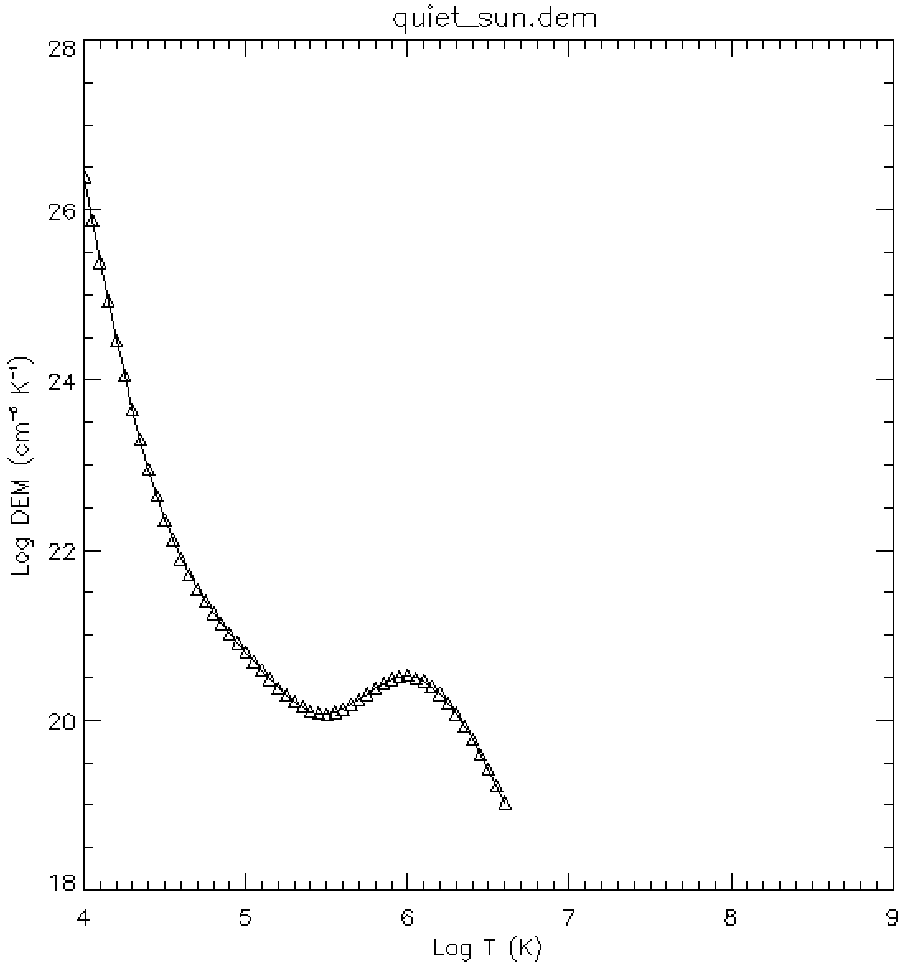

Dzifčáková & Dudík (2013), ApJS, 206, 6
Dudík et al. (2014), ApJL, 780, L12
Dzifčáková et al. (2017), A&A, 603, 14

- **For TR lines, ion abundance peaks are shifted to lower *T***
- **High-energy tail: ionization rate enhanced by orders of magnitude**
- **Recombination enhanced by a factor of < 2**

κ-distr.: Transition-Region Lines

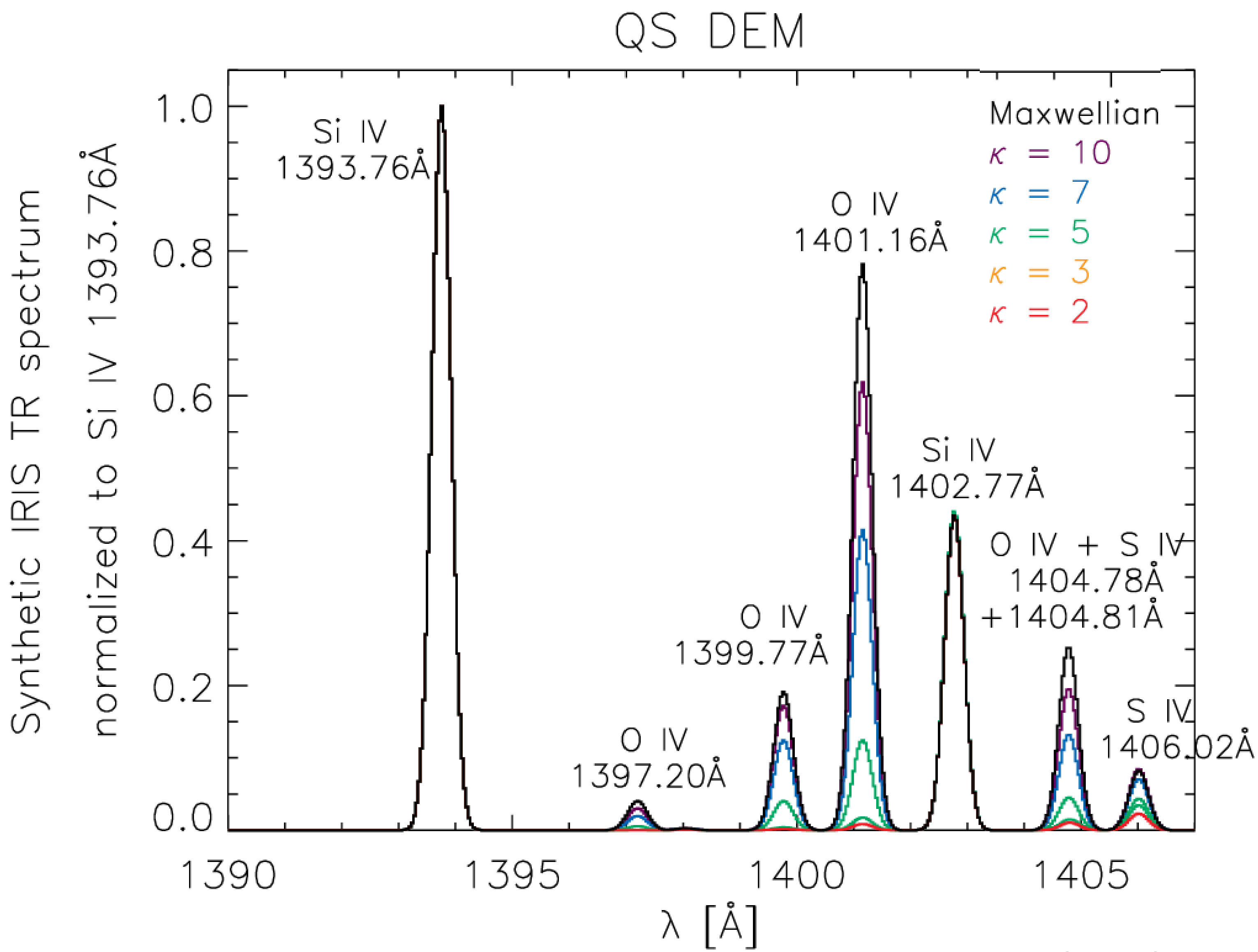

Dudík et al. (2014), ApJL, 780, 12

α Centauri A+B

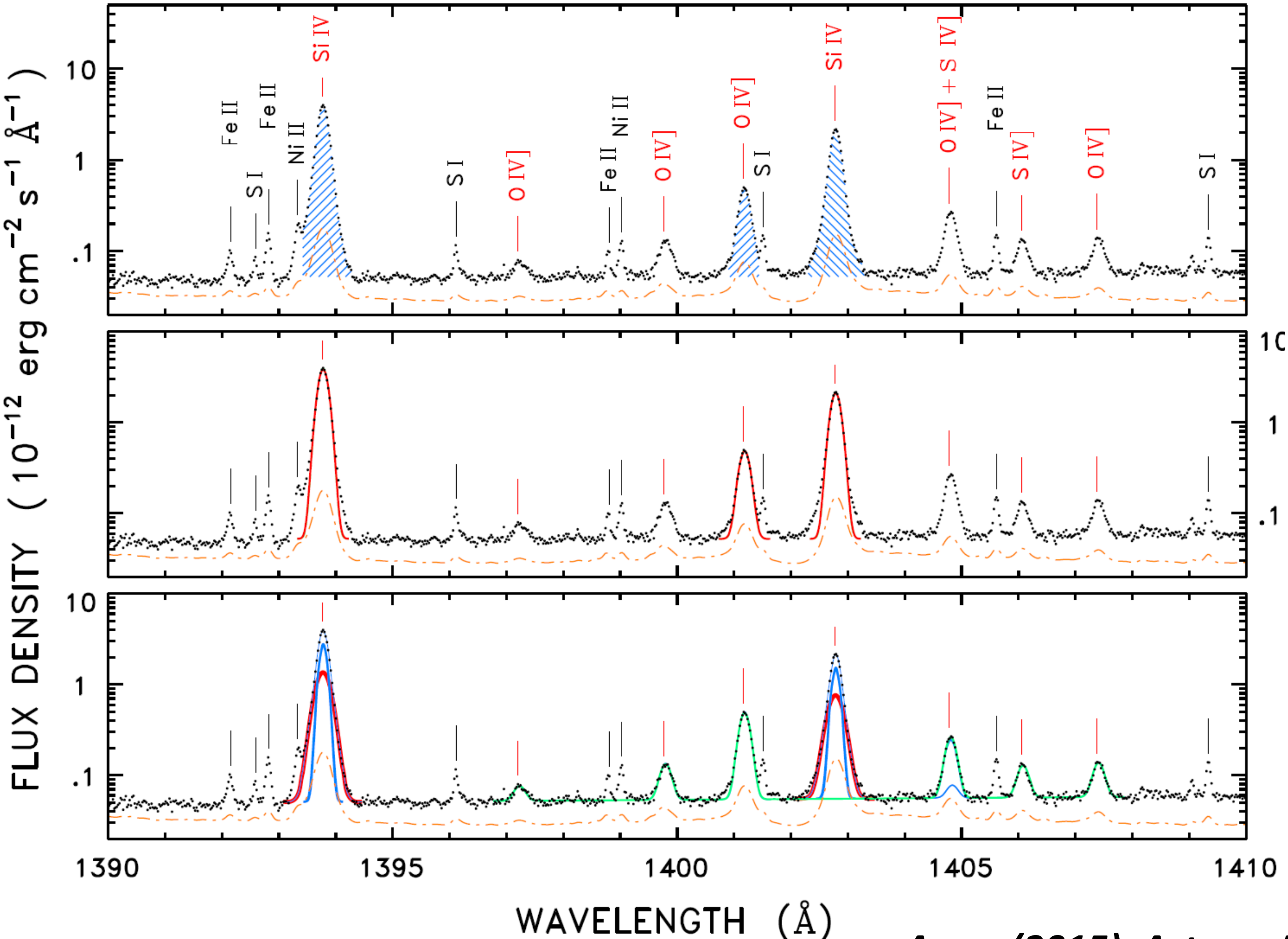

Ayres (2015), Astron. J., 149, 58

The κ-distributions: *f* (*v*)

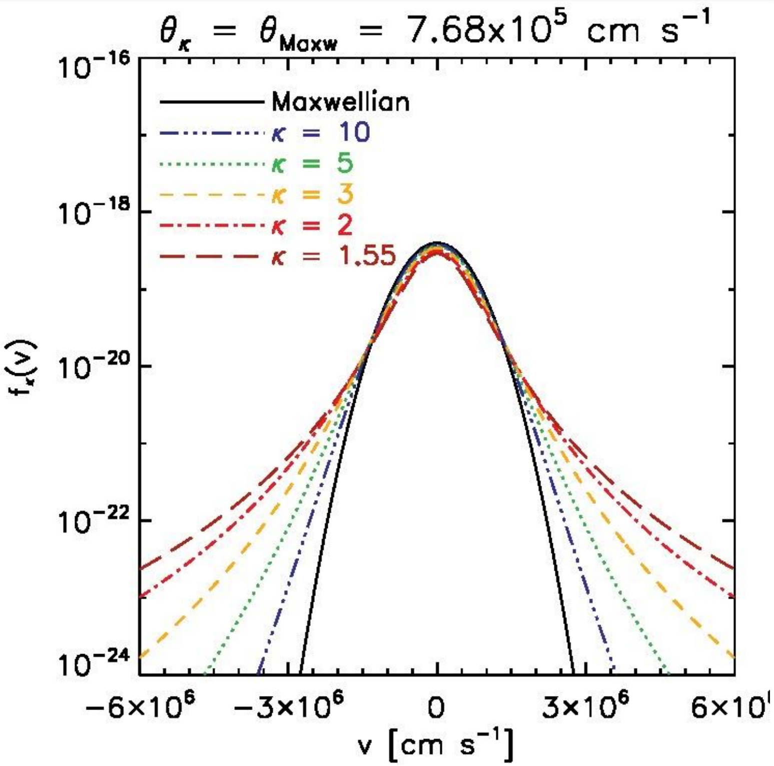

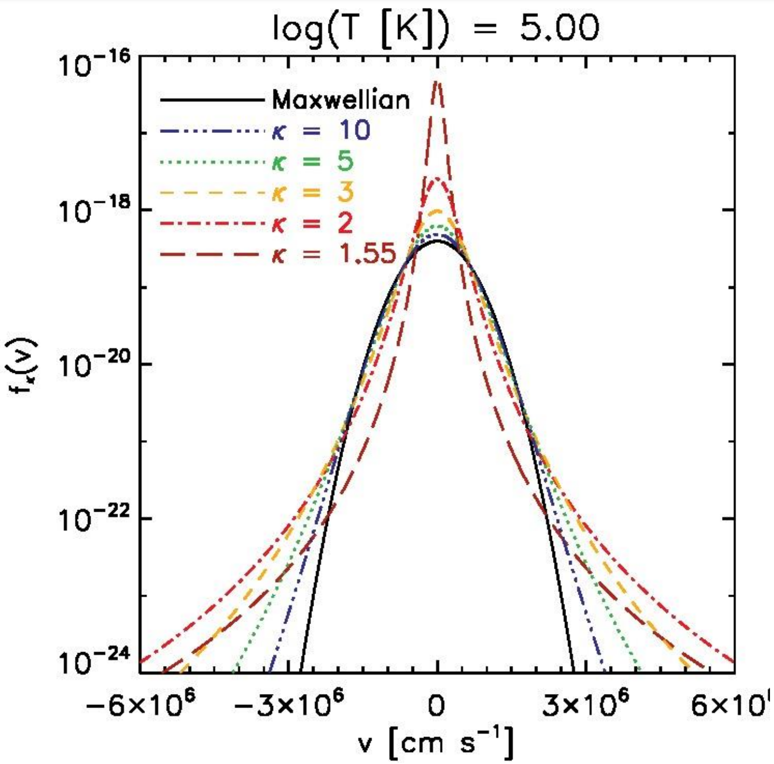

$$f_\kappa(v)\mathrm{d}v = \frac{C_\kappa}{(\pi(\kappa-3/2)\theta^2)^{3/2}} \frac{\mathrm{d}v}{\left(1+\frac{v^2}{(\kappa-3/2)\theta^2}\right)^{\kappa+1}}$$

$$T = \frac{m}{k_\mathrm{B}} \int v^2 f_\kappa(v)\mathrm{d}^3\vec{v} = \frac{m}{2k_\mathrm{B}} \frac{2\kappa}{2\kappa-3}\theta_\kappa^2$$

Olbert (1968)

Vasilyunas (1968)

Livadiotis (2015)

Lazar et al. (2016)

κ-Distributions and Line Profiles

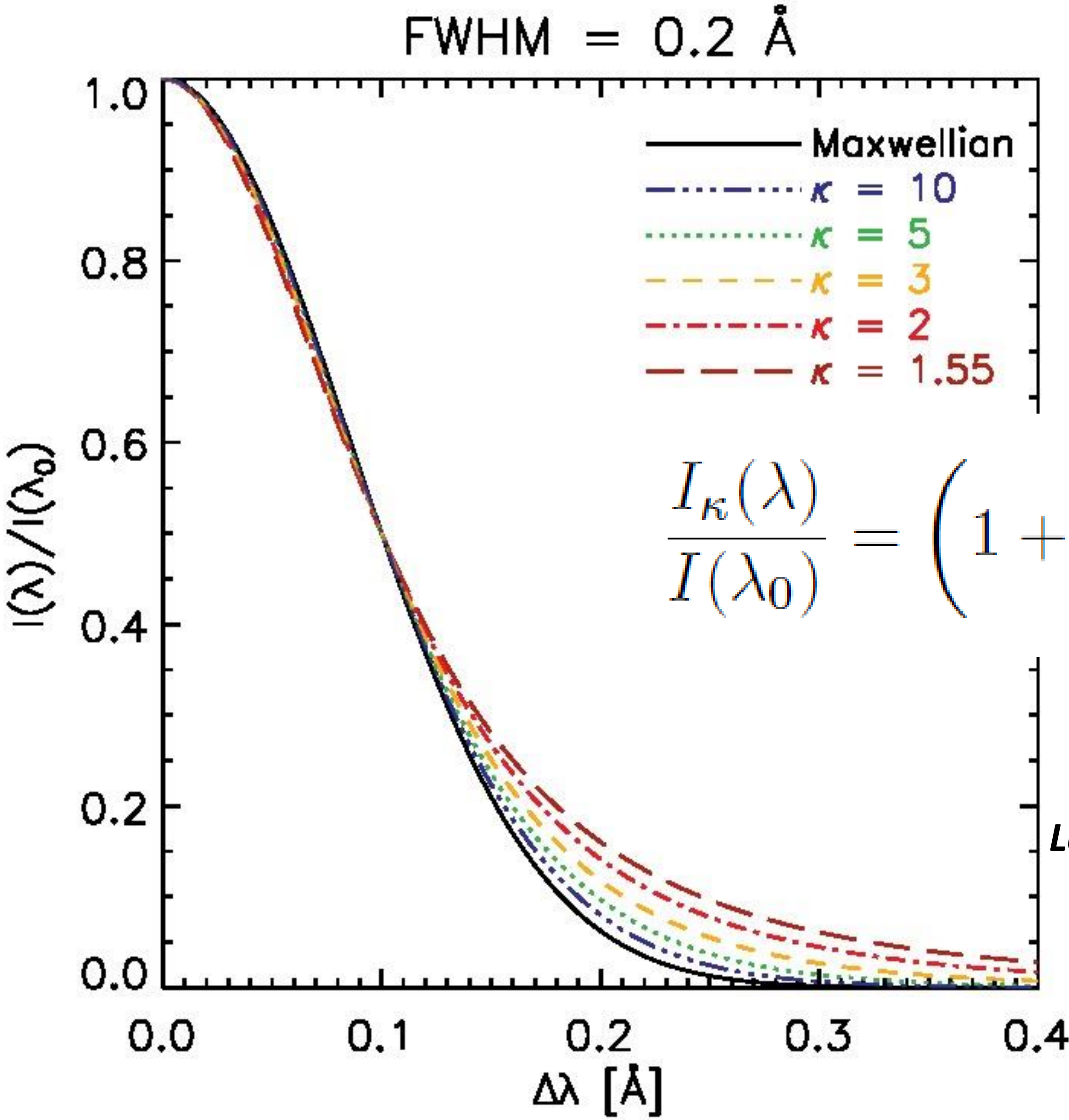

$$\Delta\lambda/\lambda_0 = v_{\|}/c$$

$$\frac{I_\kappa(\lambda)}{I(\lambda_0)} = \left(1 + \frac{mc^2(\lambda-\lambda_0)^2}{2k_\mathrm{B}T(\kappa-3/2)\lambda_0^2}\right)^{-\kappa}$$

Dzifčáková (1998), PhD Thesis
Lee, Williams & Lapenta (2013), unpubl.
Jeffrey et al. (2016), A&A, 590, A99
Jeffrey et al. (2017), ApJ, 836, 35
Jeffrey et al. (2018), ApJ, 855, 13

Dudík et al. (2017), ApJ, 842, 19

The IRIS Instrument

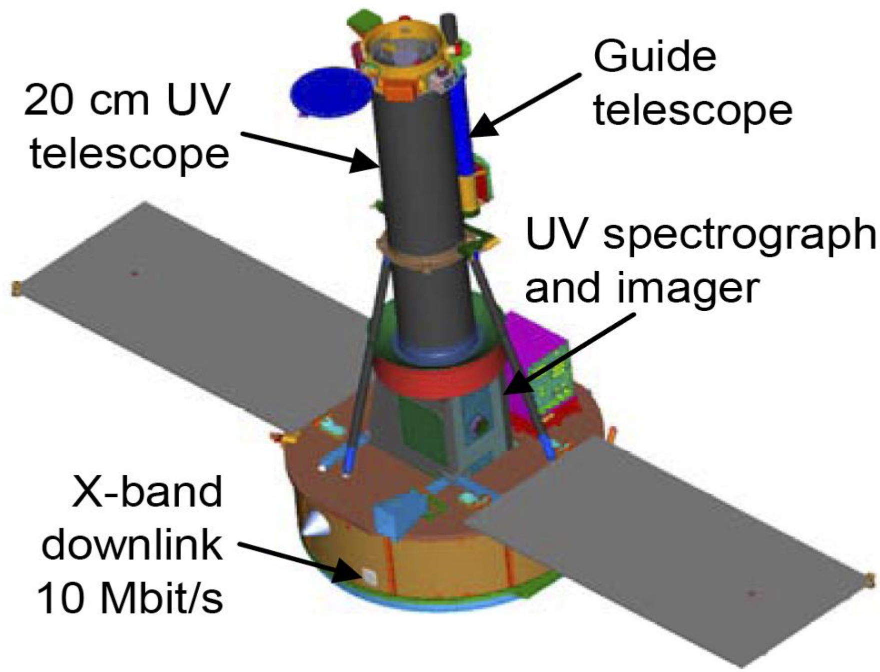

NUV and FUV Spectra Characteristics

SG Passband	Wavelength range (Å)	Spectral Dispersion (mÅ)	Spatial range (arcsec)	Spatial pixel size (arcsec)	CCD/ Camera	Shutter	Effective Area (cm^2)
FUV 1	1331.6-1358.4	12.98	175	0.166	1, CEB1	FUV SG	1.3
FUV 2	1380.6-1406.8	12.72	175	0.166	2, CEB1	FUV SG	1.3
NUV	2782.6-2833.9	25.46	175	0.166	3, CEB2	NUV SG	0.18

IRIS Example Spectrum

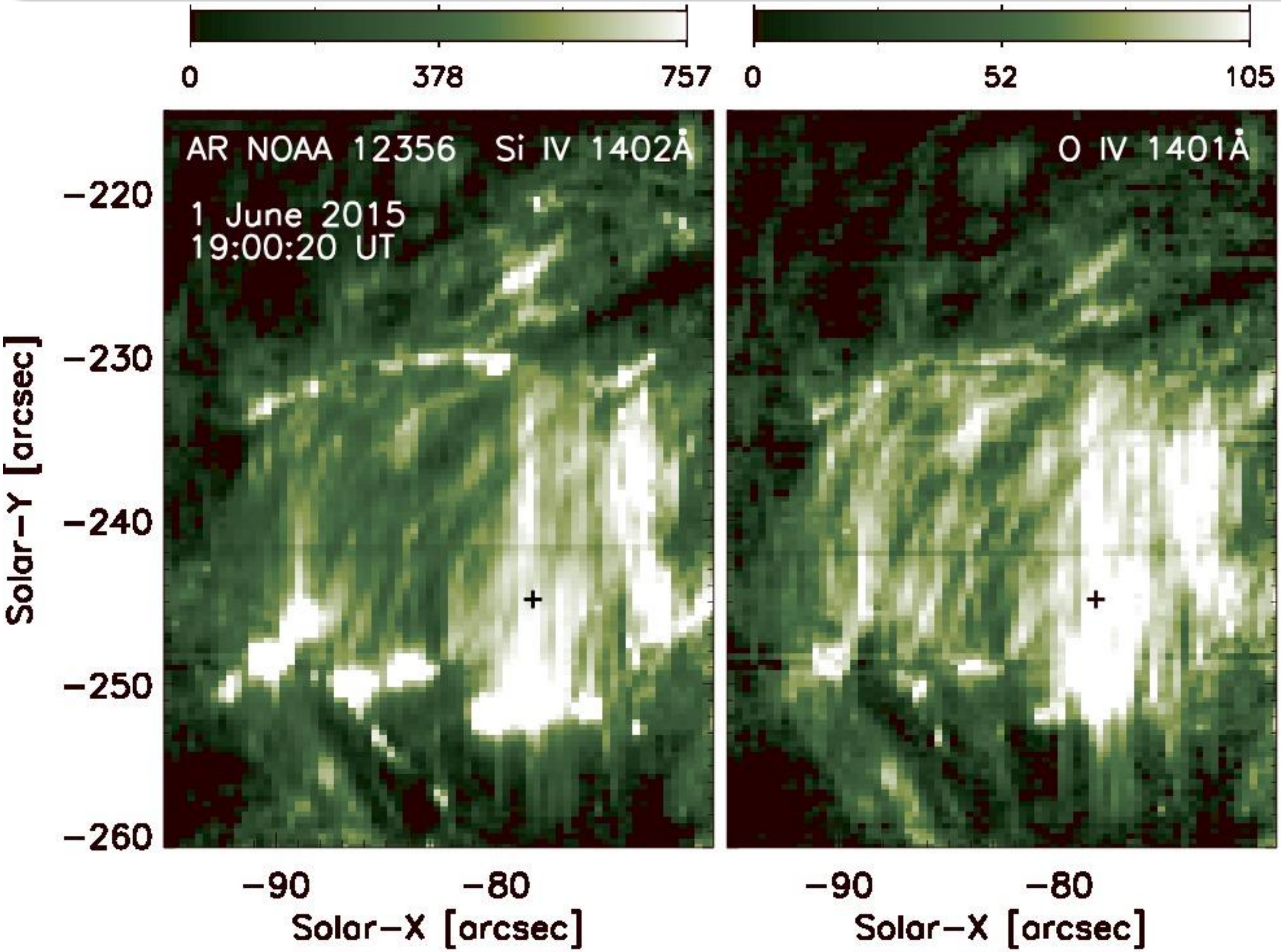

IRIS Example Spectrum: Fitting

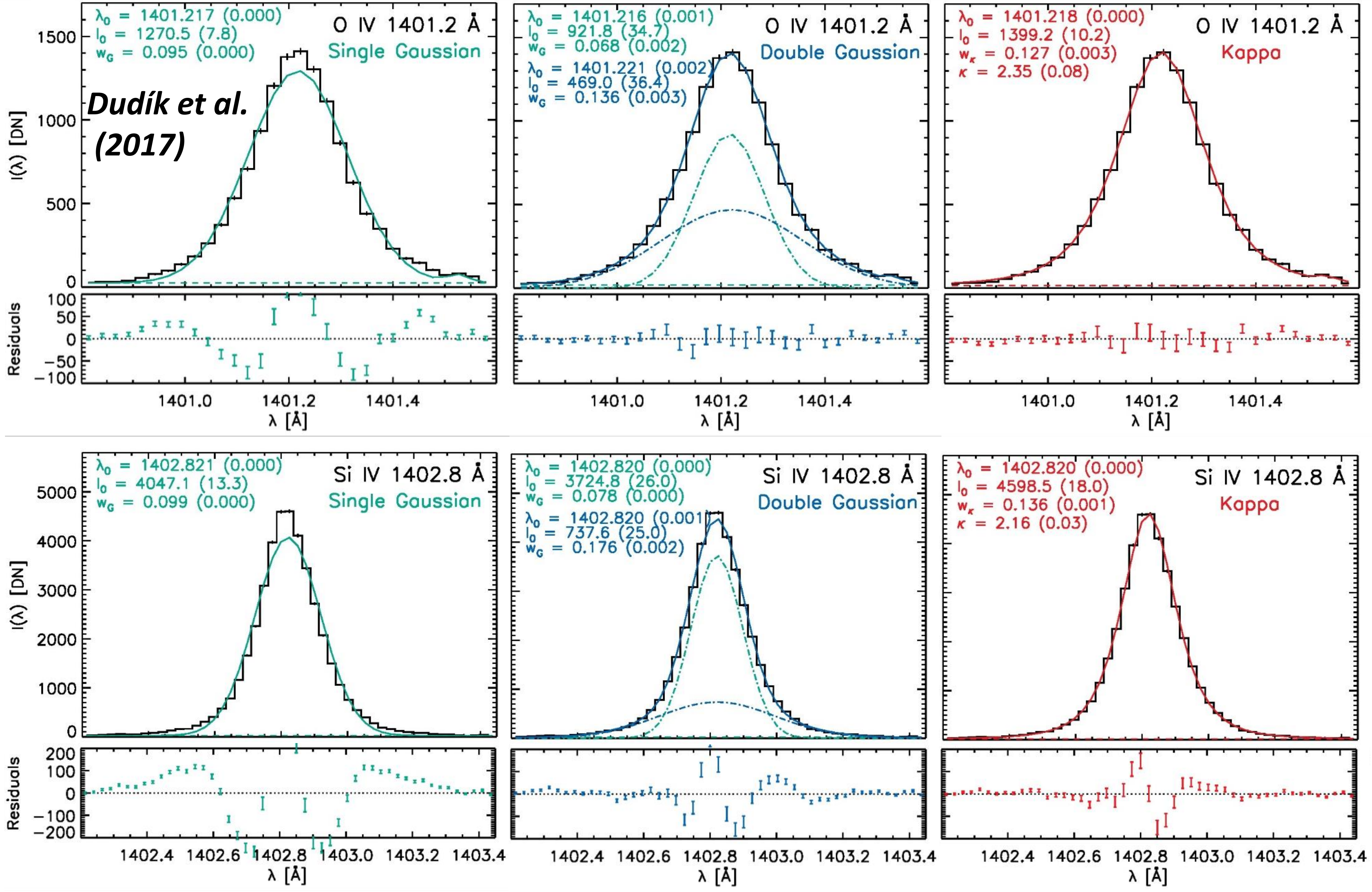

IRIS Example Spectrum: Fitting

Line	λ_0 [Å]	I_0 [DN]	w_κ [Å]	κ	FWHM_κ [Å]	T_i [MK]
O IV 1399.78 Å	1399.831 ± 0.001	385 ± 6	0.143 ± 0.010	2.16 ± 0.17	0.20 ± 0.08	1.81 ± 0.26
O IV 1401.16 Å	1401.218 ± 0.000	1399 ± 10	0.127 ± 0.003	2.35 ± 0.08	0.20 ± 0.05	1.43 ± 0.06
Si IV 1402.77 Å	1402.820 ± 0.000	4598 ± 18	0.136 ± 0.001	2.16 ± 0.03	0.19 ± 0.02	2.86 ± 0.06
O IV 1404.82 Å (bl S IV)	1404.855 ± 0.001	383 ± 6	0.163 ± 0.018	1.90 ± 0.13	0.19 ± 0.13	2.35 ± 0.52
S IV 1406.06 Å	1406.103 ± 0.001	282 ± 5	0.144 ± 0.021	1.91 ± 0.18	0.17 ± 0.17	3.64 ± 1.08

- **(Almost) consistent κ values derived from all five TR lines**
- **All five lines have the same FWHM**
- **Significant non-thermal widths**

$$w_\kappa^2 = \frac{1}{2}\frac{\lambda_0^2}{c^2}\left(\theta^2 + (\theta^{(\mathrm{nth})})^2\right) = (w_\kappa^{(\mathrm{th})})^2 + (w_\kappa^{(\mathrm{nth})})^2$$

Line	w_κ [Å]	$\log(T_{\mathrm{max,Maxw}}$ [K])	$w_{\mathrm{Maxw}}^{(\mathrm{th})}$	$w_{\mathrm{Maxw}}^{(\mathrm{nth})}$	$\log(T_{\mathrm{max},\kappa=2}$ [K])	$w_{\kappa=2}^{(\mathrm{th})}$	$w_{\kappa=2}^{(\mathrm{nth})}$
O IV 1399.78 Å	0.143 ± 0.010	5.15	0.040	0.137	4.45	0.018	0.141
O IV 1401.16 Å	0.127 ± 0.003	5.15	0.040	0.121	4.45	0.018	0.126
Si IV 1402.77 Å	0.136 ± 0.001	4.90	0.023	0.134	4.10	0.009	0.136
O IV 1404.82 Å (bl S IV)	0.163 ± 0.018	5.15	0.040	0.158	4.45	0.018	0.162
S IV 1406.06 Å	0.144 ± 0.021	5.05	0.025	0.141	4.20	0.009	0.143

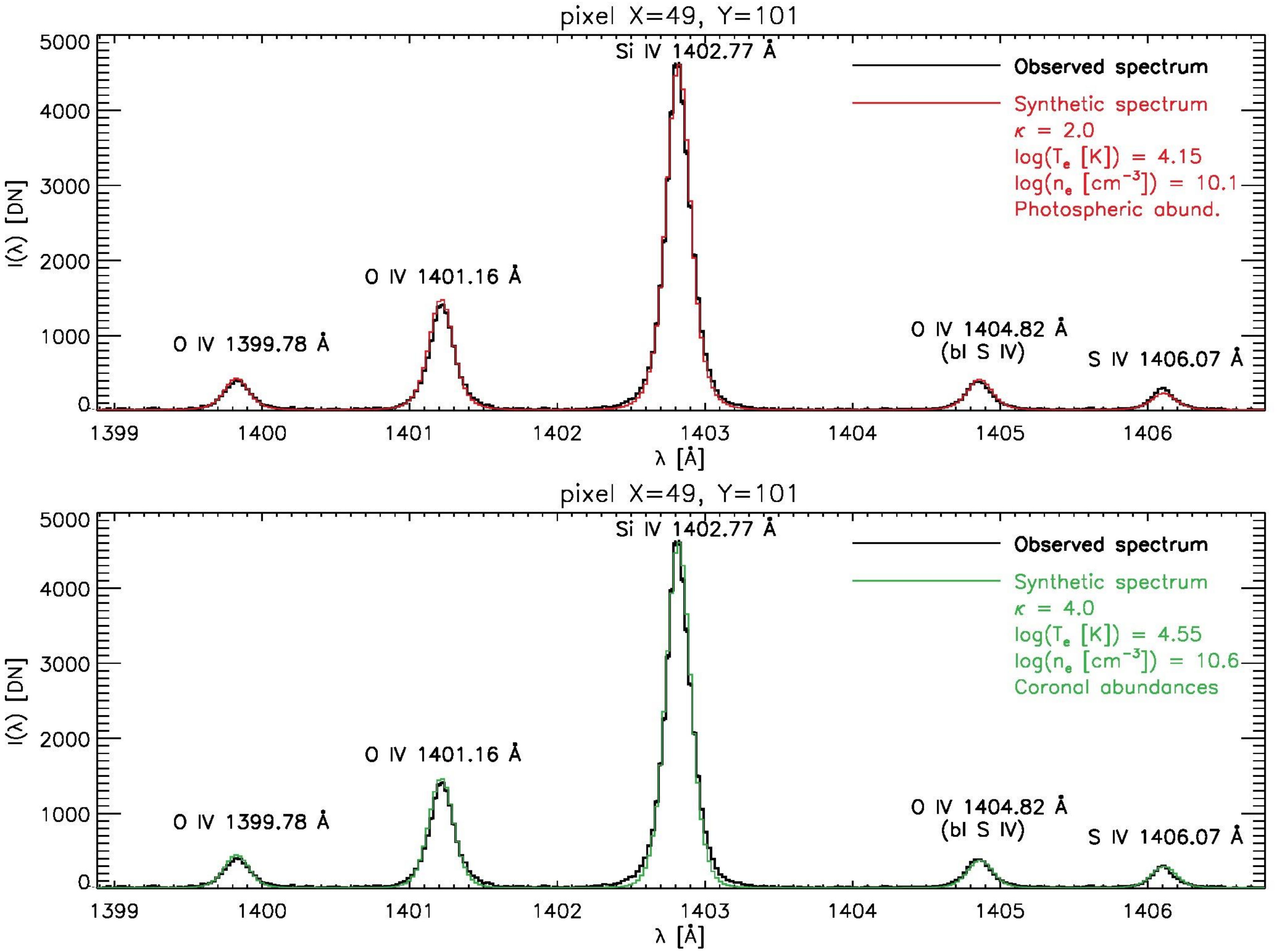
pixel X=49, Y=101
Si IV 1402.77 Å
O IV 1401.16 Å
O IV 1399.78 Å
O IV 1404.82 Å
(bl S IV)
S IV 1406.07 Å
Observed spectrum
Synthetic spectrum
κ = 2.0
log(Te [K]) = 4.15
log(ne [cm−3]) = 10.1
Photospheric abund.
I(λ) [DN]
λ [Å]
pixel X=49, Y=101
Si IV 1402.77 Å
O IV 1401.16 Å
O IV 1399.78 Å
O IV 1404.82 Å
(bl S IV)
S IV 1406.07 Å
Observed spectrum
Synthetic spectrum
κ = 4.0
log(Te [K]) = 4.55
log(ne [cm−3]) = 10.6
Coronal abundances
I(λ) [DN]
λ [Å]

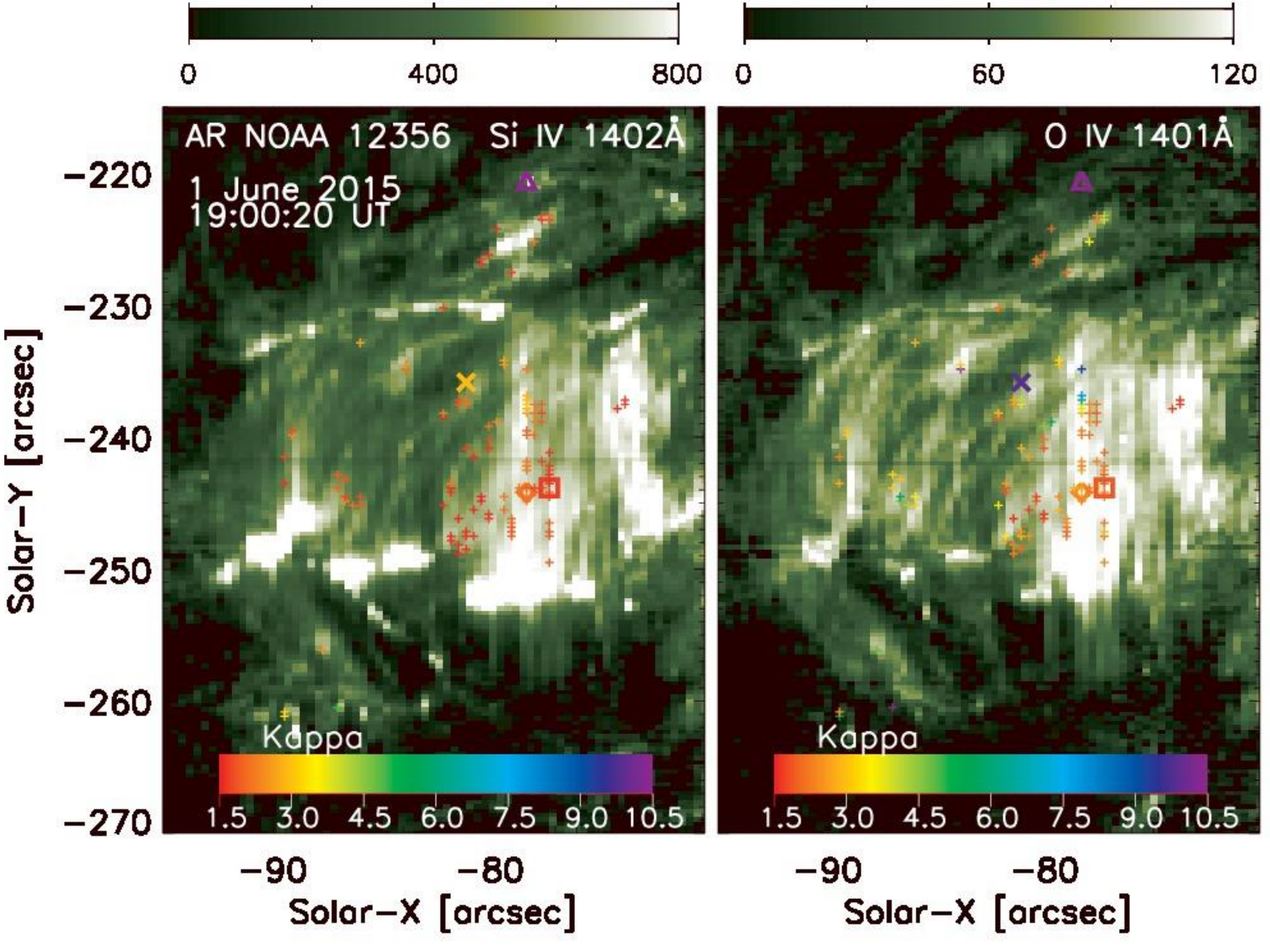

0
400
800
0
60
120
AR NOAA 12356
Si IV 1402Å
1 June 2015
19:00:20 UT
O IV 1401Å
−220
−230
−240
−250
−260
−270
Solar−Y [arcsec]
Kappa
1.5 3.0 4.5 6.0 7.5 9.0 10.5
Kappa
1.5 3.0 4.5 6.0 7.5 9.0 10.5
−90
−80
Solar−X [arcsec]
−90
−80
Solar−X [arcsec]

More cases…

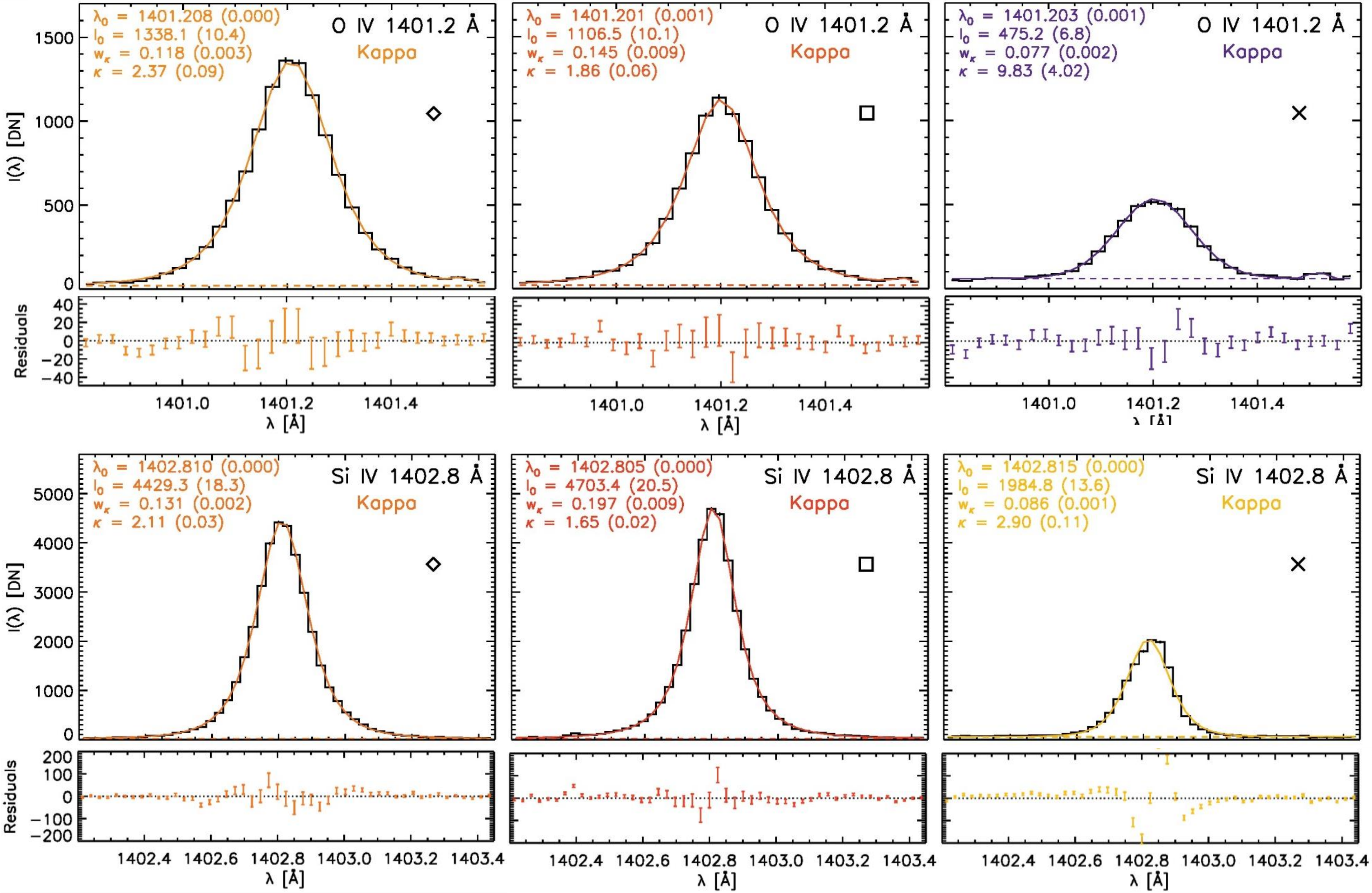

λ0 = 1401.208 (0.000)
I0 = 1338.1 (10.4)
wκ = 0.118 (0.003)
κ = 2.37 (0.09)
O IV 1401.2 Å
Kappa
λ0 = 1401.201 (0.001)
I0 = 1106.5 (10.1)
wκ = 0.145 (0.009)
κ = 1.86 (0.06)
O IV 1401.2 Å
Kappa
λ0 = 1401.203 (0.001)
I0 = 475.2 (6.8)
wκ = 0.077 (0.002)
κ = 9.83 (4.02)
O IV 1401.2 Å
Kappa
I(λ) [DN]
Residuals
λ [Å]
λ0 = 1402.810 (0.000)
I0 = 4429.3 (18.3)
wκ = 0.131 (0.002)
κ = 2.11 (0.03)
Si IV 1402.8 Å
Kappa
λ0 = 1402.805 (0.000)
I0 = 4703.4 (20.5)
wκ = 0.197 (0.009)
κ = 1.65 (0.02)
Si IV 1402.8 Å
Kappa
λ0 = 1402.815 (0.000)
I0 = 1984.8 (13.6)
wκ = 0.086 (0.001)
κ = 2.90 (0.11)
Si IV 1402.8 Å
Kappa

Gaussian pixel Δ

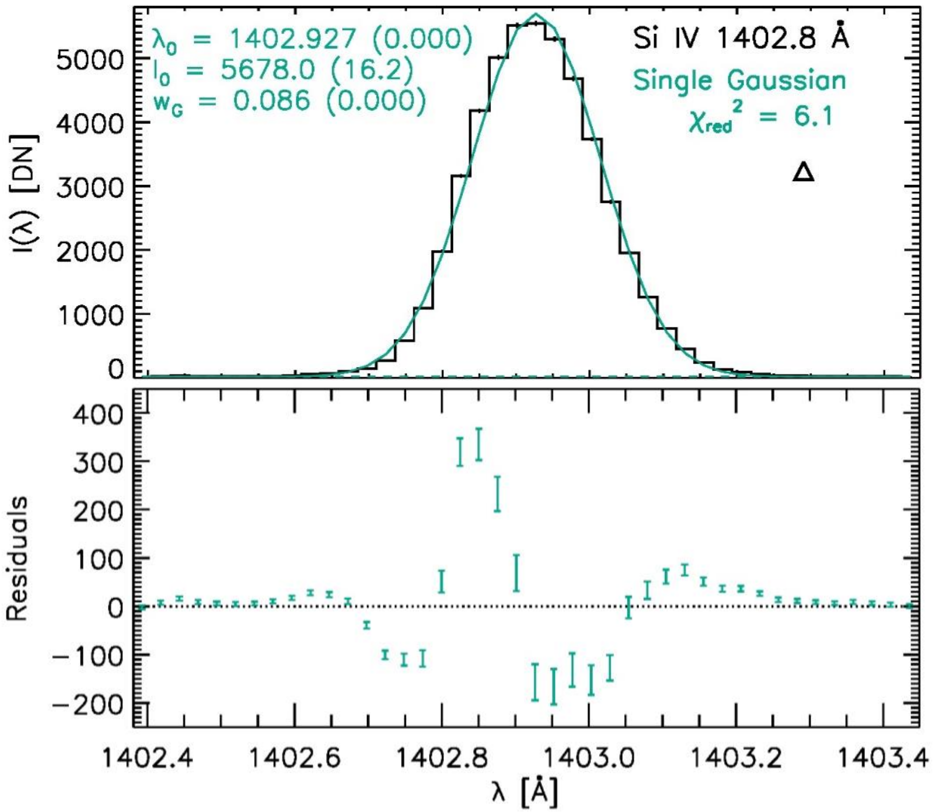

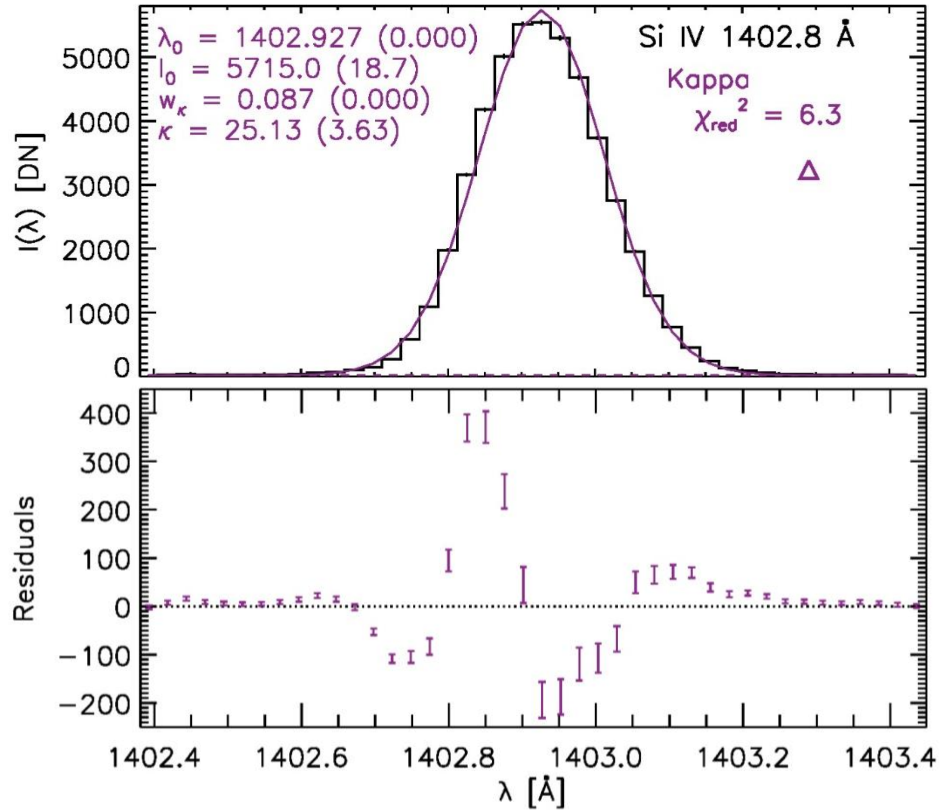

- **Detection of a single, very bright Gaussian pixel**
- **Third brightest pixel with symmetric profiles**
- **The non- Gaussian profiles are *not* caused by instrumental effects**
- **Larger / asymmetric residuals: Possibly 2 Gaussian components**

Flare of 2017-09-10

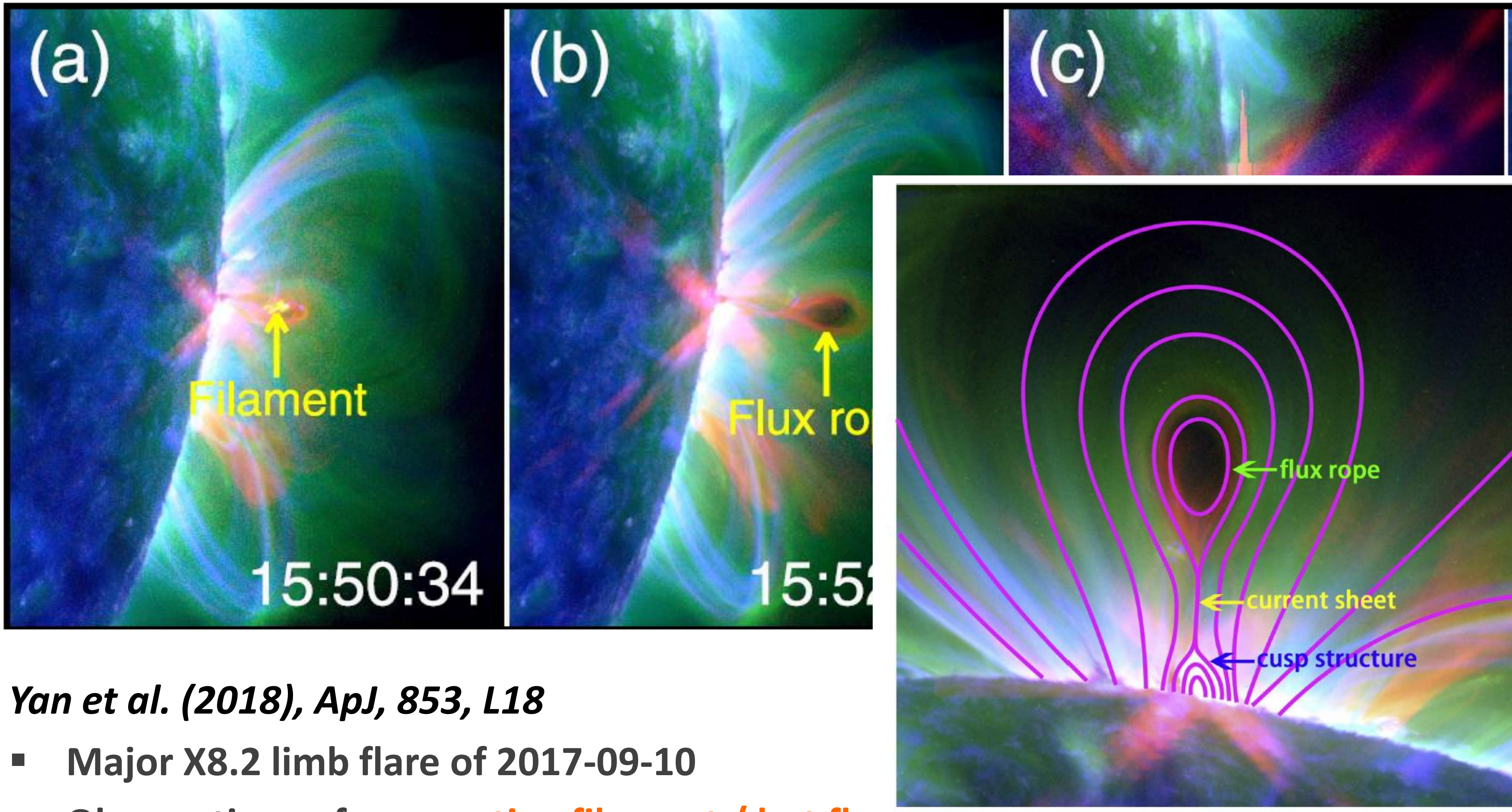

Yan et al. (2018), ApJ, 853, L18

- Major X8.2 limb flare of 2017-09-10
- Observations of an erupting filament / hot flux rope
- After eruption: Long, protruding "current sheet" structure
- Properties of the current sheet in *Warren et al. (2018, ApJ, 854, 122)*

Fe XXIV Profiles in the Flare

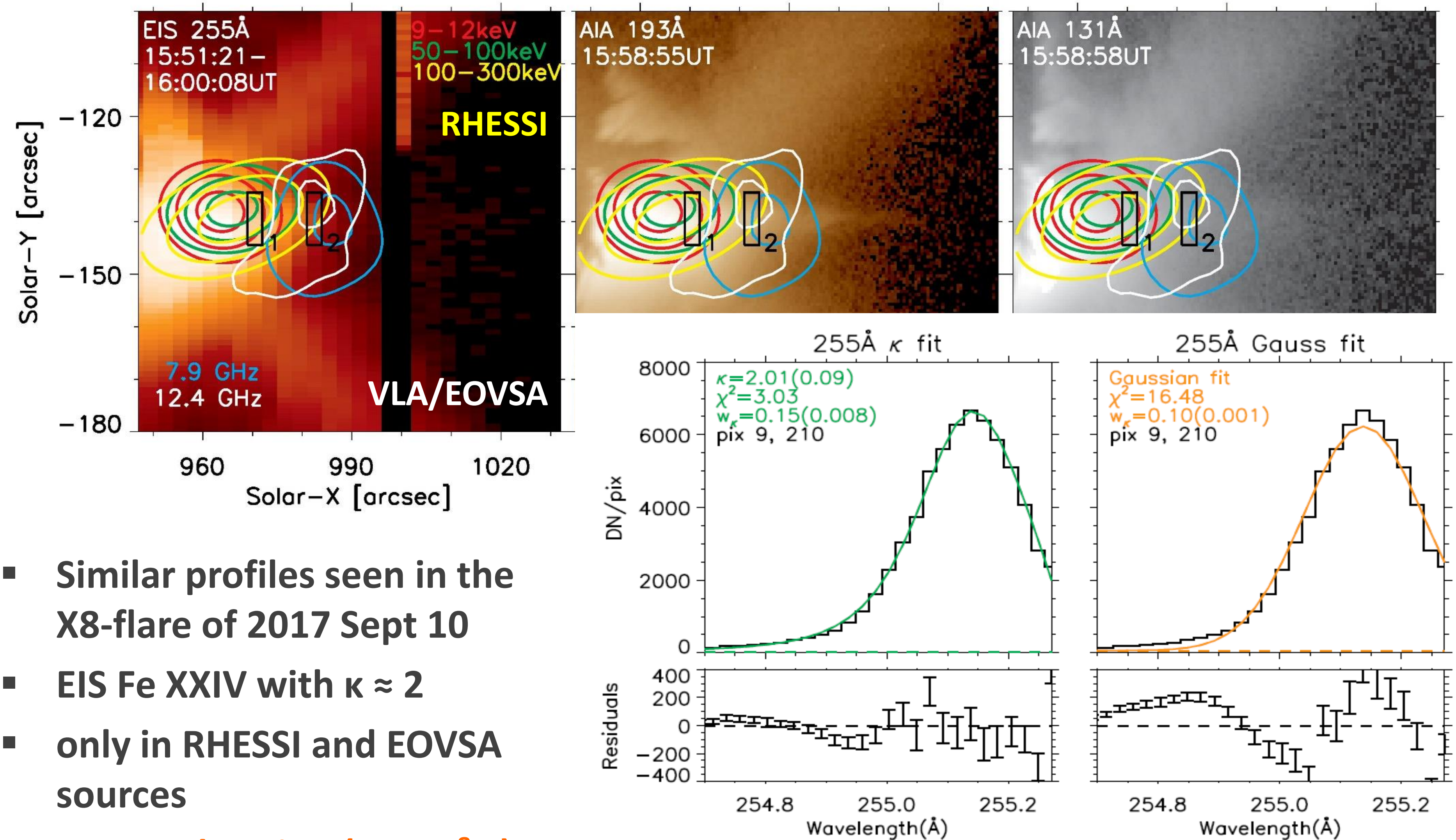

- Similar profiles seen in the X8-flare of 2017 Sept 10
- EIS Fe XXIV with κ ≈ 2
- only in RHESSI and EOVSA sources
- Ion acceleration ($T > 10^8$ K)
- Turbulence ($v_{nth} > 200$ km/s)

Polito, Dudík, et al. (2018), ApJ, 864, 63

Map of Fe XXIV Profiles

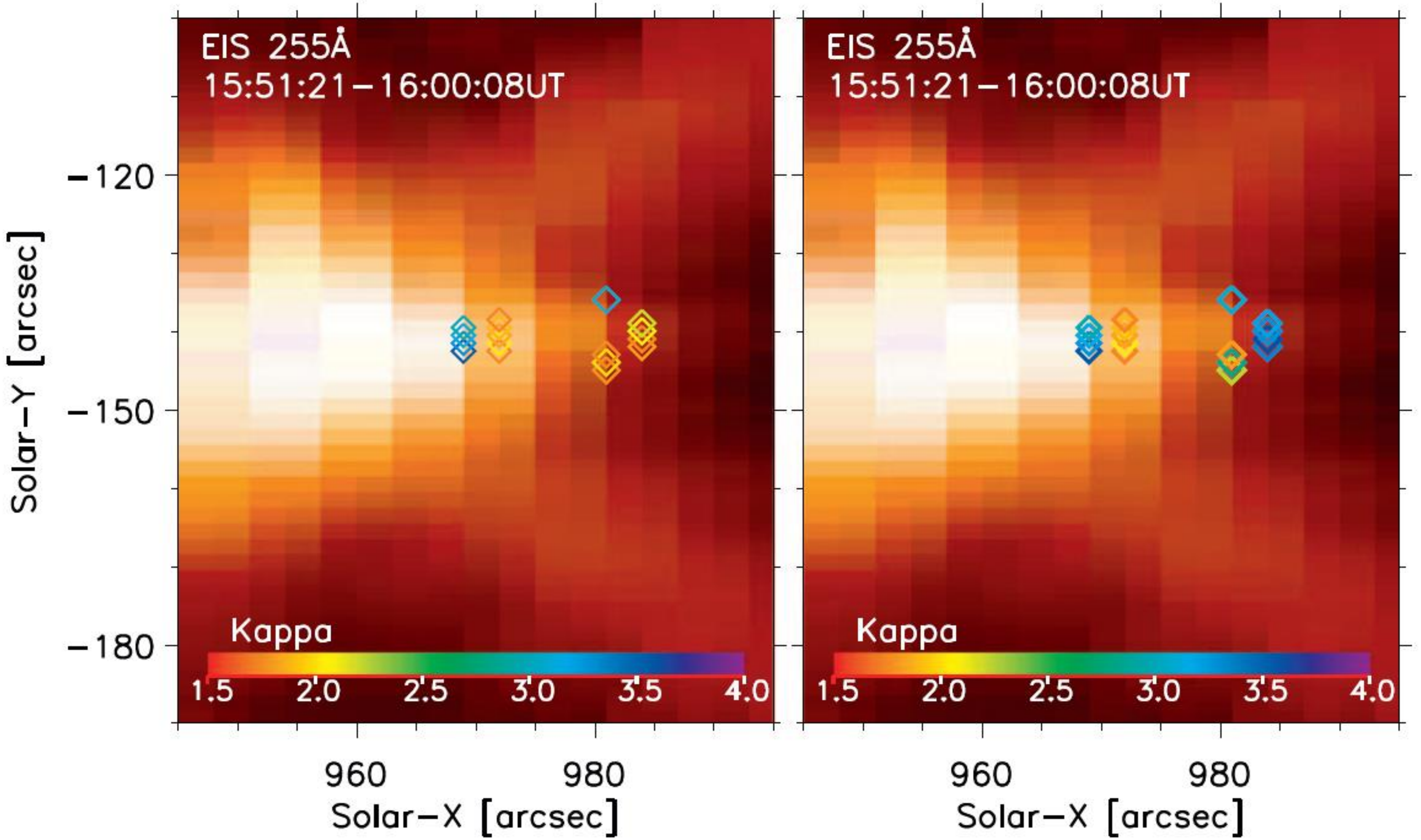

- κ derived from Fe XXIV 255 Å Fe XXIV 192 Å

Influence on Diagnostics of *T*

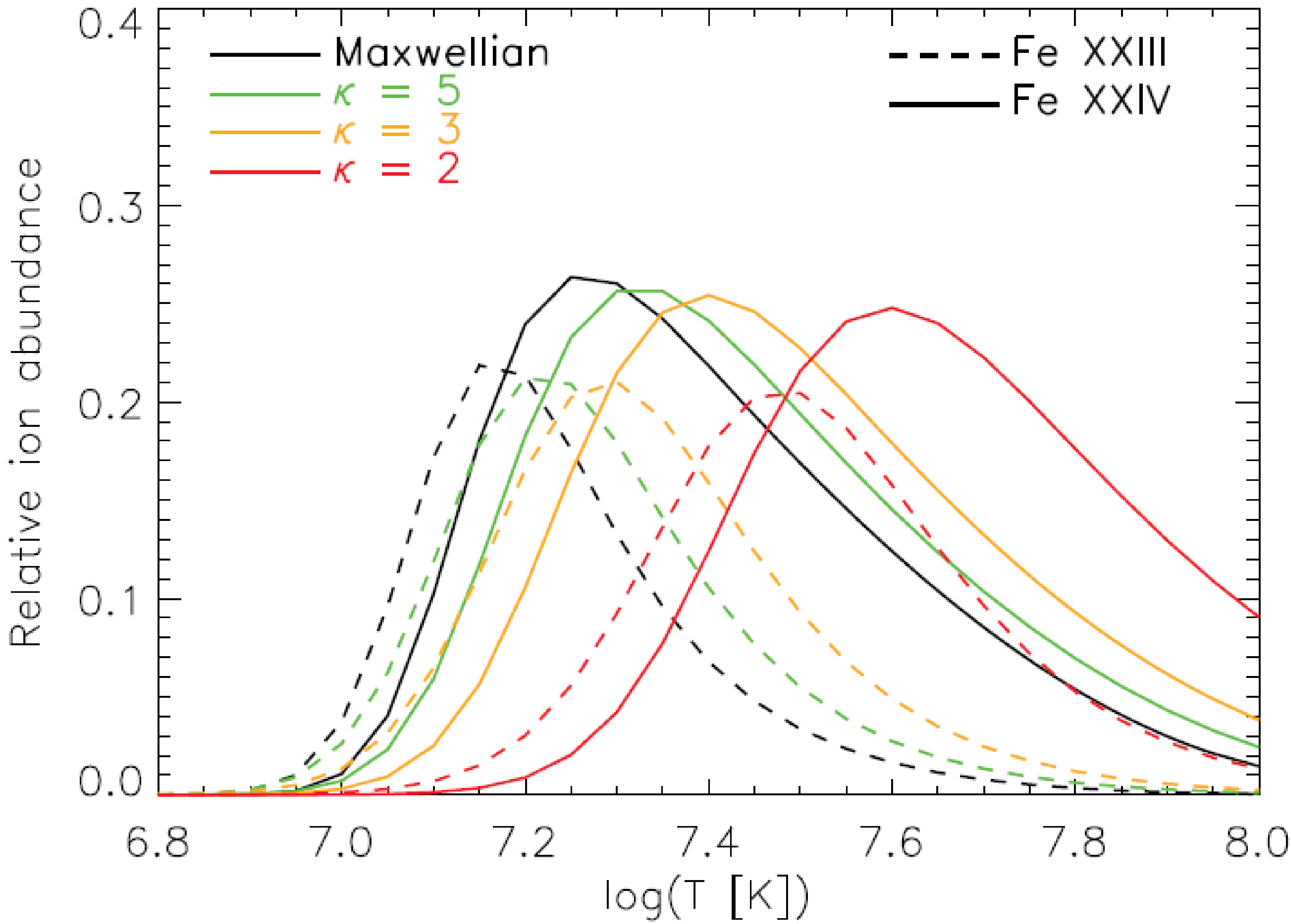

Influence on Diagnostics of *T*

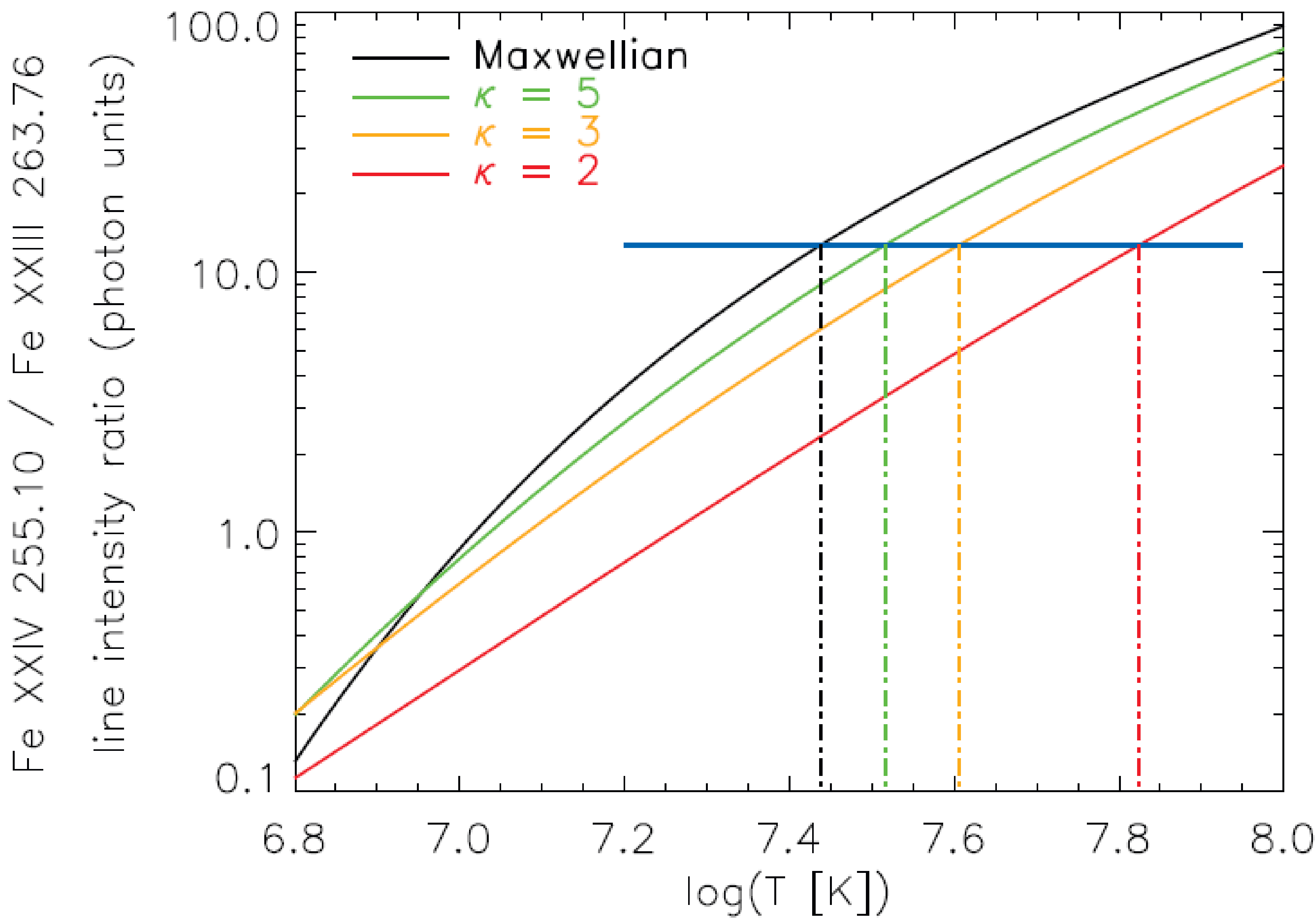

Integrating NEI and n-Maxw

- **Beam heating in HYDRAD**
  Reep et al. (2013), ApJ 778, 76
  Reep et al. (2015), ApJ, 808, 177

- **Incorporating the κ-distributions directly using KAPPA package**
  Calculation of lookup tables for:
  – ionization/recombination rates
  – ionization equilibrium
  – emissivities as a function of *T*
  – wvl resolved emissivities

- **Numerical experiments with beam passing through corona**
  – Distribution periodically changes from Maxwellian to κ = 2
  – Bulk of the distribution is the same but the temperature changes: 1 MK --> 4 MK
  – Small periods (5 – 60 s)

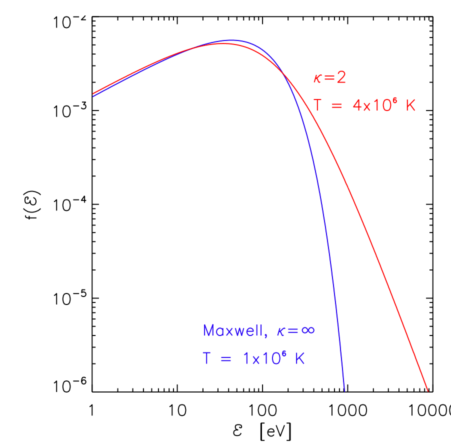

Dzifčáková et al. (2016), A&A, 589, 69

Integrating NEI and non-Maxw

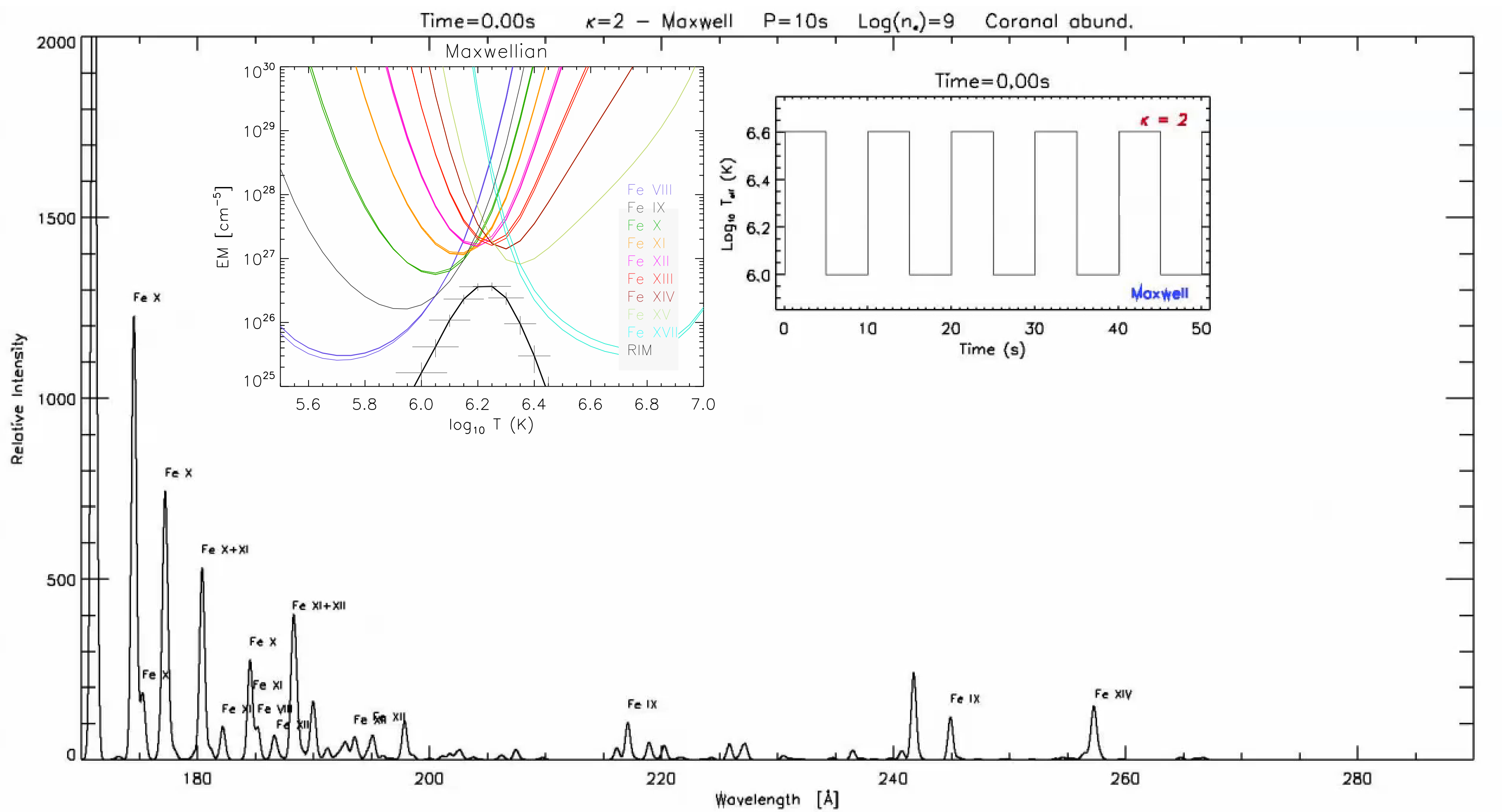

Summary: Non-Maxwellians

Non-Maxwellians observed in solar wind, flares, TR, and corona
And derived in modelling: reconnection, Si IV blue-shifts

One more parameter (at least)
Ionization, recombination, and excitation rates are strongly affected
Ionization rates are more strongly affected at low *T*
→ spectra are affected
TR line spectra can show decreased O IV compared to Si IV
AIA temperature responses, DEMs, …

Diagnostics is more difficult
requires lines with different wavelengths (instrumentation consequences)

Calculation of non-Maxwellian spectra (tools) are freely available
The KAPPA database: http://kappa.asu.cas.cz
The Maxwellian decomposition technique

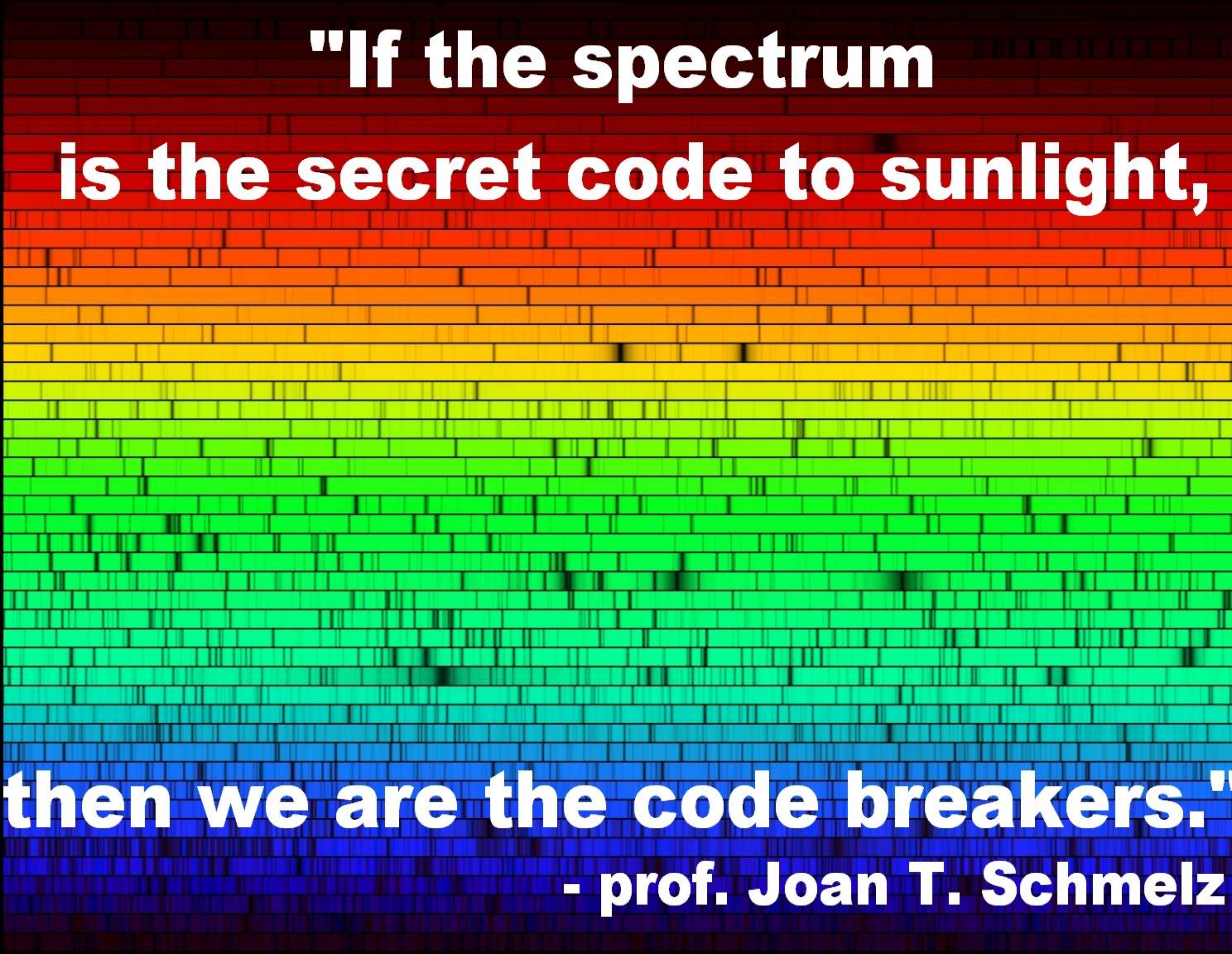
"If the spectrum
is the secret code to sunlight,
then we are the code breakers."
- prof. Joan T. Schmelz

κ-distr.: Free-free Continuum

- **Emissivity of the free-free continuum for *κ*-distributions**

$$P_{\rm ff}(\lambda,\kappa) = \mathcal{A}_\kappa C T^{1/2} \int_0^\infty \frac{g_{\rm ff}(y,w)}{\left(1+\frac{y+w}{\kappa-3/2}\right)^{\kappa+1}} {\rm d}y,$$

where $w = hc/\lambda k_{\rm B}T$

- **The constant *C* depends on abundances and the ionization equilibrium**

$$C = \frac{1}{4\pi}\frac{32\pi}{3}\frac{e^6}{m_{\rm e}c^2\lambda^2}\sqrt{\frac{2\pi k_{\rm B}}{3m_{\rm e}}}n_{\rm e}n_{\rm H}\sum_Z\sum_k k^2\frac{n_k}{n_Z}A_Z,$$

Dudík et al., 2012, A&A 539, A107

κ-distr.: Free-free Continuum

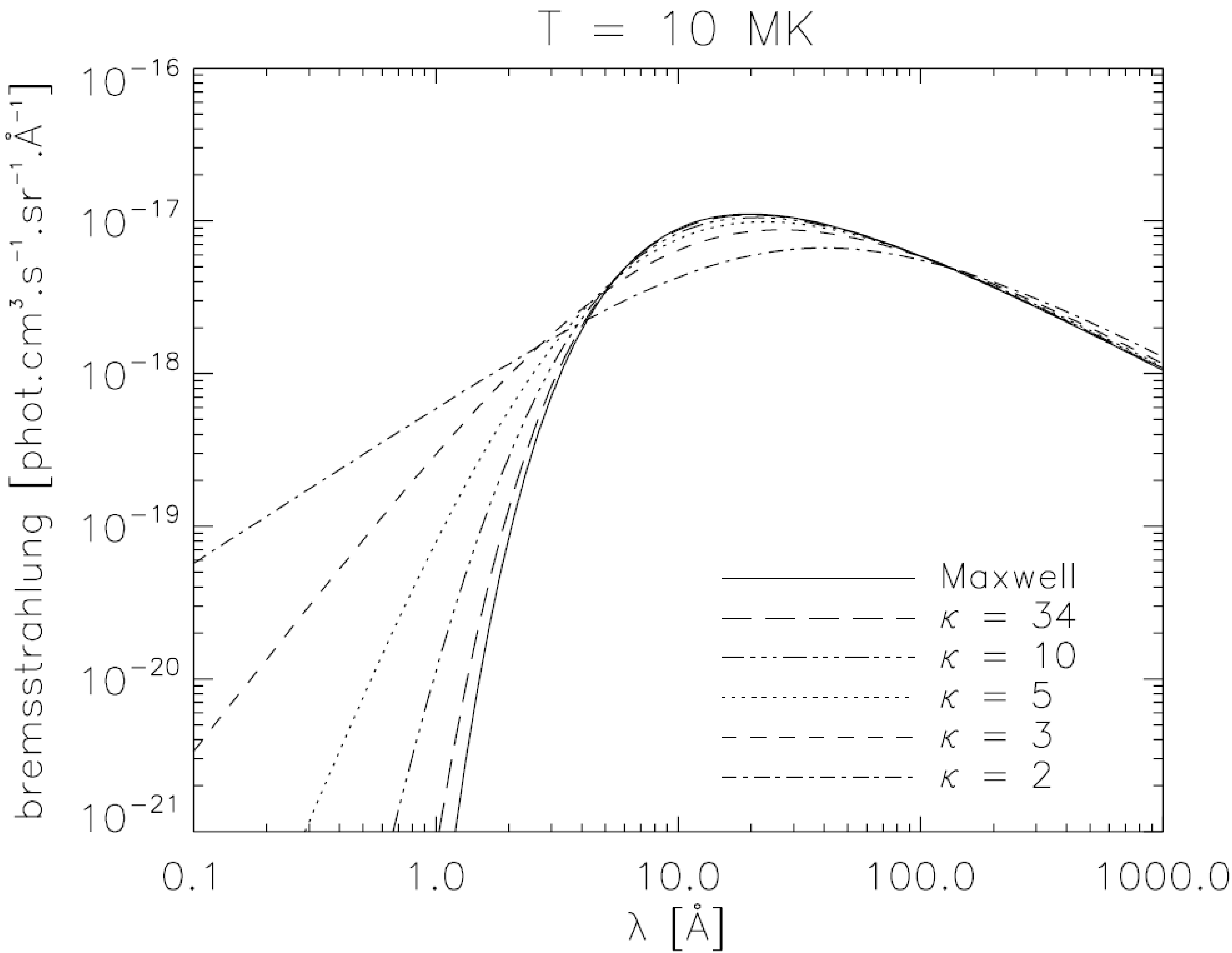

κ-distr.: Free-bound continuum

- **Emissivity of the free-bound continuum for *κ*-distributions**

$$P_{\rm fb}(E,\kappa) = \frac{1}{4\pi}\sqrt{\frac{2}{\pi}}\frac{1}{hc^3 m_{\rm e}^{3/2} k_{\rm B}^{3/2}}\frac{E^5}{T^{3/2}} n_{\rm e} n_{\rm H} \times \sum_{i,k,Z} \frac{n_{\rm k+1}}{n_Z} A_Z \frac{g_i}{g_0} \sigma_i^{\rm bf} \mathcal{A}_\kappa \frac{1}{\left(1+\frac{E-I_i}{(\kappa-3/2)k_{\rm B}T}\right)^{\kappa+1}}$$

- **Depends directly on the distribution function**
- **Influenced by the number of low-energy electrons**

Dudík et al., 2012, A&A 539, A107

κ-distr.: Free-bound continuum

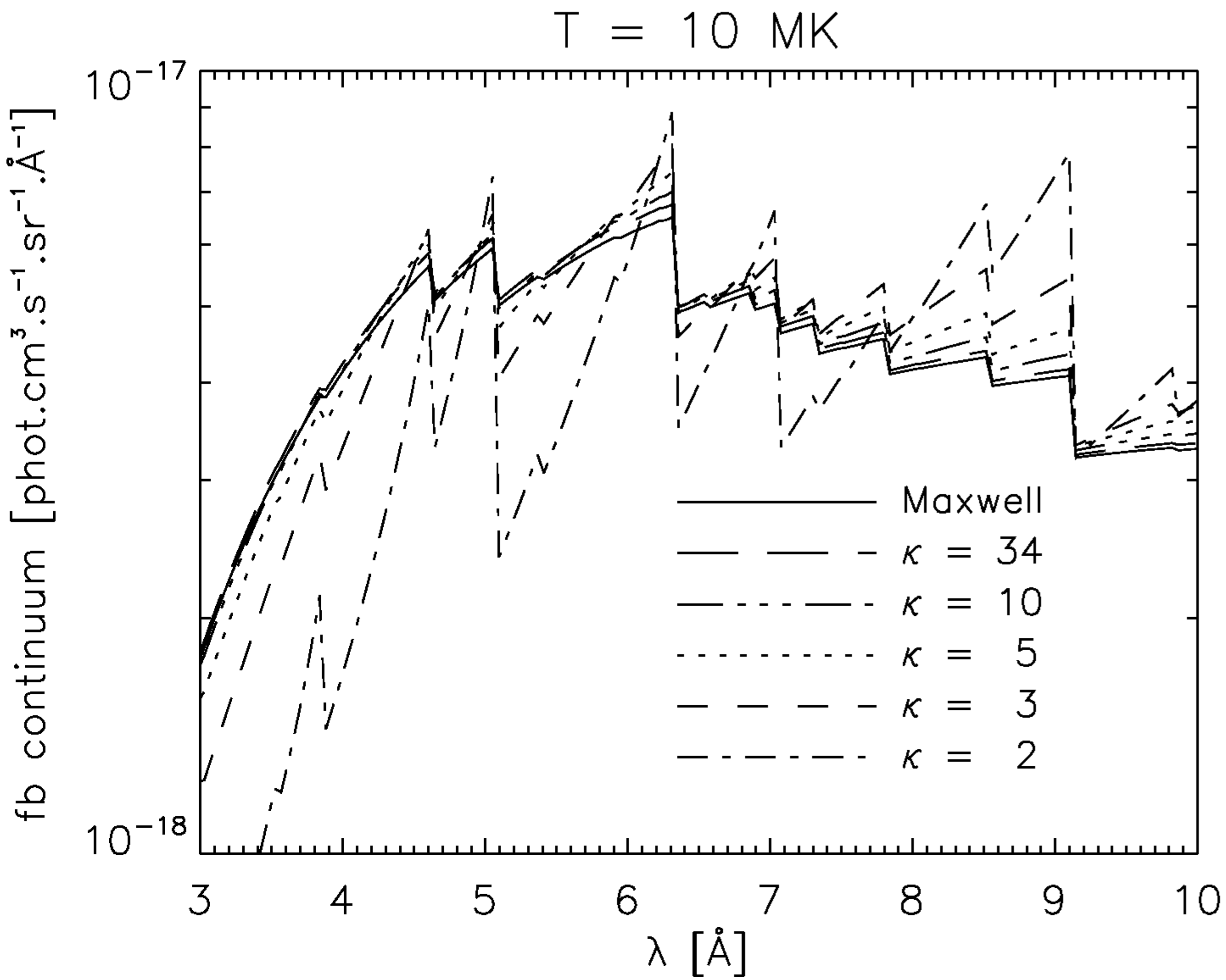

Dudík et al., 2012, A&A 539, A107

NEI and non-thermal broadening

DePontieu et al. (2015), ApJL 799, L12

- **Observed: width correlated with intensity, independent of resolution**
- **In simulations, NEI increases the broadening by 2 – 10 km s^{-1} *and produces a correlation***
- **Slow magnetoacoustic shocks**

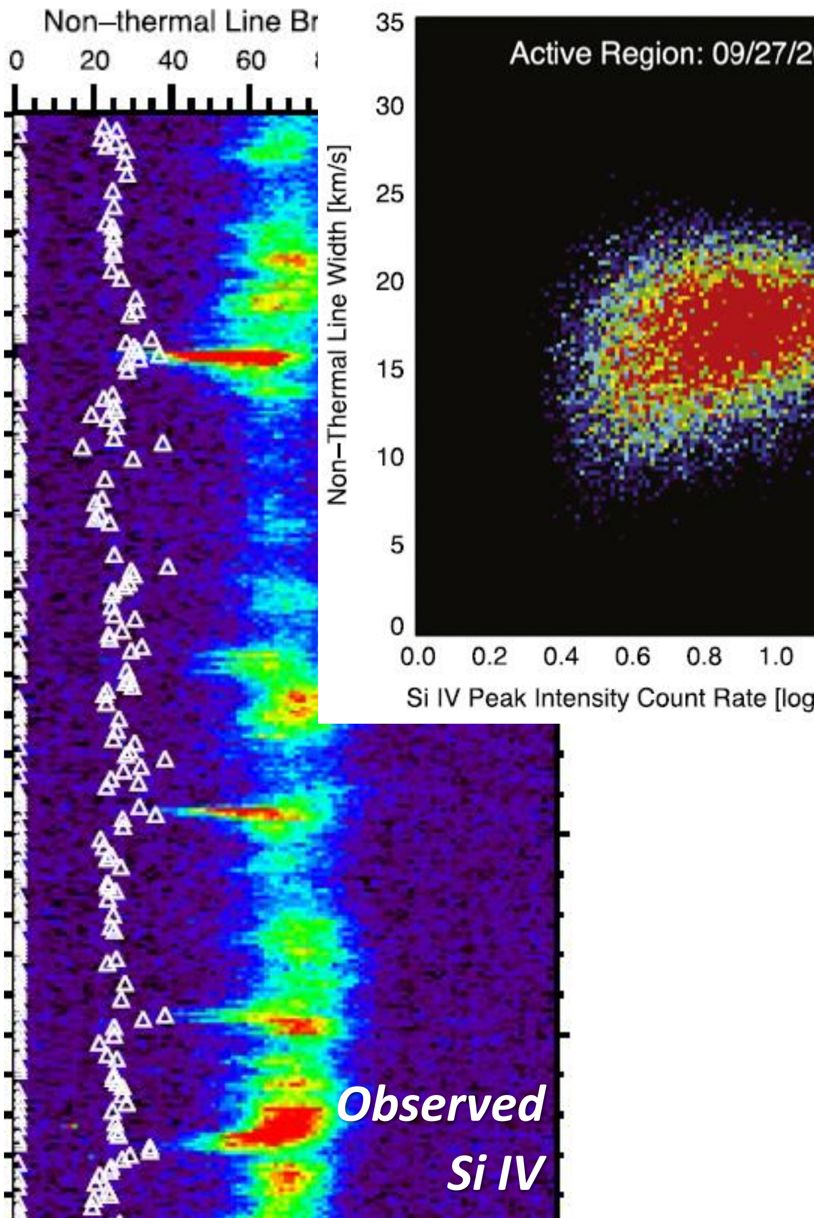

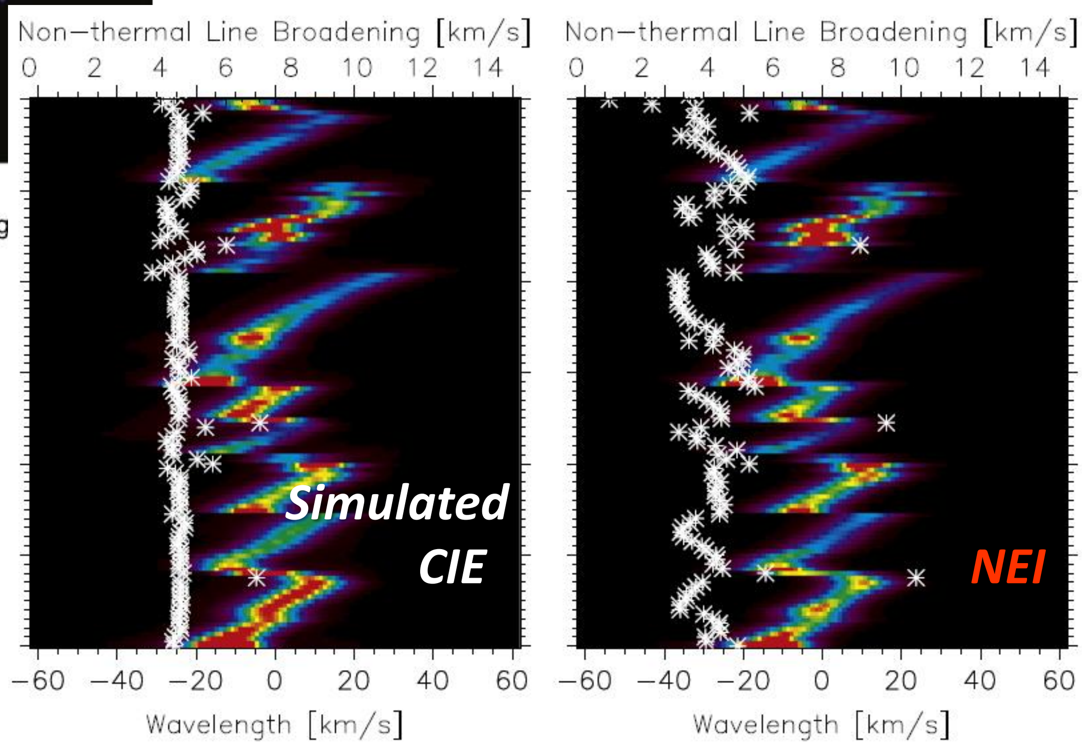

κ-distr.: Free-free Continuum

- **Emissivity of the free-free continuum for *κ*-distributions**

$$P_{\mathrm{ff}}(\lambda,\kappa) = \mathcal{A}_\kappa C T^{1/2} \int\limits_0^\infty \frac{g_{\mathrm{ff}}(y,w)}{\left(1+\frac{y+w}{\kappa-3/2}\right)^{\kappa+1}} \mathrm{d}y,$$

where $w = hc/\lambda k_{\mathrm{B}} T$

- **The constant *C* depends on abundances and the ionization equilibrium**

$$C = \frac{1}{4\pi}\frac{32\pi}{3}\frac{e^6}{m_\mathrm{e} c^2 \lambda^2}\sqrt{\frac{2\pi k_\mathrm{B}}{3 m_\mathrm{e}}} n_\mathrm{e} n_\mathrm{H} \sum_Z \sum_k k^2 \frac{n_k}{n_Z} A_Z,$$

Dudík et al., 2012, A&A 539, A107

κ-distr.: Free-bound continuum

- **Emissivity of the free-bound continuum for *κ*-distributions**

$$P_{\mathrm{fb}}(E,\kappa) = \frac{1}{4\pi}\sqrt{\frac{2}{\pi}}\frac{1}{hc^3 m_{\mathrm{e}}^{3/2} k_{\mathrm{B}}^{3/2}}\frac{E^5}{T^{3/2}} n_{\mathrm{e}} n_{\mathrm{H}} \times \sum_{i,k,Z} \frac{n_{\mathrm{k+1}}}{n_{\mathrm{Z}}} A_{\mathrm{Z}} \frac{g_i}{g_0} \sigma_i^{\mathrm{bf}} \mathcal{A}_\kappa \frac{1}{\left(1+\frac{E-I_i}{(\kappa-3/2)k_{\mathrm{B}}T}\right)^{\kappa+1}}$$

- **Depends directly on the distribution function**
- **Influenced by the number of low-energy electrons**

Dudík et al., 2012, A&A 539, A107

κ-distr.: KAPPA package

Table 1
List of Routines within the KAPPA Package

Routine name	Function
kappa.pro	interactive widget for calculation of synthetic spectra, based on ch_ss.pro
ch_synthetic_k.pro	calculates line intensities as a function of κ, n_e and T
descale_diel_k.pro	converts $\Upsilon_{ij}(T, \kappa)$ and $\mathcal{J}_{ji}(T, \kappa)$ from the scaled domain for dielectronic satellite lines and performs correction in Equation (23)
emiss_calc_k.pro	calculates $hc/\lambda\ A_{ji} n(X_j^{+k})$
freebound_ion_k.pro	calculates the free-bound continuum arising from a single ion
freebound_k.pro	calculates the free-bound continuum
free–free_k.pro	free–free continuum interpolated from pre-calculated data
free–free_k_integral.pro	calculates the free–free continuum directly
isothermal_k.pro	calculates isothermal spectra as a function of λ
make_kappa_spec_k.pro	routine for calculating the synthetic spectra
plot_populations_k.pro	calculates and plots relative level populations
pop_solver_k.pro	calculates the relative level population
read_ff_k.pro	reads the pre-calculated free–free continuum as a function of Z and T
read_rate_ioniz_k.pro	reads the total ionization and recombination rates
read_rate_recomb_k.pro	reads the total ionization and recombination rates
ups_kappa_interp.pro	routine for interpolating the $\Upsilon_{ij}(T, \kappa)$ and $\mathcal{J}_{ji}(T, \kappa)$

SDO/AIA: Transient Loop

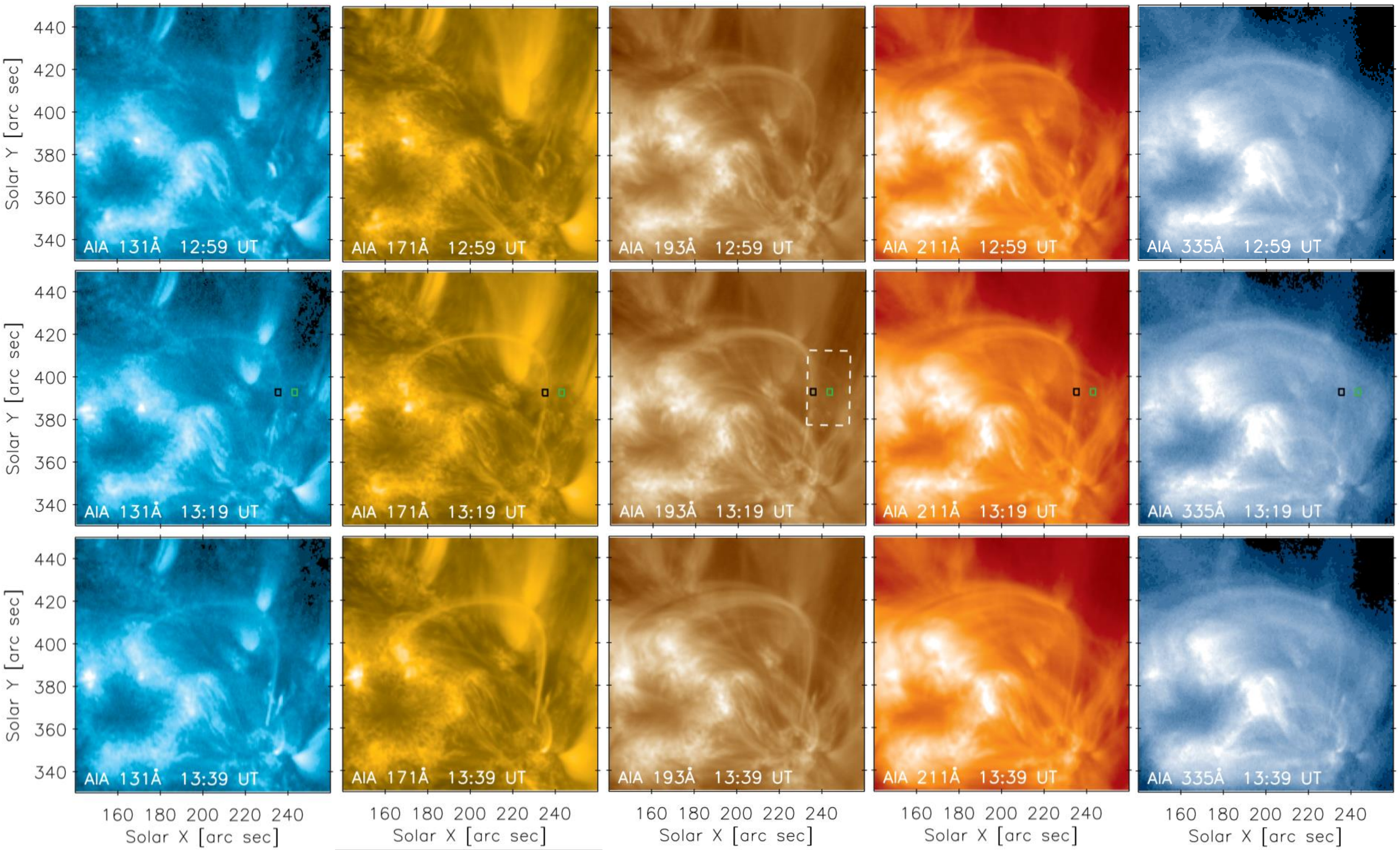

EIS Observations: HOP 226

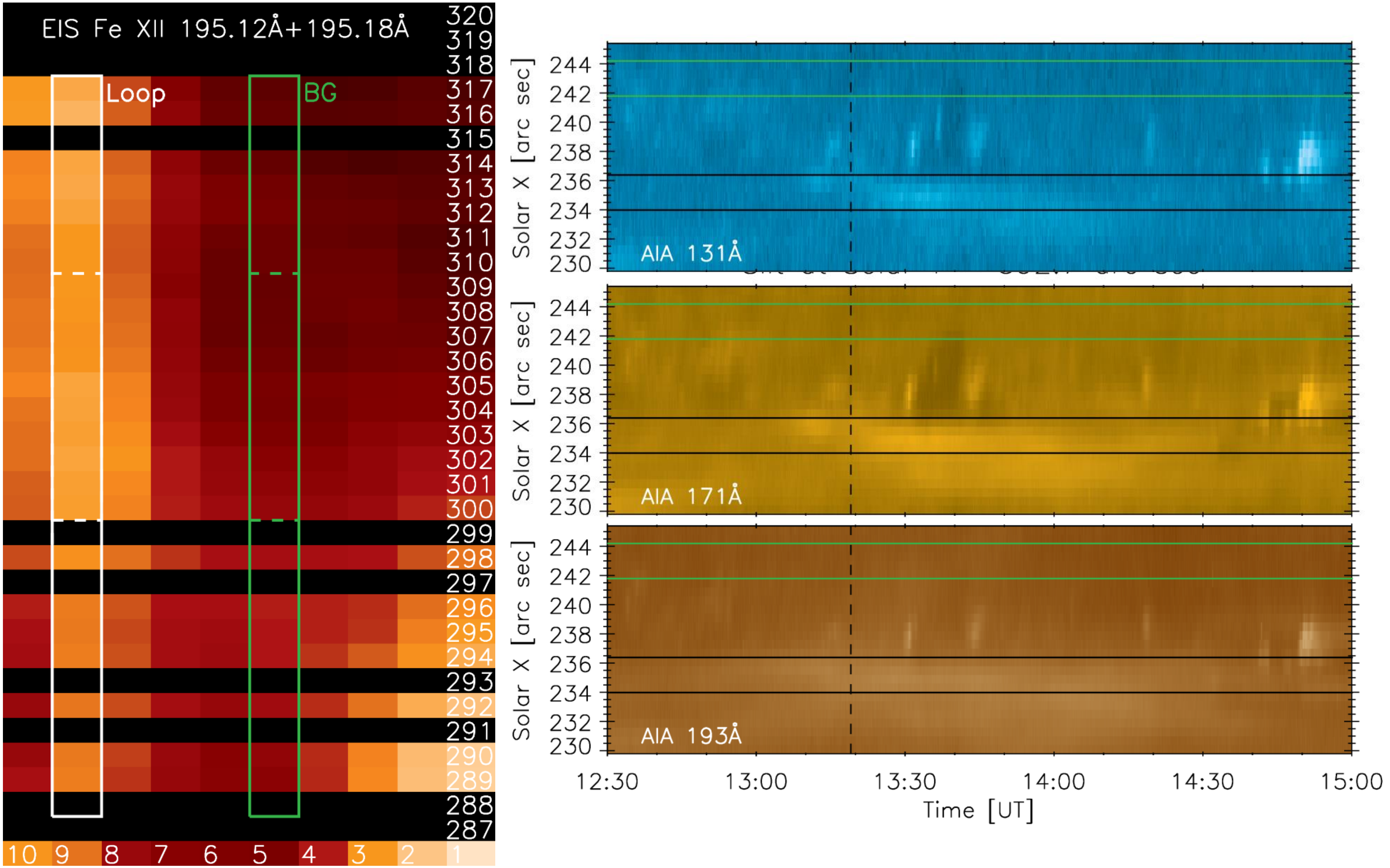

Side note: EIMI & κ-distributions

Hahn & Savin (2015), ApJ, 800, 68

Electron impact multiple ionization

- An impact of a single electron with high enough *E* can cause multiple ionization
- This contributes less than 5% for Maxwellian CIE (ionization equilibrium)
- Worsens dramatically for low κ and coronal Fe ions
- Can also be important for non-equilibrium ionization (NEI)